NASA CONTRACTOR REPORT

NASA CR-1797





# CALCULATION OF COMPRESSIBLE, NONADIABATIC BOUNDARY LAYERS IN LAMINAR, TRANSITIONAL AND TURBULENT FLOW BY THE METHOD OF INTEGRAL RELATIONS

*by Gary D. Kuhn*

*Prepared by*
NIELSEN ENGINEERING AND RESEARCH, INC.
Mountain View, Calif. 94040
*for Langley Research Center*

NATIONAL AERONAUTICS AND SPACE ADMINISTRATION • WASHINGTON, D. C. • NOVEMBER 1971

| 1. Report No. | 2. Government Accession No. | 3. Recipient's Catalog No. |
|---|---|---|
| NASA CR-1797 | | |

**4. Title and Subtitle**
CALCULATION OF COMPRESSIBLE, NONADIABATIC BOUNDARY LAYERS IN LAMINAR, TRANSITIONAL AND TURBULENT FLOW BY THE METHOD OF INTEGRAL RELATIONS

**5. Report Date**
November 1971

**6. Performing Organization Code**

**7. Author(s)**
Gary D. Kuhn

**8. Performing Organization Report No.**
NEAR TR 25

**9. Performing Organization Name and Address**
Nielsen Engineering and Research, Inc.
850 Maude Avenue
Mountain View, Calif. 94040

**10. Work Unit No.**
722-03-10-01

**11. Contract or Grant No.**
NAS1-9429

**12. Sponsoring Agency Name and Address**
National Aeronautics and Space Administration
Washington, DC 20546

**13. Type of Report and Period Covered**
Contractor Report

**14. Sponsoring Agency Code**

**15. Supplementary Notes**

**16. Abstract**

The method of integral relations has been applied to the calculation of compressible, nonadiabatic laminar, transitional, and turbulent boundary-layer characteristics. A two-layer eddy-viscosity model was employed for turbulent flow with transition produced by modulating the eddy viscosity by an intermittency function. A computer program was developed to do the calculations for two-dimensional or axisymmetric configurations from low speeds to hypersonic speeds with arbitrary Prandtl number. The program contains provisions for tabular input of arbitrary configuration shapes and arbitrary streamwise pressure, temperature, and Mach number distributions. Options are provided for obtaining initial conditions either from experimental information or from a theoretical similarity solution.

The transition region can be described either by an arbitrary distribution of intermittency or by a function based on Emmons' probability theory. Correlations were developed for use in estimating the parameters of the theoretical intermittency function. Correlations obtained from other sources are used for estimating the transition point.

Comparisons were made between calculated and measured boundary-layer quantities for laminar, transitional, and turbulent flows on flat plates, cones, cone-flares, and a waisted body of revolution. Excellent comparisons were obtained between the present theory and two other theories based on the method of finite differences.

The intermittency required to reproduce some experimental heat transfer results in hypersonic flow was found to be quite different from the theoretical function. It is suggested that the simple probability theory of Emmons may not be valid for representing the intermittency of hypersonic transitional boundary layers and that the program could be useful as a tool for detailed study of the intermittency of the transition region.

| 17. Key Words (Suggested by Author(s)) | 18. Distribution Statement |
|---|---|
| Boundary layer<br>Laminar boundary layer<br>Transitional boundary layer<br>Turbulent boundary layer | Unclassified - Unlimited |

| 19. Security Classif. (of this report) | 20. Security Classif. (of this page) | 21. No. of Pages | 22. Price* |
|---|---|---|---|
| Unclassified | Unclassified | 132 | $3.00 |

*For sale by the National Technical Information Service, Springfield, Virginia 22151

## FOREWORD

The research described herein was sponsored by Langley Research Center, NASA, under Contract NAS1-9429. Computer facilities were provided at LRC and at Ames Research Center, NASA. The assistance of the Technical Monitor, Mr. S. Z. Pinckney, in coordinating the research effort and providing technical information is gratefully acknowledged. The work was performed under the supervision of Dr. Jack N. Nielsen.

TABLE OF CONTENTS

# CALCULATION OF COMPRESSIBLE, NONADIABATIC BOUNDARY LAYERS IN LAMINAR, TRANSITIONAL AND TURBULENT FLOW BY THE METHOD OF INTEGRAL RELATIONS

By Gary D. Kuhn
Nielsen Engineering & Research, Inc.

## SUMMARY

The method of integral relations has been applied to the calculation of compressible, nonadiabatic laminar, transitional, and turbulent boundary-layer characteristics. A two-layer eddy-viscosity model was employed for turbulent flow with transition produced by modulating the eddy viscosity by an intermittency function. A computer program was developed to do the calculations for two-dimensional or axisymmetric configurations from low speeds to hypersonic speeds with arbitrary Prandtl number. The program contains provisions for tabular input of arbitrary configuration shapes and arbitrary streamwise pressure, temperature, and Mach number distributions. Options are provided for obtaining initial conditions either from experimental information or from a theoretical similarity solution.

The transition region can be described either by an arbitrary distribution of intermittency or by a function based on Emmons' probability theory. Correlations were developed for use in estimating the parameters of the theoretical intermittency function. Correlations obtained from other sources are used for estimating the transition point.

Comparisons were made between calculated and measured boundary-layer quantities for laminar, transitional, and turbulent flows on flat plates, cones, cone-flares, and a waisted body of revolution. Excellent comparisons were obtained between the present theory and two other theories based on the method of finite differences.

The intermittency required to reproduce some experimental heat transfer results in hypersonic flow was found to be quite different from the theoretical function. It is suggested that the simple probability theory of Emmons may not be valid for representing the intermittency of hypersonic transitional boundary layers and that the program could be useful as a tool for detailed study of the intermittency of the transition region.

## INTRODUCTION

Many empirical methods are available for estimating the properties of laminar and turbulent boundary layers. With the development of sophisticated electronic computers, many computer programs have also been developed for calculating the solutions of the boundary-layer equations in the laminar and turbulent regions. At the same time, much research has been done on the nature of the boundary-layer flow in the transition region between laminar and turbulent flow. Even now, however, the transition region is not completely understood. The methods of computing the boundary layer in the transition region usually employ some empirical variation of the growth of the turbulent eddy viscosity, itself an empirical quantity, along with a prediction of the starting point of the transition region developed from still other empirical correlations.

At the present time, there are two mathematical techniques for computing the details of the boundary layer. Both techniques use the boundary-layer equations together with an empirical eddy-viscosity model for the turbulent region. The techniques differ essentially in how they solve the boundary-layer equations. In the first method, an example of which is described in reference 1, the solution is sought by the method of finite differences. In the second method, described in references 2, 3, and 4, the solution is by the method of integral relations, in which the solution is represented to any degree of accuracy by partial sums of infinite series.

In the work described in this report, the method of integral relations is adapted to development of a generalized program for use as an engineering tool for the calculation of boundary-layers on arbitrary two-dimensional or axisymmetric bodies, with arbitrary flow conditions.

The method of integral relations was applied in references 2, 3, and 4 to the calculation of laminar and turbulent, nonadiabatic, compressible boundary layers. In the work described herein, the method has been extended to calculation of transitional boundary layers. In addition, the theory has been extended to include arbitrary Prandtl number, and arbitrary Chapman-Rubesin constant, thus relaxing the assumption of a linear total temperature-velocity relationship as used in the previous applications of the method.

The work presented in this report was accomplished under a 1-year effort sponsored by Langley Research Center, NASA, Contract No. NAS1-9429. The main effort was directed toward development of a computer program and the associated theory based on the method of integral relations for calculation of transitional boundary layers. Due to the general nature of the method, the program and theory are also applicable to the laminar and turbulent regions. The following sections contain the analyses which lead to the computer program and contain a substantial number of comparisons between prediction and experiment.

An operating manual and a programmer's manual for the computer program are being issued as separate documents.

## LIST OF SYMBOLS

| | |
|---|---|
| $a$ | speed of sound |
| $a_{ij}$ | elements of coefficient matrix defined by eq. (88) |
| $a'_{ij}$ | elements of coefficient matrix defined by eq. (89) |
| $A$ | parameter defined by eq. (26) |
| $\overline{A},\overline{B}$ | parameters defined by eq. (150) |
| $A_{ij}$ | elements of a coefficient matrix defined by eq. (117) |
| $B$ | parameter defined by eq. (27) |
| $B_i$ | right-hand side of eq. (86), defined by eq. (90) |
| $B'_i$ | right-hand side of eq. (87), defined by eq. (91) |
| $c_p$ | specific heat for constant pressure |
| $C$ | Chapman-Rubesin constant defined by eq. (45) |
| $C_f$ | skin-friction coefficient, $2\tau_w/\rho_e u_e^2$ |
| $C_i$ | coefficients used in specifying the velocity gradient profile, eq. (77) |
| $E_i$ | coefficients used in specifying the enthalpy function, eq. (82) |
| $f$ | frequency of Tollmien-Schlichting wave |

| | |
|---|---|
| $f_i, g_i, h_i$ | weighting functions defined in eqs. (68), (69), and (70) |
| $f_i^*$ | weighting function defined by eq. (83) |
| F,G,I | constants in transition correlation, eq. (121) |
| $F_i$ | integrand of integral defined by eq. (94) |
| h | static enthalpy |
| H | total enthalpy |
| k | transverse curvature index defined in eqs. (1), (2), and (3) |
| $k_1, k_2$ | constants in eddy viscosity, eq. (139) |
| $K_i$ | constants defined in eq. (113) |
| $\ell$ | reference length in two-dimensional coordinates or Probstein-Elliott coordinates (eq. (56)) |
| L | reference length in physical coordinate system |
| m | order of approximation of enthalpy function (eq. (82)) |
| $m_e$ | $(\gamma - 1)M_e^2/2$ |
| M | Mach number |
| n | order of approximation of velocity gradient profile, eq. (77) |
| n' | exponent of unit Reynolds number in transition correlation (eq. (121)) |
| $N_R$ | reference Reynolds number defined by eq. (160) |
| Nu | Nusselt number |
| p | pressure |
| $P_i, Q_i, R_i$ | integrals defined by equations (94), (95), and (96) |
| $P_i'$ | integrals defined by eq. (119) |
| Pr | Prandtl number |
| r | radius from axis of axisymmetric configuration or distance from datum plane of two-dimensional configuration |
| $r_L$ | laminar recovery factor |

| | |
|---|---|
| $r_T$ | turbulent recovery factor |
| $Re_{x_t}$ | transition Reynolds number, $(u_e/\nu_e)x_t$ |
| $Re_1$ | unit Reynolds number, $u/\nu$ |
| $Re_{\delta^*}$ | Reynolds number, $(u_e/\nu_e)\delta^*$ |
| $Re_{\Delta x}$ | Reynolds number of length of transition, $(u_e/\nu_e)\Delta x$ |
| $R_o$ | reference Reynolds number, $(u_{e_o}/\nu_{e_o})\ell$ |
| s' | enthalpy-Mach number parameter in transition correlations, eqs. (120), (121), and (122) |
| S | enthalpy function, $(H/H_e) - 1$ |
| St | Stanton number, $k_w(\partial T/\partial y)\Big\|_w/\rho_e u_e c_p\left[T_{aw} - T_w\right]$ |
| t | transverse curvature factor (eq. (28)) |
| T | temperature |
| u,v | velocity components in physical coordinates parallel and normal to surface, respectively |
| $\bar{u}$ | $u/u_e$ |
| $u^*$ | reference friction velocity, $(\tau_w/\rho_w)^{1/2}$ |
| $u^+$ | $u/u^*$ |
| $u_\tau$ | friction velocity, $(\tau/\rho)^{1/2}$ |
| U,V | velocity components in Stewartson plane |
| $U^+$ | velocity parameter in eddy viscosity, defined by eqs. (138) and (143) |
| $\bar{v}$ | normal velocity in Dorodnitsyn plane, $(V/U_e)\sqrt{R_o}$ |
| $\bar{w}$ | $\bar{v} + \bar{u}\eta(\dot{U}_e/U_e)$ |
| x,y | curvilinear coordinates in physical system |
| x' | axial or reference coordinate (fig. 1) |
| $\Delta x_i$ | integration step size |

$X,Y$ coordinates of the Stewartson transformation,

$$X = \int_0^x \frac{\rho_e a_e}{\rho_{e_o} a_{e_o}} dx \; ; \quad Y = \int_0^y \frac{\rho_e a_e}{\rho_{e_o} a_{e_o}} \frac{\rho}{\rho_e} dy$$

$y^+$ $\rho_w u^* y/\mu_w$

$\alpha$ angle of inclination of surface relative to reference axis (fig. 1)

$\bar{\alpha}$ exponent in transition length correlation, eq. (150)

$\beta$ eddy-viscosity parameter, $1 + \epsilon/\mu$

$\gamma$ ratio of specific heats

$\Gamma$ intermittency function

$\Gamma_B$ intermittency function defined by eq. (161)

$\delta$ boundary-layer thickness

$\delta^*$ displacement thickness

$\delta_k^*$ kinematic displacement thickness

$\epsilon$ absolute eddy viscosity

$\epsilon_H$ eddy conductivity

$\epsilon^+$ $\rho\epsilon/\mu$

$\theta$ momentum thickness

$\theta_h$ enthalpy thickness

$\lambda$ source function parameter in intermittency (eq. (147))

$\mu$ absolute molecular viscosity

$\nu$ kinematic viscosity, $\mu/\rho$

$\xi,\eta$ coordinates in the Dorodnitsyn plane,

$$\xi = \int_0^X \frac{U_e}{U_{e_o}} \frac{dx}{\ell} \; ; \quad \eta = \frac{U_e}{U_{e_o} \ell} (R_o)^{1/2} Y$$

$\rho$ density

$\sigma_1,\sigma_2,\sigma_3$ error functions defined in eqs. (65), (66), and (67)

$\Sigma_{ij}$ functions defined by eqs. (98) through (103)

$\tau$ shear stress

$\phi$ $(1/\partial\bar{u})/\partial\eta$

$\psi$ stream function

### Subscripts

aw adiabatic wall

e refers to the boundary-layer edge

L refers to laminar flow

o initial condition at $x_o$

s stagnation condition

t transition

T refers to turbulent flow

w condition at the wall

$\infty$ free-stream condition

### Special Notation

$(\bar{\ })$ denotes a time average quantity

$(\tilde{\ })$ denotes variables in the Probstein-Elliott transformation

$(\dot{\ })$ denotes differentiation with respect to $\xi$

$(\ )'$ denotes a fluctuating quantity

## THEORETICAL BASIS

The method of integral relations used herein is due to Dorodnitsyn (ref. 5). Briefly, the mathematical procedure employed is that of representing the solution of a differential equation by an infinite series. An approximation to the solution is developed by taking a partial sum of the infinite series. A discussion of some of the pertinent mathematical theorems associated with the application of the method to the partial

differential equations of the incompressible boundary layer was presented by Murphy and Rose in reference 6. In the present analysis, the method is generalized to include compressible flow with arbitrary Prandtl number.

Since the present analysis is considerably more generalized than has been presented previously, the derivation of the important equations is presented in detail. The basic analysis is presented in terms of a turbulent boundary layer since that is the most general case. The equations describing the transitional and laminar boundary layers differ from those of the turbulent case only in the definition of the effective, or eddy, viscosity.

## Assumptions

The analysis is based on the following assumptions:

(1) The governing equations are those for a compressible turbulent boundary layer.

(2) The air behaves as an ideal gas.

(3) The molecular viscosity, $\mu$, is proportional to the temperature.

(4) The specific heat of the gas is constant.

(5) The Prandtl number of the gas is constant, but arbitrary.

(6) The conditions at the edge of the boundary-layer are arbitrary.

(7) The wall is either two-dimensional or axisymmetric, but can have arbitrary variation in the direction of flow as long as the radius of curvature of the wall is large compared to the boundary layer.

(8) The pressure is constant normal to the wall.

(9) The wall temperature is prescribed and may vary arbitrarily in the direction of flow.

## Boundary-Layer Equations for Compressible Turbulent Flow

Reference 1 presents the boundary-layer equations for compressible turbulent flow in a convenient form for both axisymmetric and two-dimensional flow. The basic notation and coordinate scheme are shown in figure 1. A blunt body is shown; however, the present analysis applies equally well to a pointed body since the analysis is restricted to points downstream of a stagnation point or sharp leading edge or nose. Note also that the same symbols are used for the physical coordinates of both

two-dimensional and axisymmetric configurations. Thus, r denotes the distance of a point from the axis of an axisymmetric configuration, or from the reference plane of a two-dimensional configuration. The coordinates are a curvilinear system in which x is tne distance along the surface measured from the stagnation point or leading edge. The dimension y is measured normal to the surface. In the differential equations, the transverse curvature terms are retained because of their potential importance in predicting the boundary-layer growth on long slender bodies.

The governing equations describing the steady flow of a turbulent boundary layer are:

CONTINUITY

$$\frac{\partial}{\partial x}\left[(\rho u + \overline{\rho' u'})\, r^k\right] + \frac{\partial}{\partial y}\left[(\rho v + \overline{\rho' v'})\, r^k\right] = 0 \tag{1}$$

MOMENTUM

$$\begin{aligned}(\rho u + \overline{\rho' u'})\,\frac{\partial u}{\partial x} + (\rho v + \overline{\rho' v'})\,\frac{\partial u}{\partial y} &= -\frac{dp}{dx} - \frac{1}{r^k}\,\frac{\partial}{\partial x}\left[r^k(\overline{\rho u'^2} + \overline{u\rho' v'} + \overline{\rho' u'^2})\right] \\ &\quad + \frac{1}{r^k}\,\frac{\partial}{\partial y}\left[r^k\left(\mu\,\frac{\partial u}{\partial y} - \overline{\rho v' u'} - \overline{v\rho' u'} - \overline{\rho' u' v'}\right)\right]\end{aligned} \tag{2}$$

ENERGY

$$\begin{aligned}(\rho u + \overline{\rho' u'})\,\frac{\partial H}{\partial x} + (\rho v + \overline{\rho' v'})\,\frac{\partial H}{\partial y} &= -\frac{1}{r^k}\,\frac{\partial}{\partial x}\left[r^k(\overline{\rho u' H'} + \overline{u\rho' H'} + \overline{\rho' u' H})\right] \\ &\quad + \frac{1}{r^k}\,\frac{\partial}{\partial y}\left\{r^k\left[\frac{\mu}{Pr}\,\frac{\partial H}{\partial y} - \overline{\rho v' H}\right.\right. \\ &\quad \left.\left. + \mu\left(1 - \frac{1}{Pr}\right) u\,\frac{\partial u}{\partial y} - \overline{v\rho' H'} - \overline{\rho' v' H'}\right]\right\}\end{aligned} \tag{3}$$

where $k = 0$ for two-dimensional flow and $k = 1$ for axisymmetric flow.

The boundary layer is assumed to be thin and the terms such as $\rho$, $u$, $H$, and $x$ are assumed to be of the order of 1 and $v$ and $y$ are of the order of the boundary-layer thickness, $\delta$. This allows some of the correlation terms involving the fluctuation quantities to be neglected. Specifically, the double correlation terms $\overline{\rho'u'}$, $\overline{u'H'}$, $\overline{\rho'H'}$, and $\overline{\rho'v'}$ are of the order of $\delta$ at most, and the triple correlation terms $\overline{\rho'v'u'}$ and $\overline{\rho'v'H'}$ are of the order of $\delta^2$ at most. Away from separation, the Reynolds normal stresses $-\overline{\rho u'^2}$ and $-\overline{\rho v'^2}$ are small and can be neglected.

The Reynolds shear stress $-\overline{\rho u'v'}$ is eliminated through use of the definitions

$$\left.\begin{aligned} -\overline{\rho u'v'} &= \epsilon \frac{\partial u}{\partial y} \\ \text{and} \qquad \beta &= 1 + \frac{\epsilon}{\mu} \end{aligned}\right\} \tag{4}$$

The term $\overline{\rho v'h'}$ is eliminated through the use of an eddy-conductivity concept as follows: the total enthalpy is defined

$$H = h + h' + \frac{1}{2}\left[u^2 + v^2 + 2uu' + 2vv' + u'^2 + v'^2\right]$$

As before, the terms $u'^2$ and $v'^2$ are assumed to be of at least second order so that the total enthalpy can be expressed

$$H = \overline{H} + H'$$

where

$$\overline{H} = h + \frac{1}{2}u^2$$

and

$$H' = h' + uu' + vv'$$

Then

$$\overline{v'H'} = \overline{v'h'} + u\overline{u'v'}$$

or

$$\overline{v'H'} = \overline{v'h'} - u \frac{\epsilon}{\rho} \frac{\partial u}{\partial y}$$

If an eddy conductivity is introduced so that

$$-\overline{\rho v'h'} = \epsilon_H \frac{\partial h}{\partial y} \tag{5}$$

then

$$-\overline{\rho v'H'} = \epsilon_H \frac{\partial H}{\partial y} + (\epsilon - \epsilon_H) u \frac{\partial u}{\partial y}$$

Or, defining a turbulent Prandtl number as

$$Pr_T = \frac{\epsilon}{\epsilon_H} \tag{6}$$

gives

$$-\overline{\rho v'H'} = \frac{\epsilon}{Pr_T} \frac{\partial H}{\partial y} + \epsilon \left(1 - \frac{1}{Pr_T}\right) u \frac{\partial u}{\partial y}$$

Laufer (ref. 7) has pointed out that some of the higher order correlation terms should probably be retained in the energy equation for hypersonic flows. However, in the absence of reliable experimental or theoretical information, an appropriate model for those terms cannot be developed at the present time.

In the present analysis, the turbulent Prandtl number, $Pr_T$, has been assumed to be constant except in the transition region, where it is defined as

$$Pr_t = 1 - \Gamma(1 - Pr_T)$$

where $\Gamma$ is a modulation factor for the transition region and will be discussed in detail in a subsequent section.

Neglecting higher-order terms and incorporating the eddy-viscosity and eddy-conductivity concepts, the differential equations (1) to (3) become

CONTINUITY

$$\frac{\partial}{\partial x}\left[r^k \rho u\right] + \frac{\partial}{\partial y}\left[r^k \rho v\right] = 0 \tag{7}$$

MOMENTUM

$$\rho u \frac{\partial u}{\partial x} + \rho v \frac{\partial u}{\partial y} = - \frac{dp}{dx} + \frac{1}{r^k} \frac{\partial}{\partial y}\left[r^k \mu \beta \frac{\partial u}{\partial y}\right] \tag{8}$$

ENERGY

$$\rho u \frac{\partial H}{\partial x} + \rho v \frac{\partial H}{\partial y} = \frac{1}{r^k} \frac{\partial}{\partial y} \left\{ r^k \left[ \mu \left( \frac{1}{Pr} - \frac{1}{Pr_T} + \frac{\beta}{Pr_T} \right) \frac{\partial H}{\partial y} + \mu \left( \beta - \frac{\beta}{Pr_T} + \frac{1}{Pr_T} - \frac{1}{Pr} \right) u \frac{\partial u}{\partial y} \right] \right\} \tag{9}$$

where the term $\rho v$ is a time-averaged quantity defined by

$$\rho v = \overline{\rho v} + \overline{\rho' v'} \tag{10}$$

In solving the differential equations, it is convenient to define a new variable

$$S = \frac{H}{H_e} - 1 \tag{11}$$

with which the energy equation (eq. (9)) becomes

$$\rho u \frac{\partial S}{\partial x} + \rho v \frac{\partial S}{\partial y} = \frac{1}{r^k} \frac{\partial}{\partial y} \left\{ r^k \left[ \mu \left( \frac{1}{Pr} - \frac{1}{Pr_t} + \frac{\beta}{Pr_t} \right) \frac{\partial S}{\partial y} + \mu \left( \beta - \frac{\beta}{Pr_t} + \frac{1}{Pr_t} - \frac{1}{Pr} \right) \frac{u}{H_e} \frac{\partial u}{\partial y} \right] \right\} - \rho u \left( \frac{S + 1}{H_e} \right) \frac{\partial H_e}{\partial x} \tag{12}$$

where $H_e$ is assumed to be a function of $x$.

Equations (7), (8), and (12) are easily applicable to laminar and transitional flow. In laminar flow, substitution of $\beta = Pr_t = 1$ reduces the equations to those for a laminar boundary layer. Further, suitable variation of the eddy viscosity and turbulent Prandtl number makes the equations applicable to the transition region.

The boundary conditions for this system of equations are:

At $y = 0$:

$$u = v = 0$$

$$r = r_w$$

$$S = S_w$$

At $y = \infty$:

$$u = u_e(x)$$

$$\partial u/\partial y = 0$$

$$v = v_e(x)$$

$$S = 0$$

At $x = x_o$:

$$u = u_o(y)$$

$$S = S_o(y)$$

## Transformation of Axisymmetric Boundary-Layer Equations to Almost Two-Dimensional Form

In order to put the axisymmetric equations ($k = 1$) into a more convenient form, the Probstein-Elliott transformation (ref. 8) is applied. The coordinates of the axisymmetric body are shown in figure 1(a). The Probstein-Elliott transformation is

$$d\tilde{x} = \left[\frac{r_w(x')}{L}\right]^2 dx \tag{13}$$

$$d\tilde{y} = \frac{r(x,y)}{L}\, dy \tag{14}$$

where $r_w(x')$ is specified by the body shape and $r(x,y)$ is given by

$$r(x,y) = r_w(x') + y \cos \alpha \tag{15}$$

with

$$x = \int_0^{x'} \left[1 + (dr_w/dx')^2\right]^{1/2} dx' \tag{16}$$

A stream function that satisfies the continuity equation, equation (7), is defined by

$$\frac{\partial \psi}{\partial y} = r^k \rho u \tag{17}$$

$$\frac{\partial \psi}{\partial x} = -r^k \rho v = -r^k (\overline{\rho v} + \overline{\rho' v'}) \tag{18}$$

Let

$$\tilde{\psi} = \frac{\psi}{L} \qquad \tilde{u} = u \qquad \tilde{v} = v \tag{19}$$

$$\overline{\rho' \tilde{v}'} = \overline{\rho' v'} \qquad \tilde{\epsilon} = \epsilon \qquad \tilde{Pr}_t = Pr_t \tag{20}$$

Then the continuity equation with

$$\rho \tilde{u} = \frac{\partial \tilde{\psi}}{\partial \tilde{y}} \tag{21}$$

and

$$\rho \tilde{v} = -\frac{\partial \tilde{\psi}}{\partial \tilde{x}} = \frac{rL}{r_w^2} \rho v + \frac{L^2}{r_w^2} \frac{\partial \tilde{y}}{\partial x} \rho u \tag{22}$$

has the form

$$\frac{\partial (\rho u)}{\partial \tilde{x}} + \frac{\partial (\rho v)}{\partial \tilde{y}} = 0 \tag{23}$$

Applying the transformation to the momentum and energy equations (8) and (12) yields the transformed equations

$$\rho u \frac{\partial u}{\partial \tilde{x}} + \rho v \frac{\partial u}{\partial \tilde{y}} = -\frac{dp}{d\tilde{x}} + \frac{\partial}{\partial \tilde{y}} \left[(1 + kt\tilde{y}) \mu\beta \frac{\partial u}{\partial \tilde{y}}\right] \tag{24}$$

$$\rho u \frac{\partial S}{\partial \tilde{x}} + \rho v \frac{\partial S}{\partial \tilde{y}} = \frac{\partial}{\partial \tilde{y}} \left\{ (1 + kt\tilde{y}) \left[ \mu A \frac{\partial S}{\partial \tilde{y}} + \mu \frac{B}{H_e} u \frac{\partial u}{\partial \tilde{y}} \right] \right\}$$

$$- \rho u \left( \frac{S + 1}{H_e} \right) \frac{dH_e}{d\tilde{x}} \tag{25}$$

where

$$A = \frac{1}{Pr} - \frac{1}{Pr_t} + \frac{\beta}{Pr_t} \tag{26}$$

$$B = \beta - \frac{\beta}{Pr_t} + \frac{1}{Pr_t} - \frac{1}{Pr} \tag{27}$$

and $t$ is the transverse curvature factor

$$t = \frac{2L \cos \alpha}{r_w^2} \tag{28}$$

and

$$\tilde{y} = \frac{r_w}{L} y + \frac{\cos \alpha}{2L} y^2 \tag{29}$$

For flows in which the transverse curvature terms are negligible, letting $k = 0$ in equations (24) and (25) produces the equations of a two-dimensional boundary layer. The transverse curvature terms may be negligible for an axisymmetric flow if the body radius is large compared to the boundary-layer thickness. The Probstein-Elliott transformation is thus a first-order correction of the approximate equations for the effect of transverse curvature.

## Transformation of the Compressible Boundary-Layer Equations

In order to further simplify the equations, two additional transformations are applied. The Stewartson transformation (ref. 9) reduces the equations to a set of equations for an incompressible flow. The Dorodnitsyn transformation (ref. 5) removes the explicit dependence on the molecular viscosity. The following analysis is presented in terms

of the Probstein-Elliott coordinates, $\tilde{x}$ and $\tilde{y}$, with the understanding that in the two-dimensional case $x = \tilde{x}$ and $y = \tilde{y}$.

Stewartson transformation.- In the Stewartson transformation the following variables are introduced:

$$X = \int_0^{\tilde{x}} \frac{p_e a_e}{p_{e_o} a_{e_o}} \, d\tilde{x} \qquad Y = \int_0^{\tilde{y}} \frac{\rho_e a_e}{\rho_{e_o} a_{e_o}} \frac{\rho}{\rho_e} \, d\tilde{y} \tag{30}$$

and

$$U = \frac{a_{e_o}}{a_e} u \tag{31}$$

$$V = \frac{p_{e_o}}{p_e} \left( \frac{a_{e_o}}{a_e} \right)^2 u \frac{\partial}{\partial \tilde{x}} \int_0^{\tilde{y}} \frac{\rho_e a_e}{\rho_{e_o} a_{e_o}} \frac{\rho}{\rho_e} \, d\tilde{y} + \frac{p_{e_o} a_{e_o}}{p_e a_e} \frac{\rho}{\rho_{e_o}} v \tag{32}$$

With these the boundary conditions become:

At $\tilde{y} = 0$: $U = V = 0$

$S = S_w$

At $\tilde{y} = \infty$: $U = U_e = a_{e_o} M_e$

$\partial U / \partial Y = 0$

$S = 0$

At $X = X_o$: $U = U_o(Y)$

$S = S_o(Y)$

It is assumed that $S$, $H_e$, and the eddy-viscosity parameter, $\beta$, transform directly. That is,

$$S(X,Y) = S(\tilde{x},\tilde{y}) \tag{33}$$

$$H_e(X) = H_e(\tilde{x}) \tag{34}$$

$$\beta(X,Y) = \beta(\tilde{x},\tilde{y}) \tag{35}$$

With the above definitions, the derivatives become

$$\frac{\partial}{\partial \tilde{x}} = \frac{\partial X}{\partial \tilde{x}} \frac{\partial}{\partial X} + \frac{\partial Y}{\partial \tilde{x}} \frac{\partial}{\partial Y} = \frac{p_e a_e}{p_{e_o} a_{e_o}} \frac{\partial}{\partial X} + \frac{\partial Y}{\partial \tilde{x}} \frac{\partial}{\partial Y} \tag{36}$$

and

$$\frac{\partial}{\partial \tilde{y}} = \frac{\partial X}{\partial \tilde{y}} \frac{\partial}{\partial X} + \frac{\partial Y}{\partial \tilde{y}} \frac{\partial}{\partial Y} = \frac{\rho_e a_e}{\rho_{e_o} a_{e_o}} \frac{\rho}{\rho_e} \frac{\partial}{\partial Y} \tag{37}$$

Then with the definitions

$$U = \frac{\partial \psi}{\partial Y} \tag{38}$$

and

$$V = - \frac{\partial \psi}{\partial X} \tag{39}$$

it is easily shown, using relations (31) through (39) and the perfect gas assumption along with the relations

$$\frac{\mu}{\mu_{e_o}} = C \frac{T}{T_{e_o}} \tag{40}$$

and

$$\frac{\partial p}{\partial y} = 0 \tag{41}$$

that the boundary-layer equations in the Stewartson plane are:

CONTINUITY

$$\frac{\partial U}{\partial X} + \frac{\partial V}{\partial Y} = 0 \tag{42}$$

MOMENTUM

$$U\frac{\partial U}{\partial X} + V\frac{\partial U}{\partial Y} = (S+1)U_e\frac{dU_e}{dX} + C\nu_{e_o}\frac{\partial}{\partial Y}\left[(1+kt\tilde{y})\beta\frac{\partial U}{\partial Y}\right]$$

$$+\frac{1}{2}\frac{p_{e_o}a_{e_o}}{p_e a_e}\frac{1}{T_{s_e}}\frac{dT_{s_e}}{d\tilde{x}}\left(\frac{\rho_e}{\rho}U_e^2 - U^2\right) \qquad (43)$$

ENERGY

$$U\frac{\partial S}{\partial X} + V\frac{\partial S}{\partial Y} = C\nu_{e_o}\frac{\partial}{\partial Y}\left[(1+kt\tilde{y})A\frac{\partial S}{\partial Y}\right]$$

$$+C\frac{\nu_{e_o}}{H_e}\frac{a_e^2}{a_{e_o}^2}\frac{\partial}{\partial Y}\left[(1+kt\tilde{y})BU\frac{\partial U}{\partial Y}\right]$$

$$-\frac{a_{e_o}p_{e_o}}{a_e p_e}\frac{1}{H_e}\frac{dH_e}{d\tilde{x}}(S+1)U \qquad (44)$$

The derivatives $dT_{s_e}/d\tilde{x}$ and $dH_e/d\tilde{x}$ are not transformed because $H_e$ and $T_{s_e}$ are assumed to transform directly. Also, since $H_e(\tilde{x})$ is a boundary condition and $H_e$ and $T_{s_e}$ are related by

$$H_e(\tilde{x}) = c_p T_{s_e}(\tilde{x})$$

nothing is gained by transforming their derivatives. Likewise, the coordinate $\tilde{y}$ is not transformed in the transverse curvature terms because integration of the equations across the boundary layer is anticipated and only corresponding values are needed in those terms. The Chapman-Rubesin constant, C, is assumed to be at most a function of x. In the work presented herein, C is evaluated at the wall temperature. That is,

$$C = \frac{\mu_w}{\mu_{e_o}}\frac{T_{e_o}}{T_w} = \left(\frac{T_w}{T_{e_o}}\right)^{1/2}\left[\frac{T_{e_o}+198.6}{T_w+198.6}\right] \qquad (45)$$

where Sutherland's law is used to evaluate the viscosity.

Dorodnitsyn transformation.- The Dorodnitsyn transformation (ref. 5) converts the viscous equations in the Stewartson variables to a set of non-viscous equations in variables defined as follows:

$$\xi = \int_0^X \frac{U_e}{U_{e_o}} \frac{dX}{\ell} \qquad \eta = \frac{U_e}{U_{e_o}\ell}\left(\frac{U_{e_o}\ell}{\nu_{e_o}}\right)^{1/2} Y \tag{46}$$

$$\bar{u} = \frac{U}{U_e} \tag{47}$$

$$\bar{v} = \frac{V}{U_e}\left(\frac{U_{e_o}\ell}{\nu_{e_o}}\right)^{1/2} \tag{48}$$

$$\bar{w} = \bar{v} + \bar{u}\eta \frac{\dot{U}_e}{U_e} \tag{49}$$

where

$$\dot{U}_e = \frac{dU_e}{d\xi}$$

The boundary conditions in the Dorodnitsyn plane are:

At $\eta = 0$:

$$\left.\begin{aligned} \bar{u} = \bar{v} = \bar{w} = 0 \\ S = S_w \end{aligned}\right\} \tag{50}$$

At $\eta = \infty$:

$$\left.\begin{aligned} \bar{u} = 1 \\ \partial\bar{u}/\partial\eta = 0 \\ S = 0 \end{aligned}\right\} \tag{51}$$

At $\xi = \xi_o$:

$$\left.\begin{aligned} \bar{u} = \bar{u}_o(\eta) \\ S = S_o(\eta) \end{aligned}\right\} \tag{52}$$

As in the Stewartson transformation, it is assumed that $S$, $H_e$, and $\beta$ transform as parameters, so that

$$S(\xi,\eta) = S(X,Y) = S(\tilde{x},\tilde{y}) \tag{53}$$

$$H_e(\xi) = H_e(X) = H_e(\tilde{x}) \tag{54}$$

$$\beta(\xi,\eta) = \beta(X,Y) = \beta(\tilde{x},\tilde{y}) \tag{55}$$

The reference conditions in relations (30) through (32) and (46) through (48) have been chosen in calculations made in the present work as the conditions at the edge of the boundary layer at the station $x_o$ where the solution is considered to begin. This is a somewhat arbitrary choice, but is found to be most convenient. The reference conditions could be those at any point related isentropically to the boundary-layer edge at $x_o$. The reference length $\ell$ is completely arbitrary. However, note that for an axisymmetric body, the reference length $\ell$ in the equivalent plane must be related to the length $L$ in the physical system by the transformation relation

$$\ell = \int_o^L \frac{r_w^2}{L^2}\, dx \tag{56}$$

From relations (46)

$$\frac{\partial}{\partial X} = \frac{\partial \xi}{\partial X}\,\frac{\partial}{\partial \xi} + \frac{\partial \eta}{\partial X}\,\frac{\partial}{\partial \eta} = \frac{U_e}{U_{e_o}\ell}\,\frac{\partial}{\partial \xi} + \frac{\eta}{U_e}\,\frac{\partial U_e}{\partial X}\,\frac{\partial}{\partial \eta} \tag{57}$$

$$\frac{\partial}{\partial Y} = \frac{\partial \xi}{\partial Y}\,\frac{\partial}{\partial \xi} + \frac{\partial}{\partial Y}\,\frac{\partial}{\partial \eta} = \frac{U_e}{U_{e_o}\ell}\left(\frac{U_{e_o}\ell}{\nu_{e_o}}\right)^{1/2}\frac{\partial}{\partial \eta} \tag{58}$$

The application of relations (46) through (49) and (57) and (58) to equations (42), (43), and (44) is straightforward. The resulting equations are:

CONTINUITY

$$\frac{\partial \bar{u}}{\partial \xi} + \frac{\partial \bar{w}}{\partial \eta} = 0 \tag{59}$$

MOMENTUM

$$\bar{u}\frac{\partial \bar{u}}{\partial \xi} + \bar{w}\frac{\partial \bar{u}}{\partial \eta} = \left[S + 1 - \bar{u}^2\right]\frac{\dot{U}_e}{U_e} + C\frac{\partial}{\partial \eta}\left[(1 + kt\tilde{y})\beta\frac{\partial \bar{u}}{\partial \eta}\right]$$

$$+ \frac{1}{2}\frac{\bar{K}}{H_e}\frac{dH_e}{d\tilde{x}}\left(\frac{\rho_e}{\rho} - \bar{u}^2\right) \tag{60}$$

ENERGY

$$\bar{u}\frac{\partial S}{\partial \xi} + \bar{w}\frac{\partial S}{\partial \eta} = C\frac{\partial}{\partial \eta}\left[(1 + kt\tilde{y})A\frac{\partial S}{\partial \eta}\right] + \frac{2Cm_e}{1 + m_e}\frac{\partial}{\partial \eta}\left[(1 + kt\tilde{y})B\bar{u}\frac{\partial \bar{u}}{\partial \eta}\right]$$

$$- \frac{\bar{K}}{H_e}\frac{dH_e}{d\tilde{x}}(S + 1)\bar{u} \tag{61}$$

where

$$m_e = \frac{\gamma - 1}{2}M_e^2 \tag{62}$$

and

$$\bar{K} = \frac{p_{e_o}a_{e_o}}{p_e a_e}\frac{M_{e_o}^{\ell}}{M_e} \tag{63}$$

and it has been assumed that

$$\frac{1}{T_{s_e}}\frac{dT_{s_e}}{d\tilde{x}} = \frac{1}{H_e}\frac{dH_e}{d\tilde{x}}$$

by virtue of the assumption of constant specific heat.

## Derivation of Ordinary Differential Equations

**Development of integro-differential equations.**- The partial differential equations (59), (60), and (61) are reduced to a set of ordinary differential equations by the introduction of certain approximating functions. First, it is convenient to define a function

$$\phi = \frac{1}{\partial\bar{u}/\partial\eta} \tag{64}$$

Then, if $\phi$, S, and $\bar{w}$ are considered to be represented by approximating functions in terms of the variable $\bar{u}$, equations (59), (60), and (61) can be expressed as

$$\phi \frac{\partial\bar{u}}{\partial\xi} + \frac{\partial\bar{w}}{\partial\bar{u}} = \sigma_1 \tag{65}$$

$$\phi\bar{u} \frac{\partial\bar{u}}{\partial\xi} + \bar{w} - (S + 1 - \bar{u}^2)\phi \frac{\dot{U}_e}{U_e} - C \frac{\partial}{\partial\bar{u}} \left[(1 + kt\tilde{y}) \frac{\beta}{\phi}\right]$$

$$- \frac{1}{2} \frac{\bar{K}}{H_e} \frac{dH_e}{dx} \phi \left(\frac{\rho_e}{\rho} - \bar{u}^2\right) = \sigma_2 \tag{66}$$

$$\phi\bar{u} \frac{\partial S}{\partial\xi} + \bar{w} \frac{\partial S}{\partial\bar{u}} - C \frac{\partial}{\partial\bar{u}} \left[(1 + kt\tilde{y}) \frac{A}{\phi} \frac{\partial S}{\partial\bar{u}}\right]$$

$$- \frac{2Cm_e}{1 + m_e} \frac{\partial}{\partial\bar{u}} \left[(1 + kt\tilde{y}) \frac{B\bar{u}}{\phi}\right] + \frac{\bar{K}}{H_e} \frac{dH_e}{dx} \phi(S + 1)\bar{u} = \sigma_3 \tag{67}$$

where $\sigma_1$, $\sigma_2$, and $\sigma_3$ differ from zero by virtue of the use of approximating functions to represent $\phi$, S, and $\bar{w}$. The exact form of the approximating functions will be examined later. If the errors $\sigma_1$, $\sigma_2$, and $\sigma_3$ are required to be orthogonal to three sets of linearly independent functions $f_i$, $g_i$, and $h_i$, respectively, then

$$\int_0^1 f_i\sigma_1 \, d\bar{u} = 0 \qquad i = 1,2,\ldots,n \tag{68}$$

$$\int_0^1 g_i \sigma_2 \, d\bar{u} = 0 \qquad i = 1,2,\ldots,n \tag{69}$$

$$\int_0^1 h_i \sigma_3 \, d\bar{u} = 0 \qquad i = 1,2,\ldots,n \tag{70}$$

Requiring that

$$\left.\begin{aligned} f_i &= f_i^* \\ g_i &= \frac{\partial \bar{f}_i}{\partial \bar{u}} = f_i^{*\prime} \end{aligned}\right\} \tag{71}$$

and

$$f_i^*(1) = 0$$

and adding equations (68) and (69) gives, after some preliminary manipulation,

$$\int_0^1 \phi \frac{\partial}{\partial \xi} (f_i^* \bar{u}) \, d\bar{u} + \int_0^1 \frac{\partial}{\partial \bar{u}} (f_i^* \bar{w}) \, d\bar{u} - \frac{\dot{U}_e}{U_e} \int_0^1 \phi f_i^{*\prime} (S + 1 - \bar{u}^2) \, d\bar{u}$$

$$- C \int_0^1 f_i^{*\prime} \frac{\partial}{\partial \bar{u}} \left[ (1 + kt\tilde{y}) \frac{\beta}{\phi} \right] d\bar{u}$$

$$- \frac{1}{2} \frac{\bar{K}}{H_e} \frac{dH_e}{d\tilde{x}} \int_0^1 \phi f_i^{*\prime} \left( \frac{\rho_e}{\rho} - \bar{u}^2 \right) d\bar{u} = 0 \tag{72}$$

Note that the semi-infinite interval in the independent variable $\eta$ has been transformed into the more convenient finite interval $[0,1]$ for the independent variable $\bar{u}$.

Following the same procedure as for equation (72) it is required that

$$\left.\begin{aligned} f_i &= Sf_i^* \\ g_i &= Sf_i^{*'} \\ h_i &= f_i^* \end{aligned}\right\} \tag{73}$$

Then adding equations (68), (69), and (70) gives

$$\int_0^1 \phi \frac{\partial}{\partial \xi}\left(f_i^* S \bar{u}\right) d\bar{u} + \int_0^1 \frac{\partial}{\partial \bar{u}}\left(S f_i^* \bar{w}\right) d\bar{u} - \frac{1}{U_e}\frac{dU_e}{d\xi}\int_0^1 \phi S f_i^{*'}\left(S + 1 - \bar{u}^2\right) d\bar{u}$$

$$- C\int_0^1 \left\{ Sf_i^{*'} \frac{\partial}{\partial \bar{u}}\left[(1 + kt\tilde{y})\frac{\beta}{\phi}\right] + f_i^* \frac{\partial}{\partial \bar{u}}\left[(1 + kt\tilde{y})\frac{A}{\phi}\frac{\partial S}{\partial \bar{u}}\right] \right.$$

$$\left. + \frac{2m_e}{1 + m_e} f_i^* \frac{\partial}{\partial \bar{u}}\left[(1 + kt\tilde{y})\frac{B}{\phi}\bar{u}\right] \right\} d\bar{u}$$

$$+ \frac{\bar{K}}{H_e}\frac{dH_e}{d\tilde{x}}\int_0^1 \left[ f_i^* \phi \bar{u}(S + 1) - \frac{1}{2} f_i^{*'} S\phi\left(\frac{\rho_e}{\rho} - \bar{u}^2\right)\right] d\bar{u} = 0 \tag{74}$$

The integrals in equations (72) and (74) can be evaluated in a straightforward manner if the condition $f_i^*(1) = 0$ is considered to be satisfied by requiring that

$$f_i^* \cong 1 - \bar{u}$$

and $f_i^{*'}$ is required to be bounded as $\bar{u}$ approaches 1 ($\eta$ approaches $\infty$). Equations (72) and (74) then reduce to two integro-differential equations in the dependent variables $\phi(\xi,\bar{u})$ and $S(\xi,\bar{u})$, namely

$$\frac{d}{d\xi}\int_0^1 \phi f_i^* \bar{u}\, d\bar{u} - \frac{\dot{U}_e}{U_e}\int_0^1 \phi(S + 1 - \bar{u}^2) f_i^{*\prime} d\bar{u} + C\,\frac{f_i^{*\prime}(0)B(\xi,0)}{\phi(\xi,0)}$$

$$+ C\int_0^1 (1 + kt\tilde{y})\,\frac{f_i^{*\prime\prime}\beta}{\phi}\, d\bar{u} - \frac{1}{2}\,\frac{\bar{K}}{H_e}\,\frac{dH_e}{d\tilde{x}}\int_0^1 \left(\frac{\rho_e}{\rho} - \bar{u}^2\right)\phi f_i^{*\prime} d\bar{u} = 0 \qquad (75)$$

and

$$\frac{d}{d\xi}\int_0^1 \phi S f_i^* \bar{u}\, d\bar{u} - \frac{\dot{U}_e}{U_e}\int_0^1 (S + 1 - \bar{u}^2)\phi S f_i^{*\prime} d\bar{u}$$

$$+ CS_w f_i^{*\prime}(0)\,\frac{B(\xi,0)}{\phi(\xi,0)} + C\,\frac{f_i^*(0)A(\xi,0)}{\phi(\xi,0)}\left.\frac{\partial S}{\partial \bar{u}}\right|_{\bar{u}=0}$$

$$+ C\int_0^1 (1 + kt\tilde{y})\left\{\left[S f_i^{*\prime\prime} + f_i^{*\prime}\,\frac{\partial S}{\partial \bar{u}}\right]\frac{\beta}{\phi}\right.$$

$$\left. + \left[f_i^* A\,\frac{\partial S}{\partial \bar{u}} + \frac{2m_e}{1 + m_e} f_i^{*\prime} B\bar{u}\right]\frac{1}{\phi}\right\} d\bar{u}$$

$$+ \frac{\bar{K}}{H_e}\,\frac{dH_e}{d\tilde{x}}\int_0^1 (S + 1)\phi f_i^* \bar{u} - \frac{1}{2}\left(\frac{\rho_e}{\rho} - \bar{u}^2\right) S f_i^{*\prime}\phi\, d\bar{u} = 0 \qquad (76)$$

Note that equations (75) and (76) were obtained by linear combinations of the equations (68), (69), and (70) using particular forms for the weighting functions $f_i$, $g_i$, and $h_i$. It is clear that the conditions (68), (69), and (70) are not necessary conditions for equations (75) and (76) to be valid. In particular, this procedure offers no information to aid in selecting either the weighting function $f_i^*$ or the forms of the approximating functions for $\phi$, S, and $\bar{w}$. These functions must be determined on the basis of the boundary conditions and other conditions the functions must satisfy.

Selection of approximating functions.- The choice of functions to represent the variables $\phi$ and $S$ is not arbitrary. The functions must satisfy the boundary conditions as well as certain compatibility relations for boundary-layer flows. Specifically, the boundary conditions are:

At $\bar{u} = 0$:

$$\phi = \text{finite}$$

$$S = S_w$$

$$f_i^* = \text{bounded}$$

At $\bar{u} = 1$:

$$\phi = \infty$$

$$S = 0$$

$$f_i^* = 0$$

The Weierstrauss approximation theorem applied to the differential equations (65), (66), and (67) alone, that is, without boundary conditions, suggests that the functions $\phi$, $S$, and $\bar{w}$ could be approximated uniformly by polynomials on the closed interval $[0,1]$. However, caution must be used when applying the Weierstrauss theorem to cases with boundary conditions. In the present case the condition on $\phi$ at $\bar{u} = 1$ cannot be satisfied by a polynomial alone. Furthermore, the condition that $S$ be exactly equal to zero at $\bar{u} = 1$ is a stronger condition than continuity as required by the Weierstrauss theorem, so that uniform convergence cannot necessarily be guaranteed if the function $S$ is represented by polynomials. This is especially important in the transitional and turbulent regions as will be demonstrated subsequently.

Velocity-gradient function, $\phi$: To avoid the difficulty of the infinite condition on the function $\phi$ at $\bar{u} = 1$, Dorodnitsyn (ref. 5) introduced a profile of the form

$$\phi = \frac{1}{1 - \bar{u}} \sum_{i=1}^{n} C_i(\xi)\bar{u}^{i-1} \tag{77}$$

In references 2, 3, and 4, it was shown that a three-parameter ($n = 3$) function could adequately represent both laminar and turbulent profiles except in the vicinity of a separation point. At separation, the polynomial

formulation of equation (77) is inadequate for any order. The three-parameter formulation was used in the present study and was found to represent adequately transitional profiles as well as laminar and turbulent profiles.

Enthalpy function, S: In previous applications of the method of integral relations to boundary layers (refs. 2, 3, 4), the assumption was made that the Prandtl number is unity. Under that assumption, the energy equation takes the same form as the momentum equation and the total temperature distribution in the boundary layer is a linear function of the normalized velocity, $\bar{u}$, so that the dependent variable S can be represented by

$$S = S_w(1 - \bar{u}) \tag{78}$$

However, as shown by Schlichting (ref. 10), for non-unity Prandtl number, the velocity and thermal boundary layers are not congruent. For a laminar boundary layer on a flat plate, with constant pressure along the plate, Schlichting shows that the temperature in the boundary layer is

$$T = T_e\left[1 + r_L m_e\right](1 - \bar{u}^2) + (T_w - T_{aw})(1 - \bar{u}) \tag{79}$$

This means that the enthalpy profile parameter, S, is

$$S = (1 - \bar{u})\left[S_w + \frac{r_L - 1}{1 + m_e} m_e \bar{u}\right] \tag{80}$$

In a turbulent boundary layer, Pinckney (ref. 11) has shown that the temperature profile is a fourth-order polynomial. Converting Pinckney's static temperature function to the present notation yields

$$S = (1 - \bar{u})\left\{S_w + \left[S_{aw}(Pr)^{1/3} + S_w(1 - Pr^{1/3})\right]\bar{u} + \frac{1}{2}\frac{m_e}{1 + m_e}\frac{K}{u_e}(\bar{u}^2 + \bar{u}^3)\right\} \tag{81}$$

where K is determined by requiring the total energy deficiency of a boundary layer, obtained by integration across the boundary layer, to be equal to the energy removed from the boundary layer upstream of the local station by radiation, surface heat transfer, or any other means. In the present work, the enthalpy function was represented by

$$S = (1 - \bar{u}) \left[ S_w + \sum_{i=1}^{m} E_i \bar{u}^i \right] \tag{82}$$

This allows continuous calculation of the enthalpy profiles in laminar, transitional, and turbulent flows. For laminar flow on a cooled flat plate, the formulation was found to converge uniformly so that an adequate approximation was obtained with a profile of any order greater than $m = 2$. For turbulent flow, the combination of an approximate eddy-viscosity function and the condition at $\bar{u} = 1$ was found to cause polynomials of order greater than $m = 2$ to develop waves which rendered the polynomials inadequate to represent the variable $S$. The details of a study of the best order for the polynomial in equation (82) will be presented in a subsequent section.

In summary, the functions chosen to represent the variables $\phi$ and $S$ were

$$\phi = \frac{1}{1 - \bar{u}} \sum_{i=1}^{n} C_i(\xi) \bar{u}^{i-1}$$

and

$$S = (1 - \bar{u}) \left( S_w + \sum_{j=1}^{m} E_j \bar{u}^j \right)$$

where the values $n = 3$ and $m = 2$ were used for most of the work reported herein.

Selection of weighting functions: In order to assure that the equations to be derived from equations (75) and (76) are linearly independent, the weighting functions $f_i$, $g_i$, and $h_i$ must be families of linearly independent functions. Furthermore, the functions must be bounded as $\bar{u}$ approaches 1. The functions $f_i^*$ chosen for this analysis were the same as those used in reference 2, namely

$$f_i^* = (1 - \bar{u}) \bar{u}^{i-1} \tag{83}$$

Development of ordinary differential equations.- Substitution of equations (77), (82), and (83) into equations (75) and (76) results in a set of six ordinary nonlinear differential equations in the six unknowns $C_i(\xi)$ and $E_i(\xi)$. Since the $C_i$ and $E_i$ are functions only of the independent variable, $\xi$, the resulting equations may be expressed in terms of the independent variables, x and $\bar{u}$. Thus, with expressions (13), (36), and (57),

$$\frac{dC_i}{dx} = \left(\frac{r_w}{L}\right)^{2k} \frac{1}{\bar{K}} \dot{C}_i \tag{84}$$

and

$$\frac{dE_i}{dx} = \left(\frac{r_w}{L}\right)^{2k} \frac{1}{\bar{K}} \dot{E}_i \tag{85}$$

The differential equations to be solved are then

$$\left[a_{ij}\right] \frac{dC_i}{dx} = B_i \tag{86}$$

and

$$\left[a'_{ij}\right] \frac{dE_i}{dx} = B'_i \tag{87}$$

where

$$a_{ij} = \frac{1}{i + j} \qquad \begin{matrix} i = 1,2,3,\ldots,n \\ j = 1,2,3,\ldots,n \end{matrix} \tag{88}$$

$$a'_{ij} = \sum_{k=1}^{m} \frac{C_k}{(i + j + k)(i + j + k + 1)} \qquad \begin{matrix} i = 1,2,\ldots,m \\ j = 1,2,\ldots,m \end{matrix} \tag{89}$$

$$B_i = \left(\frac{r_w}{L}\right)^{2k} \frac{1}{\bar{K}} \left\{ C(i-1)\left[iP_{i-1} - (i-2)P_{i-2}\right] - \frac{C\beta(\xi,0) f_i^{*'}(0)}{C_1} \right\}$$

$$+ \left[\frac{1}{U_e}\frac{dU_e}{dx} + \frac{1}{2}\frac{1+m_e}{H_e}\frac{dH_e}{dx}\right]\left[(1+S_w)\Sigma_{11} + \Sigma_{12}\right] \tag{90}$$

and

$$B_i' = \left(\frac{r_w}{L}\right)^{2k} \frac{1}{\bar{K}} \left\{ -CS_w \frac{f_i^{*'}(0)\beta(\xi,0)}{C_1} - C\frac{f_i^{*}(0)}{Pr}\frac{E_1 - S_w}{C_1} \right.$$

$$\left. - C\left[(i-1)Q_{i-1} - iQ_i\right] - C(i-1)\left[(i-2)R_{i-2} - iR_{i-1}\right] \right\}$$

$$+ \frac{1}{H_e}\frac{dH_e}{dx}\left[S_w\Sigma_{i+1,4} - (1+S_w)\Sigma_{i4} - \Sigma_{i5}\right]$$

$$+ \left[\frac{1}{U_e}\frac{dU_e}{dx} + \frac{1}{2}(1+m_e)\frac{1}{H_e}\frac{dH_e}{dx}\right]\left[(i-1)\Sigma_{i-1,6} - i\Sigma_{i6}\right]$$

$$- \frac{dS_w}{dx}\Sigma_{i3} - \sum_{j=1}^{n}\left\{\frac{S_w}{(i+j)(i+j+1)}\right.$$

$$\left. + \sum_{k=1}^{m}\left[\frac{E_k}{(i+j+k)(i+j+k+1)}\right]\right\}\frac{dC_i}{dx} \tag{91}$$

in which

$$\frac{dS_w}{dx} = \frac{1}{H_e}\left[\frac{dH_w}{dx} - \frac{H_w}{H_e}\frac{dH_e}{dx}\right] \tag{92}$$

$$\frac{1}{U_e}\frac{dU_e}{dx} = -\frac{1}{\gamma}\frac{p_{e_o}}{p_e}\frac{1+m_e}{M_e^2}\left[\frac{d}{dx}\left(\frac{p_e}{p_{e_o}}\right) + \frac{p_e}{p_{e_o}}\frac{\gamma M_e^2}{H_e}\frac{dH_e}{dx}\right] \tag{93}$$

$$P_i = \int_0^1 (1 + kt\tilde{y}) \frac{\beta}{\phi} \bar{u}^{i-1} \, d\bar{u} = \int_0^1 F_i \, d\bar{u} \tag{94}$$

$$Q_i = \int_0^1 \left[ \frac{\partial S}{\partial \bar{u}} \left( 1 + \frac{A}{B} \right) + \frac{2m_e}{1 + m_e} \frac{B}{\beta} \bar{u} \right] F_i \, d\bar{u} \tag{95}$$

$$R_i = \int_0^1 SF_i \, d\bar{u} \tag{96}$$

$$\tilde{y} = \left( \frac{T_e}{T_{e_o}} \right) \frac{\bar{K}}{\sqrt{R_o}} \int_0^\eta \frac{\rho_e}{\rho} \, d\eta$$

$$= \left( \frac{T_e}{T_{e_o}} \right) \frac{\bar{K}}{\sqrt{R_o}} \left\{ \sum_{i=1}^{n} \left( \left[ (1 + m_e) S_w + m_e \right] \frac{\bar{u}^i}{i} + m_e \frac{\bar{u}^{i+1}}{i + 1} \right.\right.$$

$$\left.\left. + (1 + m_e) \sum_{j=1}^{m} \left[ \frac{\bar{u}^{i+j}}{i + 1} E_j \right] - \ln (1 - \bar{u}) - \sum_{j=1}^{i-1} \left[ \frac{\bar{u}^j}{j} \right] \right) C_i \right\} \tag{97}$$

where $R_o = u_{e_o} \ell / \nu_{e_o}$.

$$\Sigma_{i1} = \sum_{j=1}^{n} \frac{(1 - j) C_j}{(i + j - 2)(i + j - 1)} \tag{98}$$

$$\Sigma_{i2} = \sum_{j=1}^{n} \left\{ \frac{-n}{(i + n - 1)(i + n)} + \sum_{k=1}^{m} \frac{(1 - j - k) E_k}{(i + j + k - 2)(i + j + k - 1)} \right\} C_j \tag{99}$$

Nusselt Number

In this work, the Nusselt number is computed from the Stanton number as

$$Nu = (Pr)(Re_x)St$$

Displacement Thickness

$$\delta^* = \int_0^\infty \left(1 - \frac{\rho u}{\rho_e u_e}\right) dy$$

$$= \left(\frac{L}{r_w}\right)^k \frac{\bar{K}}{\sqrt{R_o}} \left\{ \sum_{i=1}^{n} \left[ (1 + m_e)(1 + S_w) \frac{1}{i} + \frac{m_e}{i+1} \right.\right.$$

$$\left.\left. + (1 + m_e) \sum_{j=1}^{m} \frac{E_j}{i+j} \right] C_i \right\} \qquad (106)$$

Momentum Thickness

$$\theta = \int_0^\infty \frac{\rho u}{\rho_e u_e} \left(1 - \frac{u}{u_e}\right) dy$$

$$= \left(\frac{L}{r_w}\right)^k \frac{\bar{K}}{\sqrt{R_o}} \sum_{i=1}^{n} \frac{C_i}{i+1} \qquad (107)$$

Enthalpy Thickness

$$\theta_h = \int_0^\infty \frac{\rho}{\rho_e} \frac{u}{u_e} \left(\frac{h}{h_e} - 1\right) dy$$

$$= \left(\frac{L}{r_w}\right)^k \frac{\bar{K}}{\sqrt{R_o}} \left\{ \sum_{i=1}^{n} \left[ S_w(1 + m_e) \frac{1}{i+1} + \frac{m_e}{i+1} + \frac{m_e}{i+2} \right.\right.$$

(eq. (108) continued on next page)

$$+ (1 + m_e) \sum_{j=1}^{m} \frac{E_j}{i + j + 1} \Bigg] C_i \Bigg\} \tag{108}$$

Velocity Profile

In the two-dimensional system or the Probstein-Elliott system, the $\tilde{y}$ coordinate is given by equation (97), and for axisymmetric flow, the physical coordinate is

$$y = \left[ \left( \frac{r_w}{\cos \alpha} \right)^2 + \frac{2L\tilde{y}}{\cos \alpha} \right]^{1/2} - \frac{r_w}{\cos \alpha} \tag{109}$$

Velocity Gradient

$$\frac{\partial \bar{u}}{\partial (y/L)} = \left( \frac{r}{L} \right)^k \frac{M_e}{M_{e_o}} \left( \frac{T_{e_o}}{T_e} \right)^{1/2} \left( \frac{T_e}{T} \right) \frac{L}{\ell} \sqrt{R_o} \; \frac{(1 - \bar{u})}{\sum_{i=1}^{n} C_i \bar{u}^{i-1}} \tag{110}$$

If $k = 0$, then $L = \ell$.

Mach Number Profile

$$\frac{M}{M_e} = \frac{\bar{u}}{\left\{ (1 + m_e) \left[ 1 + (1 - \bar{u}) \left( S_w + \sum_{j=1}^{m} E_j \bar{u}^j \right) \right] - m_e \bar{u}^2 \right\}^{1/2}} \tag{111}$$

Temperature and Density Profiles

$$\frac{T}{T_e} = \frac{\rho_e}{\rho} = (1 + m_e) \left[ 1 + (1 - \bar{u}) \left( S_w + \sum_{j=1}^{m} E_j \bar{u}^j \right) \right] - m_e \bar{u}^2 \tag{112}$$

## Initial Conditions

In order to solve the differential equations (86) and (87), initial values of $C_i$ and $E_i$ must be specified. The required values can be determined in several ways. The ways that have been found to be most useful are discussed in this section.

Similarity solution.- For laminar flow on a flat plate at uniform temperature with constant pressure, similarity is known to exist. Solution of equation (86) under those conditions yields

$$C_i = K_i \left(\frac{x}{\ell}\right)^{1/2} \tag{113}$$

where $K_i$ is a constant. So the initial values of $C_i$ are simply

$$C_{i_o} = K_i \left(\frac{x_o}{\ell}\right)^{1/2} \tag{114}$$

For the laminar similarity case, the equation (86) does not depend upon the $E_i$. Therefore, it is easy to show from equation (87) that for the laminar similarity case

$$\frac{dE_i}{dx} = 0 \tag{115}$$

and equation (87) can be expressed as

$$\left\{A_{ij}\right\} E_i = B_i \tag{116}$$

where

$$\begin{aligned} A_{ij} = \sum_{k=1}^{n} \frac{C_k}{(i + j + k)(i + j + k + 1)} + \frac{Cf_i^*(0)}{C_1 Pr}\,\delta_{j1} \\ + \left(1 + \frac{1}{Pr}\right) C \Big\{ (i - 1)\left[j(P'_{i+j-2} - P'_{i+j-1}) - P'_{i+j-1}\right] \\ - i\left[j(P'_{i+j-1} - P'_{i+j}) - P'_{i+j}\right] \Big\} \\ + C(i - 1)\left[(i - 2)(P'_{i+j-2} - P'_{i+j-1}) - i(P'_{i+j-1} - P'_{i+j})\right] \end{aligned} \tag{117}$$

and

$$B_i = S_w \left\{ \frac{Cf_i^*(0)}{C_1 Pr} - \sum_{k=1}^{n} \frac{\dot{C}_k}{(i+k)(i+k+1)} - \frac{Cf_i^{*'}(0)}{C_1} \right.$$

$$+ C\left(1 + \frac{1}{Pr}\right)\left[(i-1)P'_{i-1} - iP'_i\right] + C(i-1)\left[i(P'_{i-1} - P'_i)\right.$$

$$\left. \left. - (i-2)(P'_{i-2} - P'_{i-1})\right]\right\} - \frac{2m_e}{1+m_e} C\left(1 - \frac{1}{Pr}\right)\left[(i-1)P'_i - iP'_{i+1}\right] \tag{118}$$

where

$$\delta_{j1} = \begin{cases} 1 & \text{for } j = 1 \\ 0 & \text{for } j > 1 \end{cases}$$

and

$$P'_i = \int_0^1 \frac{\bar{u}^{i-1}}{\phi} \, d\bar{u} \tag{119}$$

Solution of the equations (116) for the values of $E_i$ is accomplished by substituting the values

$$C_i = K_i$$

and

$$\dot{C}_i = \frac{1}{2} K_i$$

into equations (117), (118), and (119).

The values $K_i$ have been determined by computing the solution to the equations (86) from arbitrary initial conditions. The similar solution is obtained asymptotically. The results for $n = 3$ are

$$K_1 = 3.006443(C)^{1/2}$$

$$K_2 = -3.041346(C)^{1/2}$$

$$K_3 = 0.7048994(C)^{1/2}$$

The same procedure as used to obtain $K_i$ in the laminar case can also be used to compute initial values of $C_i$ and $E_i$ for a fully turbulent boundary layer on a flat plate or for higher orders of approximation ($n > 3$). This procedure was discussed in reference 2.

Direct fit of known velocity and temperature profiles.- If the velocity profile, y versus $\bar{u}$, and the total temperature profiles can be known at the initial station, the required values of $E_i$ are easily obtained from equation (82) by substituting the values of S and $\bar{u}$ at m points in the boundary layer at that station. Then, the required values of $C_i$ are obtained by substituting the n values of y corresponding to the n values of $\bar{u}$ into equation (97) and solving the resulting set of n algebraic equations simultaneously. Note, however, that for an axisymmetric configuration, the coordinate y must be transformed to the Probstein-Elliott value, $\tilde{y}$, before equation (97) is used. It must be noted that this technique depends on the choice of the points at which values of $\bar{u}$ and T are obtained in the boundary layer. Thus, if all points are near the edge of the boundary layer, a different fit may be obtained than for points near the wall.

Known boundary-layer parameters.- A third method of obtaining initial values of $C_i$ and $E_i$ for a three-parameter ($n = 3$) velocity gradient profile depends upon knowledge of the parameters $C_f$, St, $\delta^*$, and $\theta$ plus knowledge of the total temperature at $(m - 1)$ values of $\bar{u}$. The skin-friction coefficient, $C_f$, is used to obtain $C_1$ from equation (104). Then the parameter $E_1$ is obtained from equation (105) with the known value of the Stanton number. The $(m - 1)$ values of $T_t$ are then used in equation (82) to obtain the remaining $E_i$. Finally, the equations (106) and (107) are used to obtain the remaining two parameters, $C_2$ and $C_3$.

This method can be used for any order of approximation on the enthalpy profile, but is limited to a three-parameter velocity-gradient profile.

Least squares fit of velocity and temperature profiles.- A fourth method of obtaining initial conditions consists of solving the the required

parameters from known distributions of $y$ versus $\bar{u}$ and $S$ versus $\bar{u}$ by the method of least squares. This method was used in the work of reference 2. The method was not used in the present work, but is outlined here to generalize the presentation.

Least squares fitting of the enthalpy function is straightforward. The residual equations are written in the form

$$R_i = S_i - (1 - \bar{u}_i)S_w - (1 - \bar{u}_i)E_1\bar{u}_i$$

$$- (1 - \bar{u}_i)E_2\bar{u}_i^2 - \ldots - (1 - \bar{u}_i)E_m\bar{u}_i^m$$

and the coefficients $E_i$ are obtained by solving the set of equations given by

$$\sum_{i=1}^{m'} R_i \frac{\partial R_i}{\partial E_j} = 0; \quad j = 1,2,\ldots,m$$

where $m'$ is the number of data points.

Fitting of the velocity profiles is a more complicated process. First the data must be expressed in terms of a distribution of $\partial\bar{u}/\partial\eta$ versus $\bar{u}$. That is,

$$\left(\frac{\partial\bar{u}}{\partial\eta}\right)_i = \frac{1 - \bar{u}_i}{\sum_{j=1}^{n} c_j\bar{u}^{j-1}}$$

The residual equations are then written as

$$R_i = \frac{\left(\frac{\partial\bar{u}}{\partial\eta}\right)_i \sum_{j=1}^{n} c_j\bar{u}^{j-1}}{\sum_{j=1}^{n} c'_j\bar{u}^{j-1}} - \frac{1 - \bar{u}_i}{\sum_{j=1}^{n} c'_j\bar{u}_i^{j-1}}$$

An iteration procedure is then used to compute the required values of $C_j$. First it is assumed that

$$\sum_{j=1}^{n} C_j \bar{u}_i^{j-1} = 1$$

for all $\bar{u}_i$ and the $C_j$ are computed by least squares. Then these $C_j$ are used to compute the denominators of the residual equations and new values of $C_j$ are obtained. This is repeated until successive iterations yield the same solution within a desired degree of accuracy.

## CALCULATION OF TRANSITIONAL BOUNDARY LAYERS

As discussed previously, the only thing that distinguishes between laminar, transitional, and turbulent flow in the present formulation is the parameter $\beta$ in the dissipation integrals $P_i$, $Q_i$, and $R_i$ (eqs. (94), (95), and (96)). Thus, the requirements of calculating transitional flow are (1) knowledge of the point where transition begins, (2) a function representing the turbulent eddy-viscosity $\beta$, (3) a modulation function to cause the parameter $\beta$ to go smoothly from its laminar value of unity to its fully turbulent distribution, and (4) knowledge of where transition ends.

In this section, the methods chosen for treating the requirements for calculating transitional boundary layers will be discussed. For greater detail regarding the theoretical aspects of boundary-layer stability and transition, the reader is referred to the many excellent references on the subject. In particular, the report by M. V. Morkovin (ref. 12) is an excellent review of all aspects of the transition problem and contains an extensive list of references for the reader desiring detailed knowledge of specific topics. The report by L. Mack (ref. 13) is, to the author's knowledge, the most current and comprehensive study of laminar boundary-layer stability theory.

## Prediction of the Transition Point

At the present time, the transition point cannot be predicted with confidence by purely theoretical methods. While sophisticated methods of solving the equations describing the stability of the laminar boundary layer have been developed in recent years (refs. 13, 14, 15) these methods are unable to predict the point where the growing linearized disturbances characteristic of boundary-layer stability theory become large enough to trigger the breakdown which creates the transition region. A promising method of approach was taken by Donaldson (ref. 16) who devised a model of the transitional boundary-layer two-dimensional in the mean flow but three-dimensional in the disturbance flow. The model was apparently capable of predicting an onset of transition boundary for the case of fairly large disturbances introduced into a flat plate boundary layer. However, although the method appears to be an effective way of studying the transition process, it has not been developed into a general engineering tool. Purely empirical methods are also limited in application due to the myriad of factors affecting the transition. Some of these factors are Reynolds number, Mach number, unit Reynolds number, pressure gradients, nose bluntness, surface roughness, free-stream turbulence level, angle of attack, and radiated aerodynamic noise. In a recent paper, Morkovin (ref. 12) indicates that even though a large amount of experimental transition data exists much of the information has not been recorded in sufficient detail to allow the separation of the effects of all the different parameters. For this reason, the approach usually taken for engineering applications is to try to correlate data with certain parameters or groups of parameters. Even though limited in scope depending upon the parameters chosen for the correlation, this method at least can provide a first approximation over a reasonably wide range of parameters.

Definition of the transition point is difficult since experimentally transition takes place over a finite region and different kinds of data produce different indications of the point of transition. Optical techniques such as schlieren photographs indicate a point of transition which is somewhere near the middle of the transition region (ref. 17). Wall temperature or recovery factor determinations indicate a peak value which is also considered by Brinich (ref. 18) to correspond approximately to the mean point of the transition zone. The only quantities which yield well-defined points near the beginning of the transition zone are the

Stanton number, the skin-friction coefficient, and the pressure indicated by a pitot probe placed near the surface (surface pitot pressure). Those quantities exhibit maxima and minima. The minimum of any of those quantities occurs near the point of onset of transition. It is not clear, however, that the minimum values of each of the three quantities would necessarily occur at the same point.

It was found that the calculated boundary-layer quantities, skin-friction coefficient, $C_f$, and Stanton number, St, tended to develop the same form of variation in the transition region as the imposed intermittency distribution. A well-defined minimum is obtained for both quantities. On the other hand, the minimum of the surface pitot pressure distribution is less well defined. The surface pitot pressure is a quantity which depends on the velocity profile in the boundary layer. Because of this, the surface pitot pressure distribution depends to some extent on the size of the probe relative to the boundary layer, and on the position of the probe within the boundary layer. In addition, the possible effect of the probe on starting the transition cannot be dismissed. For these reasons, correlations based on measurements of surface quantities such as $C_f$ or St are believed to be the most reliable for predicting the onset of transition.

In the present work, two methods are used for estimating the location of the transition point. These methods are (1) correlations based on collection of experimental data over a broad range of experimental conditions and (2) use of the experimental location of transition. When the transition point is determined by one of these methods, it is used as a direct input into the analytical solution. The remainder of this section will be devoted to discussion of correlations for the transition Reynolds number.

In recent years, several correlations have been developed for predicting transition Reynolds numbers. Some of these are described in references 19 through 23. Pate and Schueler (ref. 19) and Pate (ref. 20) showed that data on flat plates and cones in wind tunnels could be correlated using parameters characteristic of the boundary layer on the wind-tunnel walls. However, that kind of correlation is restricted to use in wind tunnels and hence cannot be extended to predicting transition on models in a ballistic range or in free flight. Deem et al. (ref. 21)

developed a correlation for sharp and cylindrically blunted flat plates at zero angle of attack based on Mach number, unit Reynolds number, leading-edge bluntness, leading-edge sweep angle, and wall-to-adiabatic-wall temperature ratio. Their correlation, applicable only to wind tunnels, predicted the Reynolds number of the end of transition within a factor of less than 2 for most of the data used. This correlation was developed into a set of charts by Hopkins, Jillie, and Sorensen (ref. 22), who pointed out that the correlation can provide only a first approximation of the transition Reynolds number expected for flight vehicles. Correlation parameters developed at NASA Langley Research Center by Bertram and Beckwith (ref. 23) were able to predict the onset of transition Reynolds number for sharp-nosed cones within a factor of 2 when wind-tunnel, ballistics range, and flight data were considered separately. Researchers at Langley Research Center have recently developed an improved correlation for the onset of transition on sharp cones in wind tunnels and ballistics ranges. The specific relations for these correlations will be presented subsequently.

The correlation relations to be presented in this report will be directly applicable to sharp-nosed cones or sharp-leading-edged flat plates or hollow cylinders. The relations may be used as first approximations for determining the transition point on other configurations with sharp noses or leading edges. The effects of nose or leading-edge bluntness and pressure gradients have been studied by a number of investigators (refs. 24, 25, 26). However, a completely general correlation accounting for all the various parameters affecting the transition point does not exist at this time.

The correlations recommended for use with the present theory are as follows:

Sharp Flat Plates

$$Re_{x_t} = \frac{1}{2} R_{e_1}^{0.6} \frac{10^{2[0.95 + 0.187 s']}}{\left(0.094 M_e^2 + 1.22 \frac{h_w}{h_e}\right)^2} \qquad (120)$$

where

$$s' = M_e \left(\frac{h_w}{h_e}\right)^{0.7 \exp(-0.05 M_e^2)}$$

This relation was obtained by dividing the expression given in reference 23 for sharp cones in wind tunnels by 3. A sample of the success of the relation is shown in figure 2 where the predicted value of $Re_{x_t}$ is compared with experimental values from different sources (refs. 18 and 27 through 32 and unpublished data from LRC). The prediction is within a factor of 2 for most of the data.

Sharp Cones

Wind Tunnels and Ballistics Ranges*

$$Re_{x_t} = Re_1^{n'} \, 10^{[F + Gs' + I(s')^2]} \tag{121}$$

where n', F, G, and I depend on the experimental environment as follows:

| Facility | n' | F | G | I |
|---|---|---|---|---|
| Wind Tunnel | 0.4 | 4.5158 | -0.29861 | 0.027300 |
| Ballistics Range | 0.6 | 2.5955 | -0.13680 | 0.014578 |

Free Flight (ref. 23)

$$Re_{x_t} = \frac{3}{2} Re_1^{0.6} \frac{10^{2[1.32 + 0.130 s']}}{\left(0.094 M_e^2 + 1.22 \frac{h_w}{h_e}\right)^2} \tag{122}$$

For estimating the transition Reynolds number on blunt leading-edge flat plates or hollow cylinders or other two-dimensional or open-nosed axisymmetric configurations, the reader is referred to the charts of Hopkins, Jillie, and Sorensen (ref. 22). It must be remembered, however, that those charts refer to the end of the transition region. A correlation for estimating the length of the transition region will be discussed

*The author gratefully acknowledges the cooperation of Mr. P. Calvin Stainback of LRC in providing this correlation relation.

in a subsequent section of this report. For blunted cones or other closed-nose axisymmetric configurations, the work of Stetson and Rushton (ref. 25) and Moeckel (ref. 26) and Zakkay and Krause (ref. 33) may be helpful. Some effects of nose bluntness on cones were studied experimentally by Stainback (ref. 34) and by Softley, Graber and Zempel (ref. 35). However, the generality of the results is uncertain since each investigator examined flow over a limited range of Mach numbers and Reynolds numbers.

## Turbulent Eddy-Viscosity Model

Several authors have developed eddy-viscosity models for use in solving the turbulent boundary-layer equations. Some of these models are described in references 1,.2, 36, 37, and 38. Several models are compared in references 36 and 39. The criteria used for choosing a particular model for the present work were that the model yield results which agreed reasonably well with those of other models and that the model formulation be as simple as possible. The latter criterion dictated that the best model for the present theory would be one which could be described in terms of the independent variable $\overline{u}$ rather than the boundary-layer coordinate y. This makes calculation of the actual velocity profiles at each integration step unnecessary except at stations where they are desired for output, or in cases where transverse curvature is being accounted for, thus maximizing the speed of the computer program.

The eddy-viscosity model employed in the present work is a two-layer model based on the work of Kleinstein (ref. 38) and of Clauser (ref. 40). Kleinstein derived an expression for the eddy-viscosity of the inner layer of an incompressible boundary layer (the laminar sublayer and the law of the wall region). Clauser proposed that the eddy viscosity in the outer layer was constant at the value

$$\beta = 0.0168\ Re_{\delta^*} \tag{123}$$

for an incompressible boundary layer.

Inner Layer Eddy-Viscosity Model

Extension of Kleinstein's model for the inner layer to compressible flow is straightforward. With the definitions

$$y^+ = \frac{\rho_w u^*}{\mu_w} y \tag{124}$$

$$u^+ = u/u^* \tag{125}$$

$$u^* = (\tau_w/\rho_w)^{1/2} \tag{126}$$

$$\epsilon^+ = \rho\epsilon/\mu \tag{127}$$

$$u_\tau = (\tau/\rho)^{1/2} \tag{128}$$

$$u_\tau^+ = \frac{u_\tau}{u^*} \tag{129}$$

the turbulent shear stress

$$\tau = (\mu + \rho\epsilon) \frac{\partial u}{\partial y} \tag{130}$$

where it has been assumed that

$$-\overline{\rho u'v'} = \rho\epsilon \frac{\partial u}{\partial y}$$

becomes

$$\tau = \rho \frac{\nu}{\nu_w} (1 + \epsilon^+) \frac{\partial u^+}{\partial y^+} u^{*2} \tag{131}$$

from which

$$\frac{\tau}{\tau_w} = \frac{\rho}{\rho_w} \frac{\nu}{\nu_w} (1 + \epsilon^+) \frac{\partial u^+}{\partial y^+} \tag{132}$$

and

$$\beta = 1 + \epsilon^+ = \frac{\nu_w}{\nu} (u_\tau^+)^2 \frac{\partial y^+}{\partial u^+} \tag{133}$$

For incompressible flow, Kleinstein found that Prandtl's mixing length theory gave

$$\epsilon^+ = k_1^2 (y^+)^2 \frac{du^+}{dy^+} \tag{134}$$

For compressible flow, the assumption is made that the fluid properties do not change significantly in a distance dy. The major contributions to the turbulent shear then come from the velocity correlation $\overline{u'v'}$ so that with the mixing length hypothesis $\epsilon = k_1^2 y^2 (du/dy)$ and the definitions (124) through (127), the expression (134) becomes

$$\epsilon^+ = k_1^2 (y^+)^2 \frac{\nu_w}{\nu} \frac{du^+}{dy^+} \tag{135}$$

For large distances from the wall such that $\epsilon^+$ is large compared to unity, equation (133) can be expressed

$$\frac{du^+}{dy^+} = \frac{\nu_w}{\nu} (u_\tau^+)^2 \frac{1}{\epsilon^+} \tag{136}$$

so that with equations (135) and (136)

$$\epsilon^+ = k_1 y^+ u_\tau \frac{\nu_w}{\nu} \tag{137}$$

Retaining Kleinstein's definition, a new variable is introduced, namely

$$U^+ = \int_0^{u^+} \frac{du'}{u_\tau^+} \tag{138}$$

where $u_\tau^+$ can be variable due to variations of both the turbulent shear and the density. Following Kleinstein, it is easily shown that the turbulent eddy-viscosity can be represented by the expression

$$B = 1 + \frac{\nu_w}{\nu} \frac{k_1}{k_2} u_\tau^+ \left\{ e^{k_1 U^+} - \left[ 1 + k_1 U^+ + \frac{1}{2} (k_1 U^+)^2 \right] \right\} \qquad (139)$$

where the values 0.41 and 7.7 are used for $k_1$ and $k_2$, respectively. With the conditions

$y = 0$: $\tau = \tau_w$

$$\frac{\partial \tau}{\partial y} = \frac{\partial p}{\partial x}$$

$y = \delta$: $\tau = 0$

$$\frac{\partial \tau}{\partial y} = 0$$

it can be shown that the variation of the shear stress in a boundary layer can be represented by

$$\tau = \tau_w \left[ 1 - 3 \left( \frac{y}{\delta} \right)^2 + 2 \left( \frac{y}{\delta} \right)^3 \right] + \delta \frac{dp}{dx} \left[ \frac{y}{\delta} - 2 \left( \frac{y}{\delta} \right)^2 + \left( \frac{y}{\delta} \right)^3 \right] \qquad (140)$$

For an equilibrium turbulent boundary layer in which $dp/dx = 0$ and

$$\frac{y}{\delta} \cong \bar{u}^7$$

it is easy to see that the shear stress can be assumed to be constant for the inner layer calculations, since values of $y/\delta$ at which significant deviations of $\tau$ from $\tau_w$ occur require values of $\bar{u}$ near unity, corresponding to the outer layer of the boundary layer. Of course, flows with significant adverse pressure gradients may require the full polynomial expression. In the present work it was always assumed that $\tau = \tau_w$ throughout the inner layer. This assumption is the "Prandtl hypothesis" which results in the classical law of the wall.

The Kleinstein model of the inner layer eddy viscosity is conveniently expressed in terms of $\bar{u}$ as follows. Since

$$\frac{\tau_w}{\rho_w} = \frac{1}{2} \frac{\rho_e}{\rho_w} u_e^2 C_f \qquad (141)$$

it follows that

$$u^+ = u(\rho_w/\tau_w)^{1/2} = \bar{u}\left[(2/C_f)(\rho_w/\rho_e)\right]^{1/2} \tag{142}$$

So

$$U^+ = \int_0^{\bar{u}} \left[\frac{2}{C_f} \frac{\tau_w}{\tau} \frac{\rho}{\rho_e}\right]^{1/2} d\bar{u} \tag{143}$$

In the computer program written for the present analysis, the expression (143) is evaluated using simple trapezoidal integration for 11 values of $\bar{u}$.

Outer Layer Eddy Viscosity

Herring and Mellor (ref. 36) extended Clauser's model to compressible flow by defining the eddy viscosity in the outer layer as

$$\beta = 0.0168 \frac{u_e}{\nu} \delta_K^* \tag{144}$$

where $\delta_K^*$ is called the kinematic displacement thickness defined by

$$\delta_K^* = \int_0^{\infty} (1 - \bar{u})\, dy \tag{145}$$

Other authors (refs. 1 and 41) have used an intermittency function in the outer layer to cause the eddy viscosity to decay to zero at the edge of the boundary layer. The major effect of such an intermittency function is confined to the region $\bar{u} > 0.9$. The intermittency function is thus of secondary importance in calculation of the boundary-layer solutions. For this reason, no intermittency function was used in the outer layer in the present analysis.

## Modulation of the Eddy Viscosity in the Transition Region

The functional form of the eddy viscosity in the transition zone is defined in the present work as

$$\beta_{\pm}(x,y) = 1 - \left[\beta(x,y) - 1\right] \Gamma(x) \tag{146}$$

where $\Gamma(x)$ is called the intermittency. The intermittency must satisfy the conditions that $\Gamma = 0$ when $x = x_t$ and $\Gamma = 1$ when $x$ is far downstream of $x_t$. In the present work, the intermittency is specified in one of two ways: (1) an analytical expression derived from considerations of the probability of the flow being turbulent at a given station or (2) an empirical distribution. The analytical function chosen to represent $\Gamma(x)$ is the Gaussian distribution derived by Emmons (ref. 42). In this analysis, the function is expressed as

$$\Gamma = 1 - e^{-\lambda(x-x_t)^2} \tag{147}$$

In the present analysis, the parameter $\lambda$ is determined by calculating the length of the transition region and requiring that $\Gamma = 0.95$ at the point of maximum skin friction or heat transfer. This process will be described in greater detail in a subsequent section concerned with correlation of the length of the transition region.

Emmons derived the intermittency function after observing turbulent spots form in a water flow. He introduced a source-density function (related to the parameter $\lambda$) to describe the production of turbulent spots, and showed that the probability of the flow being turbulent at a given point is the intermittency factor, $\Gamma$, given by equation (147).

The existence of turbulent spots in a boundary layer has been confirmed in a water flow by Mitchner (ref. 43), by Schubauer and Klebanoff (ref. 44) in low-speed air flows, and by James (ref. 45) in air flows at Mach numbers from 2.7 to 10. Emmons' assumption that the spots grow independently of each other was confirmed by the experiments of Elder (ref. 46). Dhawan and Narasimha (ref. 47) used their own and Schubauer and Klebanoff's (ref. 44) experiments to show that Emmons' source density function could be best represented by a delta function in $x$, implying that the spots originate essentially along a single line transverse to the

flow. Nagel (ref. 48), in extending the theory to hypersonic flow, showed that a key factor in the source density function is the frequency of spot formation. That frequency was found to require the existence of a characteristic length which was identified as the average lateral spacing of the turbulent spots. This length was found to be related to free-stream disturbances which could be related to wind-tunnel size, model vibrations, or other external causes.

The intermittency distribution across the boundary layer in the transition region is a function of the shape of the turbulent spots. Schubauer and Klebanoff (ref. 44) showed that at low speeds the spots have a nearly constant cross sectional area close to the surface and taper toward the outer edge of the boundary layer. Owen (ref. 49) reported that the intermittency distributions across the boundary layer in the transition region were similar to those reported by Corrsin and Kistler (ref. 50) in turbulent boundary layers. That is, the intermittency varies from some maximum value near the wall to zero toward the outer edge of the boundary layer. The intermittency distribution in the direction normal to the wall is of secondary importance in relation to the streamwise distribution in determining the mean profiles and the heat transfer and shear stress at the wall. This is especially true in the present analysis, since the intermittency is nearly constant across the inner part of the boundary layer from which come the major contributions to the integrals involved in the solution. For this reason, in this work no intermittency distribution was applied in the direction normal to the wall.

That Emmons' theory may not be generally applicable was discovered by Morkovin (ref. 12), who found that in plotting the distributions of a number of surface variables from different experiments through the transition region, only about half of those examined could be fitted to the probability distribution curves of Dhawan and Narasimha (ref. 47). Likewise, the present author found that for some hypersonic flows the intermittency tends to increase faster toward the end of transition than the low-speed probability theory predicts. One reason for this may be that some of the higher instability modes found by Mack (ref. 13) become excited and contribute to the breakdown so that the source function is not adequately represented by a single line source, but should include new sources introduced downstream of the original transition point. In the absence of a more satisfactory theory of the spot distribution in hypersonic flow, the

simple probability theory of Emmons was chosen to be used in the computer program written for the present theory. Provision was also made for the input of an arbitrary distribution of the function $\Gamma(x)$. In this way, known deviations from the Emmons function can be accommodated in the computer program. In the test calculations to be discussed in this report, the experimental intermittency distributions were used whenever they could be clearly determined.

It is important to note at this point that the capability of using an arbitrary distribution of $\Gamma(x)$ allows the determination of the experimental intermittency distribution from data. Thus, the computer program can provide a useful engineering tool for studying hypersonic transition or transition under other circumstances where the simple probability theory is inadequate.

### Correlation for the Extent of the Transition Zone

In the present work, the parameter $\lambda$ in equation (147) is determined from relations describing the length of the transition region. The length of the region is defined as the distance between the minimum and the maximum of the heat transfer, skin-friction coefficient, or surface pitot pressure. A typical distribution is shown in figure 3. It was found that when the expressions (139) and (146) were used for the eddy viscosity, the minimum of the calculated heat transfer and skin-friction coefficient occurred at approximately $\Gamma = 0.01$, and the maximum occurred at approximately $\Gamma = 0.95$. These values were used to determine the point of onset of transition and the parameter $\lambda$ so that if the Reynolds number of the length of the transition region is known, the location of the point of onset of transition is given by

$$Re_{x_t} = Re_{x_{min}} - 0.061\ Re_{\Delta x} \tag{148}$$

and the factor $\lambda$ is given by

$$\lambda = 2.66/(\Delta x)^2 \tag{149}$$

In most cases, due to the uncertainty involved with locating the transition point, the correction described in equation (148) is a minor one and may be neglected. The correction is necessary if the minimum point is known from specific data.

In reference 47, it is shown with data for a limited range of Mach numbers that the quantity $Re_{\Delta x}$ could be represented by the expression

$$Re_{\Delta x} = 5\ Re_{x_t}^{0.8}$$

Potter and Whitfield (ref. 31) studied the transition zone over a broad range of Mach numbers ($2 \leq M \leq 8$). They observed that the parameter $Re_{\Delta x}$ is independent of the unit Reynolds number and leading-edge geometry, and is basically only a function of the transition Reynolds number and the Mach number. That is,

$$Re_{\Delta x} = f(Re_{x_t}, M_e)$$

Some insight into the variation of $Re_{\Delta x}$ with Mach number can be obtained by examining the work of Nagel (ref. 48), Lees and Reshotko (ref. 51), and Mack (ref. 13). Nagel showed that the source function in the intermittency (eq. (147)) could depend upon the frequency, f, of the Tollmien-Schlichting wave most unstable with respect to the breakdown process. Nagel further showed that the Reynolds number based on the distance from the onset of transition to a given point in the transition region was inversely proportional to the square root of that frequency. That is,

$$Re_{\Delta x} = Re_x - Re_{x_t} \cong \sqrt{1/f}$$

Lees and Reshotko showed by boundary-layer stability theory that the most unstable frequency was inversely proportional to $M^2$ for high Mach numbers. Thus, the length of transition Reynolds number, $Re_{\Delta x}$, would be linear with Mach number for high supersonic and hypersonic flows.

Formulas for $Re_{\Delta x}$ were developed by examination of experimental data. For flat plates and hollow cylinders, the data of Potter and Whitfield (ref. 31) were used. For cones, data were obtained from references 20, 28, 34, and 52 through 61. The data of Potter and Whitfield were found to suggest a form

$$Re_{\Delta x} = f(M_e)\, Re_{x_t}^{\bar{\alpha}}$$

The function $f(M_e)$ was assumed to be linear so that

$$Re_{\Delta x} = (\bar{A} + \bar{B}M_e)Re_{x_t}^{\bar{\alpha}} \tag{150}$$

The parameter $\bar{\alpha}$ was determined as the slope of a plot of $\log (Re_{\Delta x})$ versus $\log (Re_{x_t})$ for fixed Mach number. Then the parameters $\bar{A}$ and $\bar{B}$ were determined from a plot of $Re_{\Delta x}(Re_{x_t})^{-\bar{\alpha}}$ versus $M_e$. For cones, this was a trial and error process, since the data exhibited a considerable amount of scatter. Thus, the formula arrived at can be considered a first approximation for arbitrary flow conditions. The values obtained for the parameters are as follows:

| Configuration | $\bar{\alpha}$ | $\bar{A}$ | $\bar{B}$ |
|---|---|---|---|
| Flat plates, hollow cylinders | 0.575 | 237.5 | 61.8 |
| Cones | .6 | 20.0 | 34.5 |

Comparisons of the predicted value of $Re_{\Delta x}$ with experimental values from several sources are shown in figure 4. All data were obtained in wind tunnels except for one free-flight case shown in figure 4(b). Some of the scatter of the data can be attributed to the quality and quantity of available data. In many instances, insufficient experimental data were obtained to locate accurately the ends of the transition region. Also, the data shown in figure 4 were obtained by several different methods. As for the location of the beginning of transition, as discussed previously, the observed location of the end of transition depends upon the quantity being observed. Included in figure 4 are data from heat-transfer measurements, surface pitot probe measurements, and wall temperature measurements. It is not clear that all three quantities will exhibit a maximum at the same point for a given flow situation.

## DETERMINATION OF ORDER OF APPROXIMATION FOR THE ENTHALPY FUNCTION

The selection of the best order of the polynomial in equation (82) was done by examining the solutions produced by various orders in both laminar and turbulent flow. The solutions were compared with other theories as well as with experimental data.

First, it can be shown that for a laminar boundary layer on a flat plate, the $E_i$ are functions only of the Prandtl number, Pr. For such a case, the velocity profiles are similar and the solution for the coefficients of the approximating polynomial in the function $\phi$ (eq. (81)) is given by equation (113), and the solution for the $E_i$ is obtained from equations (116).

In order to evaluate the order of approximation of the enthalpy function, equations (116) were solved for values of m of 0, 1, 2, 3, 4, 5, and 6. The results are shown in figures 5 and 6 for a Prandtl number of 0.72 and a wall-to-total temperature ratio of 0.3086. In figure 5 is shown the variation of total temperature as a function of $\bar{u}$. The profiles appear to converge uniformly so that there is only a slight difference between the curves for $m = 2$ and $m = 3$ and the higher-order curves are the same as that for $m = 3$. The variation of the static temperature is shown in figure 6. The manner of convergence is more apparent for the static temperature than for the total temperature. The curve for $m = 0$ is relatively high, while that for $m = 1$ is low. The higher-order curves then appear to approach a limiting curve between those for $m = 0$ and 1 as m increases. The curve for the temperature profile discussed by Schlichting (eq. (79)) is also shown in figure 6. That curve is slightly higher than the apparent limiting curve for the present approximate profile except in the outer region ($\bar{u}$ greater than 0.7 in the figure).

Another test that can be given the enthalpy function approximation in the laminar boundary layer is the value of the recovery factor. If $E_1$ is set equal to $S_w$, then the heat transfer to the wall is zero, since

$$\left.\frac{\partial T}{\partial y}\right|_w \cong \left.\frac{\partial S}{\partial \bar{u}}\right|_w \frac{1}{\phi(\xi,0)} = \frac{E_1 - S_w}{C_1} \tag{151}$$

Then solution for $S_w$ yields the adiabatic wall temperature. The recovery factor is then computed from the relation

$$r_L = 1 + S_{aw}\left(\frac{1 + m_e}{m_e}\right) \tag{152}$$

where

$$S_{aw} = \frac{T_{a_w}}{T_{t_e}} - 1 \tag{153}$$

The variation of $r_L$ with the order of the approximating function for $S$ is shown in figure 7. The recovery factor appears to converge in approximately the same manner as the temperature profiles shown in figures 5 and 6. As the order of approximation, $m$, is increased from 1, $r_L$ appears to approach the theoretical value of $(Pr)^{1/2}$ asymptotically. For $m = 3$, the error in the recovery factor is approximately 4 percent, with the error decreasing as $m$ is increased.

Finally, the approximating function for $S$ must be able to represent the enthalpy profile in a turbulent boundary layer. In this case, the $E_i$ cannot be obtained as simply as for the laminar similarity case. Furthermore, the $E_i$ will depend to some extent upon the particular model used to represent the eddy viscosity as well as upon the accuracy with which the velocity profiles are represented. In order to examine the effect of the order of approximation of the variable $S$ in turbulent flow, the solution for a boundary layer was calculated for $m = 0$, 1, 2, 3, and 4, starting in laminar flow with a similarity solution, going through a transition zone, and terminating after the boundary layer had become fully turbulent. Both the eddy viscosity model chosen for the present work and that used in reference 2 were used for this study. Similar results were obtained with both models.

The variation of the total temperature profile at a station near the end of the transition zone for the present eddy-viscosity model is shown in figure 8. The total temperature profiles for $m = 3$ and 4 are quite different from the profiles for $m = 0$, 1, and 2. The profiles for $m = 3$ and 4 display a waviness not indicated by the lower-order profiles. This phenomenon is explained by the fact that the equations used to calculate the profiles (eqs. (86) and (87)) contain an approximate function, namely the eddy viscosity. Because of this, the function being represented by the approximate series is not precisely defined. This fact alone might only serve to require higher orders for convergence since the Weierstrauss approximation theorem guarantees convergence if the functions are simply continuous. However, the imposition of the additional condition on the

function $S$ at $\bar{u} = 1$ removes the guarantee of convergence and as the order of the approximation is increased the higher-order functions develop waves as they try to satisfy both the boundary condition at $\bar{u} = 1$ and the differential equations.

The importance of the temperature profile approximation is shown in figure 9 where the distribution of the Stanton number in a transitional boundary layer is shown for values of $m$ of 0, 1, 2, 3, and 4. The present eddy-viscosity model was used in those calculations. The approximation produces a solution for the Stanton number which appears to converge as does the temperature profile for $m = 0$, 1, and 2. Then for $m = 3$ and 4, a completely different solution is obtained.

Convergence in the turbulent boundary layer will probably depend on the velocity profiles as well as the eddy viscosity. It was found in previous investigations (refs. 2 and 6) that the three-parameter velocity gradient profile given by equation (77) is not the best for all conditions on a turbulent boundary layer. Specifically, that kind of profile was found in both references cited to be inadequate for accurately representing the turbulent profile close to separation. However, since the three-parameter profile is found to be accurate for a wide range of conditions, its use represents a reasonable engineering compromise.

In view of the results shown in figures 5, 6, 7, 8, and 9 and the preceding discussion, it is believed that the value of $m = 2$ is a reasonable order of approximation for the enthalpy function. The apparent discrepancy between this series and the profile of Pinckney (eq. (81)) is explained by the fact that the present formulation is an approximation to the true profile function. Some effort was expended to modify the formulation by specifying the slope of the enthalpy function at $\bar{u} = 0$ in terms of Pinckney's function (eq. (81)). However, such a device reduces the generality and predictive nature of the solution since knowledge of the recovery factor becomes a necessary part of the solution of the equations. Specification of the value of the parameter $E_i$ and the recovery factor is tantamount to specifying the Reynold's analogy factor since from equation (105)

$$\frac{2St}{C_f} = \frac{S_w - E_1}{(S_w - S_{aw})Pr}$$

It was reported by Cary (ref. 62) that a comprehensive definition of Reynolds analogy is not available. In the absence of reliable information, from which $E_1$ could be specified, it was decided to let $E_1$ vary independently along with the other parameters, $E_2$, $E_3$,..., $E_m$. A comprehensive search for more sophisticated approximating functions was beyond the scope of the present effort and was not undertaken. It should be emphasized that the present formulation allows prediction of boundary-layer properties for both adiabatic and nonadiabatic conditions. Some error may be encountered at adiabatic wall conditions since the recovery factor of the present theory for low orders of approximation is about 4 percent lower than the theoretical value of $(Pr)^{1/2}$. However, it will be shown subsequently that the theory yields predictions of heat transfer, skin-friction coefficient and other boundary-layer properties in excellent agreement with experimental data over a wide range of conditions.

It is also believed that improvement of the eddy-viscosity model so that the equations being solved more exactly represent the true physical situation will help the present enthalpy profile formulation to converge for turbulent flow as well as for laminar flow. Until a more exact representation of the eddy viscosity is found, it is recommended that values of m greater than 2 be used with caution.

## DESCRIPTION OF COMPUTER PROGRAM

A generalized computer program was written to calculate laminar, transitional, and turbulent boundary layers of a perfect gas on arbitrary two-dimensional or axisymmetric bodies with arbitrary prescribed edge conditions and wall temperature. The program was based on equations (86) and (87) and their accompanying relations (88) through (103) as well as the auxiliary relations (104) through (112). The options for initial conditions discussed in a previous section were included in the program.

The basic input data required for the computer program are as follows:

1. Reference flow conditions, $Re_{1_o}$, $M_{e_o}$, $T_{s_{e_o}}$, $p_{e_o}$. These are most conveniently chosen as the conditions at the initial station although they can be the conditions at any point in a shock-free flow. The edge pressure, $p_{e_o}$, and the edge pressure distribution may be input in arbitrary units since the distribution is normalized with respect to the reference value when calculations are performed.

2. Prandtl numbers $Pr_L$ and $Pr_T$ and recovery factors $r_L$ and $r_T$. The turbulent Prandtl number, $Pr_T$, is defined to be equal to 1.0 in laminar flow and is modulated to change continuously to the turbulent value by the expression

$$Pr_t = 1 - \Gamma(1 - Pr_T) \tag{154}$$

Recovery factors can be inputted arbitrarily or automatically computed as

$$r_L = (Pr_L)^{1/2} \tag{155}$$

$$r_T = (r_L)^{2/3} \tag{156}$$

In the transition region, the recovery factor is then computed as

$$r_t = r_L + \Gamma(r_T - r_L) \tag{157}$$

3. Information for transition, $Re_{x_t}$, $Re_{\Delta x}$, $\lambda$. Options are included in the program for input of an arbitrary tabular distribution of $\Gamma$ versus $x$ or calculating $\Gamma$ from equation (147). If equation (147) is used, then the parameter $\lambda$ may be either inputted or computed from equation (149). If $\lambda$ is to be computed, then $Re_{\Delta x}$ is required as input.

4. Distributions of the required edge conditions, wall temperature, and configuration coordinates are provided as input to the computer program in tabular form. A list of values of each quantity, $p_e$, $T_{s_e}$, $M_e$, and $T_w$ can be input with a corresponding list of values of $x$. For the configuration coordinates a subroutine is provided to compute a table of values of $x$ corresponding to the input values of $x'$ and $r_w$. Interpolation for values of any quantity between the input values is accomplished by second-order interpolation. Tables of values of derivatives of the quantities at the input stations are obtained by averaging the slopes on either side of a given input station computed using the first differences between stations. Subsequent values of derivatives at stations between input stations are computed by linear interpolation. In the present work, it was found that adequate smoothness of the input data was easily achieved by obtaining the data from a smooth curve drawn to a scale from which three significant figures could be read. The most important requirement is that enough data

be input in regions of rapid changes that the values obtained from the interpolation schemes can adequately represent the input distribution.

An option is provided so that the edge conditions may be computed from isentropic flow relations. In that case, only the pressure distribution is necessary as input. The Mach number distribution is then computed from the relation

$$M_e = \left\{ \frac{2}{\gamma - 1} \left[ \left( \frac{p_{e_o}}{p_e} \right)^{\left[ (\gamma-1)/\gamma \right]} \left( 1 + \frac{\gamma - 1}{2} M_{e_o}^2 \right) - 1 \right] \right\}^{1/2} \qquad (158)$$

5. Initial conditions. Four options are provided: (1) input of n values of $C_i$ and m values of $E_i$; (2) input of n values of $\bar{u}$ and $\tilde{y}$ and m values of $\bar{u}$ and $T_t$; (3) input of values of $C_f$, St, $\delta^*$, $\theta$, and (m - 1) values of $\bar{u}$ and $T_t$; (4) calculation of $C_i$ and $E_i$ from a similarity solution as described previously.

Output from the computer program consists of values of x, x', $Re_x$, $r_w$, $dr_w/dx'$, $p_e/p_{e_o}$, $T_{s_e}/T_{s_{e_o}}$, $M_e$, $d(p_e/p_{e_o})/dx$, $\delta^*$, $\theta$, $C_f$, $\theta_h$, St, Nu, $\Gamma$, $\Delta x_i$, $C_i$, $E_i$, and C at each station at which output is required. In addition, the profiles of $\bar{u}$, y, $y/\delta$, $\partial\bar{u}/\partial\eta$, $d\bar{u}/d(y/L)$, $M/M_e$, $T/T_e$, $T_s/T_{s_e}$, and $\beta$ may be printed at the output stations if desired.

The integration of equations (86) and (87) is accomplished using a fourth-order Adams-Moulton predictor-corrector integration scheme (refs. 2, 3, and 63) with a fourth-order Runge-Kutta scheme used to obtain starting values. By doubling or halving the integration step size, the integration scheme is capable of some optimization of the integration. Thus, numerical errors are kept within certain bounds by dividing the integration step by 2 whenever the error is too large and by multiplying the interval by 2 whenever less accuracy is necessary than is being attained. Because of this feature, the running time of the program is somewhat dependent upon the rate at which quantities are changing. Typical run times for the flat-plate and cone calculations to be discussed in the following section of this report were 1.0 to 2.0 minutes per run on the IBM 7094. The calculations described in this report were performed on the IBM 7094.

## EVALUATION OF THE METHOD

The method of integral relations solution technique together with the transitional flow structure and eddy-viscosity model discussed in previous sections of this report are applied in this section to a number of boundary-layer calculations. Included are comparisons with experimental measurements on various two-dimensional and axisymmetric configurations as well as comparisons with calculated solutions obtained by the method of finite differences. Cases were selected to demonstrate the ability of the method to compute boundary-layer solutions over a wide range of flow parameters as well as to demonstrate the flexibility of the program for calculating boundary layers on arbitrary configurations.

In all cases, air is assumed to be a perfect gas with a constant ratio of specific heats, $\gamma$, equal to 1.4 and constant laminar and turbulent Prandtl numbers. Unless otherwise stated, the conditions at the edge of the boundary layer were computed assuming isentropic flow. Initial conditions for most of the calculations were obtained assuming a similar solution from the leading edge or nose to the initial station of the calculations. In all calculations of transitional boundary layers, the velocity gradient and enthalpy function approximations employed three-parameter expressions ($n = 3$ and $m = 2$ in equations (77) and (82)).

### Incompressible Transitional Flow on a Flat Plate

The first case to be examined is the data of Schubauer and Klebanoff (ref. 44). These data were shown by Dhawan and Narasimha (ref. 47) to fit the probability theory of Emmons (ref. 42) describing the intermittency of the transition region. Because of this, the case is an excellent one for demonstrating that the boundary-layer calculations have the correct response to the modulation of the eddy viscosity by the intermittency factor, $\Gamma$. Also, the case demonstrates the applicability of the theory for low Mach numbers.

The test conditions used for the calculations were:

$$M_e = 0.072$$

$$Re_1 = 0.44(10^6)\ ft^{-1}$$

$$T_s = 530^{\circ}R$$

$$T_w = 530^{\circ}R$$

$$Re_{x_t} = 2.31(10^6)$$

$$\lambda = 0.838\ ft^{-2}$$

Values of transition Reynolds number and the source factor of the intermittency function (eq. (147)) were determined from the data. The configuration was a sharp-leading-edge flat plate of length 12 feet.

In figure 10(a) is shown a series of calculated velocity profiles through the transition region compared with the experimental profiles. Excellent agreement is achieved for the entire region. Likewise, the agreement between the experimental values of the skin-friction coefficient and the theory shown in figure 10(b) is excellent.

### Compressible Transitional Flow on a Sharp Flat Plate

The next case to be examined is for compressible flow on a flat plate. Some data were obtained from the Langley Research Center for the heat transfer to a sharp-leading-edge flat plate. The data were obtained on a model of length 2.5 feet in the Continuous Flow Hypersonic Wind Tunnel. The tunnel Mach number was 10.39. Mach numbers from 6 to 10 on theplate were produced by varying the angle of attack of the plate. Due to the rapid expansion required to produce a Mach number of 10 in the tunnel, an error of 4 percent existed in the static temperature and pressure at the edge of the boundary layer on the plate. This error in the temperature was accounted for in the calculations by defining an effective total temperature so that the calculated local static temperature agreed with the data.

A characteristic of the experimental data was that all of it displayed an intermittency distribution in the transition region different from that

given by Emmons' probability analysis represented by equation (147). For this reason, the experimental intermittency distribution was used in calculations.

Recall that the intermittency represents the fraction of turbulence existing in the boundary layer at a given station. The procedure for determining the intermittency is somewhat iterative since the fraction of turbulence cannot be determined directly from the experimental data. To make a direct calculation of $\Gamma$, it would be necessary to know both the laminar and the fully turbulent conditions at each station. This is clearly impossible for the turbulent conditions since the virtual origin of the turbulent boundary layer is unknown. Accordingly, the procedure followed was to first use equation (147) to compute the intermittency, then, by comparing the results of the boundary-layer calculation with the data the intermittency distribution could be modified to fit the data. Two or three trials were sufficient to produce good comparisons with the data.

The results for three sets of data are shown in figure 11 where the calculated distributions of the Stanton number are compared with the experimental data. Also shown in the figures is the intermittency distribution used in the calculations as well as that given by equation (147). The conditions used in the calculations were as follows:

| Case 1 | Case 2 | Case 3 |
|---|---|---|
| $M_e = 6.18$ | $M_e = 6.18$ | $M_e = 6.18$ |
| $Re_1 = 1.32(10^6)\ ft^{-1}$ | $Re_1 = 1.63(10^6)\ ft^{-1}$ | $Re_1 = 2.03(10^6)\ ft^{-1}$ |
| $T_s = 1860^\circ R$ | $T_s = 1815^\circ R$ | $T_s = 1829^\circ R$ |
| $T_w = 549^\circ R$ | $T_w = 552^\circ R$ | $T_w = 553^\circ R$ |
| $Pr_L = 0.72$ | $Pr_L = 0.72$ | $Pr_L = 0.72$ |
| $Pr_T = 1.0$ | $Pr_T = 1.0$ | $Pr_T = 1.0$ |
| $T_{aw} = 1526^\circ R$ | $T_{aw} = 1525^\circ R$ | $T_{aw} = 1527^\circ R$ |

In the reduction of the experimental heat-transfer data for presentation in terms of the Stanton number, the recovery factor was assumed to be constant along the plate at the laminar value. In the theoretical

calculations shown in figure 11, the same assumption was used with the values of $r_L$ and $r_T$ taken to be equal to the value required to make $T_{aw}$ correspond to the value used for the experimental data.

In each case, it was discovered that the intermittency distribution required to fit the experimental data deviated from the distribution of equation (147) by increasing more rapidly than that distribution near the end of transition. A possible reason for this was that the end of the transition zone coincided with the end of the plate. The laminar heat transfer was predicted quite well without any adjustments. The solution generated by the intermittency of equation (147) with the parameter $\lambda$ determined from the indicated $\Delta x$ is shown in figures 11(a), (b), and (c) for comparison. The experimental data indicate that the intermittency at first increases more slowly than for the probability function but then rises to its ultimate value more rapidly than the probability function. In figure 11(b), it is seen that intermittency values greater than unity are required to match the data.

## Transitional Flow on a Sharp Cone

Fischer (ref. 52) recently conducted a study of boundary-layer transition on a $10^{\circ}$ half-angle sharp-nosed metal cone at a free-stream Mach number of 7. The data provide an excellent case for comparison as well as for demonstrating the flexibility of the computer program. Three cases were selected at random from reference 52 for comparison. The test conditions used for the sample calculations were as follows:

| Case 1 | Case 2 | Case 3 |
|---|---|---|
| $M_e = 5.54$ | $M_e = 5.54$ | $M_e = 5.54$ |
| $Re_1 = 6.69(10^6)\ ft^{-1}$ | $Re_1 = 7.01(10^6)\ ft^{-1}$ | $Re_1 = 7.48(10^6)\ ft^{-1}$ |
| $T_{s_{e_o}} = 1040^{\circ}R$ | $T_{s_{e_o}} = 1070^{\circ}R$ | $T_{s_{e_o}} = 1075^{\circ}R$ |
| $T_w = 551^{\circ}R$ | $T_w = 556^{\circ}R$ | $T_w = 548^{\circ}R$ |
| $Pr_L = 0.72$ | $Pr_L = 0.72$ | $Pr_L = 0.72$ |
| $Pr_T = 1.0$ | $Pr_T = 1.0$ | $Pr_T = 1.0$ |

In all three cases, the laminar and turbulent recovery factors were taken to be $(Pr_L)^{1/2}$ and $(Pr_L)^{1/3}$, respectively. The experimental location of transition and the experimental intermittency distribution determined in the same manner as for the previous examples were used in the numerical calculations.

Comparisons of the calculated results with the experimental Stanton number distributions are presented in figure 12. The agreement between the numerical results and the experimental data is very good for all three test cases. Also shown with the Stanton number distributions are the intermittency distributions as determined to match the data and as given by equation (147).

### Adverse Pressure Gradient Flow on a Cone-Flare

The previous examples have demonstrated the ability of the theory and the computer program to calculate transitional boundary layers on flat plates and cones on which a constant pressure existed. In the next example, a case in which transition occurs in an adverse pressure gradient is considered. The data were obtained by Zakkay, Bos, and Jensen (ref. 64) on a cone-flare model on which a $7.5^{\circ}$ half-angle cone was blended smoothly into an axisymmetric flare body with a constant radius of curvature. The data are an excellent case for demonstrating the ability of the theory and the computer program to calculate boundary layers under nonzero pressure gradients. In addition, since both the pressure distribution and the Mach number distribution are presented in reference 64, the case is also a demonstration of the ability of the program to accept arbitrary boundary-layer edge conditions. A sketch of the configuration and the coordinates used in the computer program is shown in figure 13.

The reference conditions used in the theoretical calculations corresponded to the conditions on the cone and were as follows:

$$Re_{1_o} = 4.86(10^6)\ ft^{-1}$$

$$M_{e_o} = 8.0$$

$$T_s = 1800^{\circ}R$$

$$T_w = 520^{\circ}R$$

$$Pr_L = 0.70$$

$$Pr_T = 1.0$$

$$\lambda = 42 \text{ ft}^{-2}$$

$$Re_{x_t} = 6.88(10^6)$$

Calculations were initialized on the cone 9 inches from the nose. Initial conditions for the calculations were obtained from the similarity solution built into the computer program. The experimental distributions of the Mach number at the edge of the boundary layer and the static pressure in the boundary layer shown in figure 14 were used for the calculations. Transition was assumed to begin at a point estimated from the experimental data. The intermittency of the transition region was calculated by equation (147).

Experimental data are presented in reference 64 for the heat transfer on the body in terms of a parameter $Nu/N_R^{1/2}$ where the Nusselt number and Reynolds number are defined in terms of local stagnation conditions. That is,

$$Nu = \frac{q_e C_{p_{s_e}} L_z}{k_{s_e}(h_{s_e} - h_w)} \tag{159}$$

and

$$N_R = \frac{\rho_{s_e} u_e L_z}{\mu_{s_e}} \tag{160}$$

where $L_z$ is a reference length equal to 1 inch. The results of the theoretical calculations in terms of the heat-transfer parameter compare quite well with the data as shown in figure 15.

## Comparison with a Finite-Difference Method

The technology of finite-difference methods of solving the boundary-layer equations has recently been applied to solution of transitional boundary layers by Harris (ref. 41). That technique apparently provides good comparisons with experimental measurements. Therefore, it was

considered worthwhile to compare the results of a calculation made with that technique with the present theory. Accordingly, some calculations made by the technique of reference 41 were obtained and are compared with calculations from the present theory in figure 16. The flow conditions of the calculations were as follows:

$$Re_1 = 1.706(10^7)\ ft^{-1}$$

$$M_e = 6.21$$

$$T_s = 1367^{\circ}R$$

$$T_w = 584^{\circ}R$$

$$Pr_L = 0.7$$

$$Pr_T = 0.9$$

$$Re_{x_t} = 4.45(10^6)$$

$$\lambda = 160.0$$

The configuration is a $10^{\circ}$ half-angle sharp-nosed cone, 2.5 feet in length. The calculations of the present theory were initialized at $x = 0.1$ utilizing the internally generated similarity solution of the computer program. The intermittency was computed from equation (147), using a value of the parameter $\lambda$ determined from the referenced calculations.

In figures 16(a), (b), and (c), the initial velocity and temperature profiles of the two theories are compared. The initial velocity profiles show excellent agreement between the two theories. The temperature profiles show excellent agreement near the wall, but only fair agreement near the outer edge of the boundary layer. Comparison of turbulent profiles from a station downstream of the transition is presented in figures 16(d) and (e). In this case, both the temperature profiles and the velocity profiles given by the two theories show good agreement over the entire boundary layer. In the referenced theory, the inner layer eddy viscosity was based on Prandtl's mixing-length hypothesis as described by Van Driest (ref. 65), while the outer layer was described by the same function as used in the present theory (eq. (144)) except that an intermittency factor was used.

Comparison of the two models at the turbulent station of figures 16(a) and (e) is shown in figure 16(f).

Skin-friction coefficient and Stanton number predictions for the two theories are compared in figures 16(g) and (h). The two theories are in excellent agreement in the laminar region for the skin-friction coefficient, displaying slight differences in the transitional and turbulent regions. For the Stanton number, a slight difference between the two theories is noted for the entire length of the calculation. Finally, the two theories are in excellent agreement for the displacement and momentum thicknesses as shown in figure 16(i).

## Calculations with Specified Initial Conditions

One of the useful features of the present theory is that initial conditions may be obtained in a number of ways. Four methods were discussed in a previous section of this report. One of these methods is the similarity solution used for initializing the previous test cases. The other three methods require known profiles. Two of these were tested by comparison with results of another theoretical calculation. The comparison calculations were produced by the finite-difference technique of Bushnell and Beckwith described in reference 66. Those authors extended the calculation technique to transitional flow by the use of an intermittency function like equation (147). In addition, their intermittency function was multiplied by a factor which was specified as a function of $\Gamma$. That is,

$$\Gamma_B(x) = f(\Gamma)\Gamma \tag{161}$$

where $\Gamma$ is given by equation (147).

In the calculations obtained from the authors of reference 66 for comparison, the intermittency, $\Gamma_B(x)$ was specified at four points. These values of $\Gamma_B(x)$ were plotted and a smooth distribution of $\Gamma$ for use with the present theory was obtained graphically. The distribution is shown in figure 17(a). It should be noted that the distribution of $\Gamma(x)$ shown in figure 17(a) was used only as an illustrative example to compare the present theory with another theory. No special significance is implied by values of $\Gamma$ greater than unity.

The configuration was a sharp-leading-edge flat plate. The reference conditions used for the calculations were as follows:

$$M_{e_o} = 8.5$$

$$Re_{1_o} = 2.295(10^7)\ ft^{-1}$$

$$T_s = 640^oR$$

$$T_w = 526^oR$$

$$Pr_L = 0.688$$

$$Pr_T = 0.9$$

$$r_L = r_T = 0.89$$

The turbulent Prandtl number of the reference calculation varied across the boundary layer from 0.9 to 1.5. The value of 0.9 was chosen for the present calculations. Two cases were computed with the present theory, corresponding to the two methods of obtaining initial conditions from known quantities. The initial conditions were as follows:

Case 1:

| $\bar{u}$ | y | $T_t$ |
|---|---|---|
| 0.30097 | 0.020068 | 570.0 |
| .50396 | .0336 | 590.0 |
| .80428 | .05361 | |

Case 2:

$$C_f = 0.00019736$$

$$\delta^* = 0.006595$$

$$\theta = 0.00014955$$

$$St = 0.00076354$$

$$\bar{u} = 0.50396$$

$$T_s = 590.0$$

The initial temperature profiles are compared in figure 17(b). For Case 1, the fitted profile matches the reference profile very well over the entire profile while the profile for Case 2 exactly matches the reference profile at the wall and at the specified point ($\overline{u} = 0.5$) with good fit elsewhere.

Comparison of the initial velocity profiles is presented in figure 17(c). As with the temperature profiles, an excellent fit was obtained for the conditions of Case 1. Only at the outer edge of the boundary layer does the fitted profile deviate from the reference profile. For Case 2, with the integral and wall quantities matched, the fitted profile is slightly different from the reference profile in shape.

Comparison of the skin-friction coefficient and the displacement and momentum thickness variation along the plate is shown in figures 17(d) and 17(e). The reference calculations and the present calculations are in excellent agreement for both Case 1 and Case 2. Note in particular that both calculative methods show the same response to the rather unusual intermittency variation.

In figures 17(f), (g), and (h) are shown comparison of the velocity and temperature profiles at two stations downstream of the transition point. The first station was in the transition region where the intermittency factor, $\Gamma$, was approximately equal to 3. The second station was near the end of the transition region, where $\Gamma = 1$. At the first station, the temperatures within the boundary layer predicted by the present theory are slightly lower than those of the reference calculation. However, at the second station, the temperature profiles are in excellent agreement. Note also, that the temperature profiles corresponding to Case 1 and Case 2 of the present theory are identical with each other at both of the stations shown in figures 17(g) and 17(i).

There is slightly more difference between the velocity profiles of the present theory and the reference theory than between the temperature profiles, as shown in figures 17(f) and 17(h). At both stations, the reference theory predicts a profile which has higher velocities through a greater portion of the boundary layer than does the present theory. Recall, however, that the wall and integral quantities predicted by both theories were in excellent agreement as shown in figures 17(d) and 17(e).

## Effect of Transverse Curvature in Laminar Flow

On axisymmetric configurations, the effects of transverse curvature can be important if the thickness of the boundary layer is comparable to the radius of the configuration. The effect of transverse curvature on a laminar boundary-layer calculation is illustrated in figure 18. The configuration being examined is the $10^{\circ}$ half-angle cone of reference 52 in a flow with a Mach number of 6.9. The pressure was assumed to be constant along the cone surface and unit Reynolds number $10^4$ $ft^{-1}$ was chosen for illustrative purposes. The effects of transverse curvature (TVC) on the calculated Stanton number distribution are evident from figure 18(a). The calculation in which transverse curvature was accounted for predicts a higher value of St than for the calculation in which transverse curvature is neglected. However, the effect diminishes as the calculation proceeds downstream, as evidenced by the fact that the error between the two predictions decreases from 29 percent at $x = 0.2$ foot to 14 percent at $x = 1.0$ foot. Similar results are found for the displacement thickness of the boundary layer as shown in figure 18(b). The calculated velocity and temperature profiles are shown in figure 18(c) and (d). Since increasing the Reynolds number has the effect of decreasing the boundary-layer thickness, it is expected that in most cases of interest for transitional boundary-layer calculations transverse curvature can be neglected. This was indeed found to be true for the data of figure 12, discussed previously. The inclusion of transverse curvature in the calculations for that figure had no effect on the results.

The initial conditions for both cases shown in figure 18 were obtained from the similarity solution built into the computer program. This resulted in an initially transient solution for the case with transverse curvature included. However, the solution approached a unique variation within a few integration steps (each step was approximately 0.0001 foot).

## Turbulent Flow with Transverse Curvature

A good example of turbulent boundary-layer data for flows with variable pressure gradients and significant transverse curvature effects was presented by Winter, Smith, and Rotta (ref. 67). The data provide a particularly good case for comparison with the present theory because they allow the demonstration of many different capabilities of the theory all in two calculations.

The configuration is an axisymmetric, piecewise continuous, waisted body (fig. 19). The data presented in reference 67 for $M_\infty = 1.4$ were chosen for comparison. The transition point was assumed to be at 1.5 inches from the nose of the body, corresponding to the location of a boundary-layer trip as reported in reference 67.

The test conditions for the case considered were as follows:

$$M_\infty = 1.398$$

$$Re_{1_\infty} = 2.02(10^6)\ ft^{-1}$$

$$T_s = 536^\circ R$$

$$T_w = 524^\circ R$$

$$M_{e_o} = 1.06$$

$$Re_{1_o} = 2.02(10^6)\ ft^{-1}$$

$$Re_{x_t} = 0.252(10^6)$$

The reference conditions for the calculations were taken to be the conditions on the conical nose section of the body. The calculations were started at $x = 0.1$ foot using the similarity solution built into the computer program. Transition from laminar to turbulent flow was computed automatically from the given value of $Re_{x_t}$ with the intermittency given by equation (147). The source function in equation (147) was computed assuming the transition region to be equal in length to the length of the laminar boundary layer. The experimental Mach number distribution is presented in figure 19 along with the configuration. The isentropic pressure distribution corresponding to the given Mach number distribution was used as input to the computer program. The conditions behind the nose shock wave were obtained from reference 68.

This case was a good one for demonstrating the smoothness requirements of the input distributions. The smoothness of the distribution describing the configuration is not critical since the body slope does not enter the calculations directly. However, the distributions of pressure, Mach number, wall temperature, and total temperature must be smooth so that the

interpolation of the first derivatives required will be smooth. In the calculations discussed in this section, it was found to be sufficient to plot the distribution to a scale at which three significant figures could be obtained from a smooth curve drawn through the data.

The configuration being described has received considerable attention by authors of theoretical methods. Calculations on this configuration have been made by Cebeci, Smith, and Mosinskis (ref. 69), Herring and Mellor (ref. 36), and Harris (ref. 41). All of these authors used finite-difference methods. Until now, only Harris was able to compute a completely theoretical solution with no dependence on experimental profile or skin-friction information for initial conditions. To the author's knowledge, the solution presented here is the first to be obtained by the method of integral relations.

The calculated results are compared with the experimental data for momentum thickness and skin-friction coefficient distributions in figure 20. The agreement between the theoretical and experimental distributions is very good. In particular, note the erratic behavior of the data and the theory for the skin-friction coefficient in the region $x < 1$ foot. Also, note that the inclusion of the transverse curvature terms in the solution had a significant effect on the momentum thickness. The transverse curvature effect is the same as found by the authors of references 36, 41, and 69. The skin friction is predicted quite well both with and without transverse curvature, particularly at the point of minimum skin friction. Without transverse curvature, the momentum thickness is overpredicted near the downstream end of the model, but is in good agreement with the data when transverse curvature is included in the calculations.

## CONCLUDING REMARKS

The method of integral relations has been applied to the calculation of laminar, transitional, and turbulent boundary layers on arbitrary axisymmetric or two-dimensional configurations. The technique employed is a new application of a method previously used successfully to predict the characteristics of separated laminar boundary layers and unseparated turbulent boundary layers. An eddy-viscosity model has been developed for use in the turbulent boundary-layer equations along with an intermittency function for the transition region. A computer program has been written to solve the

equations with arbitrarily prescribed boundary-layer edge conditions, wall-temperature distributions, and Prandtl number for flows from low speeds to hypersonic speeds.

A number of methods of obtaining initial conditions are discussed. The solution can be started from known information such as velocity and temperature profiles or known values of skin friction, heat transfer, and other boundary-layer properties, or from a similarity solution which assumes constant pressure from the leading edge of the configuration and has no dependence on experimental or empirical data. Other theoretical initial conditions could also be used but were not included in the work described here. Thus, the calculative method can either be self-starting or rely on experimental information as the user chooses.

The computer program can be used to calculate the transition region between other laminar and turbulent boundary-layer calculations or it can be used to compute the entire solution from laminar through turbulent flow. Prediction of the transition point is performed by the user of the computer program using approximate formulas developed by correlating experimental data. The intermittency of the transition region can be computed using a function based on probability theory, or it can be provided as an arbitrary distribution. The computer program may be used to determine the intermittency corresponding to experimental data.

Good comparisons between the theory and experimental data for heat transfer and skin friction were made on various kinds of configurations in both subsonic and supersonic flows. Transitional heat transfer on both sharp-leading-edged flat plates and sharp-nosed cones was calculated by determining an intermittency distribution to fit the data. Comparisons of the present theory with calculations made using finite-difference theory indicated excellent agreement between the two theories. Calculation of the turbulent boundary layer on a body of revolution having both favorable and adverse pressure gradients yielded excellent agreement with the experimental skin-friction coefficient and momentum thickness, when the effects of transverse curvature were included. Most significantly, that calculation was made using no experimental information to obtain initial conditions.

Finally, some comments are in order regarding the intermittency distribution in hypersonic boundary layers. The exact details of the transition

region flow structure remain as one of the major unsolved problems of fluid mechanics. Data examined in this research corroborated the finding of Morkovin (ref. 12) that the intermittency distributions of hypersonic boundary layers do not always fit the simple probability distribution of Emmons as used by Dhawan and Narasimha (ref. 47). Morkovin stated that of many hypersonic cases he examined, only about half of them could be fitted to the low-speed probability distribution curves of Dhawan and Narasimha. Cases were presented in this report in which the intermittency distributions found to fit the data were quite different from that given by Emmons' function.

The cases presented herein were presented to demonstrate the accuracy and flexibility of the computer program and were not intended as evidence of the validity of the probability theory. However, the results suggest that the intermittency function should be a more complicated function than that given by the simple theory of Dhawan and Narasimha. The results also suggest an important use of the computer program as a research tool in the study of hypersonic transition, but such a study must be accompanied by further experimental research before meaningful results can be obtained. Many experimental data are available for heat transfer to flat plates and cones in wind tunnels. However, in order to study the intermittency in the transition region comprehensively, more data are needed from free-flight experiments as well as from configurations with significant pressure variation. It is possible that the higher modes of instability described by Mack (ref. 13) could produce potential turbulent sources which would be triggered by the relatively high disturbance level of a wind tunnel, but might not be triggered in free flight. However, available free-flight data are not adequate to determine the detailed distribution of the intermittency. Use of the computer program along with experimental data to determine the intermittency in boundary layers over a wide range of parameters could lead to correlations with which the intermittency could be predicted with greater confidence than with the simple probability function of Dhawan and Narasimha. Moreover, such correlations could lead to extension of the probability theory to more complicated source functions, than the delta-function of Dhawan and Narasimha, with sources of turbulence being introduced downstream of the original point of onset of transition.

Most available experimental data in hypersonic flow are for heat transfer alone. Experiments in which both heat transfer and skin friction were measured for several Mach numbers would substantially improve the state of knowledge of the transition region. These measurements could be accompanied by measurements of the intermittency as determined from fluctuating quantities in the boundary layer. Calculations could then be made to verify whether the intermittency determined to match transitional heat transfer data is the same as required to match skin-friction data. The experiments would also provide information about Reynolds analogy in the transition region. This might be useful in improving the present formulation of the enthalpy profiles in the theory.

Another area in which reliable experimental information is needed is the effect of pressure gradients on the transition zone. This is needed for development of improved models of the eddy viscosity and turbulent Prandtl number as well as for the improvement of the theory regarding the intermittency.

In conclusion, the method has been found to be a fast, flexible, and accurate method of computing unseparated laminar, transitional, and turbulent boundary layers. As input, the computer program requires only very basic information such as the flow conditions and data describing the configuration, plus information on the initial conditions. Use of the program as an engineering tool requires only a minimum amount of knowledge of the theoretical methods used in the calculations.

Nielsen Engineering & Research, Inc.
Mountain View, California
October 5, 1970

## REFERENCES


1. Smith, A. M. O. and Cebeci, T.: Numerical Solution of the Turbulent Boundary-Layer Equations. Douglas Aircraft Corp. Rep. No. DAC 33735, May 29, 1967.

2. Lynes, L. L., Nielsen, J. N., and Kuhn, G. D.: Calculation of Compressible Turbulent Boundary Layers with Pressure Gradients and Heat Transfer. NASA CR-1303, Mar. 1969.

3. Goodwin, F. K., Nielsen, J. N., and Lynes, L. L.: Inhibition of Flow Separation at High Speed. AFFDL-TR-68-119, Vols. I through III, Mar. 1969.

4. Kuhn, G. D., Goodwin, F. K., and Nielsen, J. N.: Prediction of Supersonic Laminar Separation by the Method of Integral Relations with Free Interaction. AFFDL-TR-69-87, Jan. 1970.

5. Dorodnitsyn, A. A.: General Method of Integral Relations and Its Application to Boundary Layer Theory. Advances in Aeronautical Sciences, vol. 3, von Karmán Ed., The MacMillan Co., New York, N. Y., 1962, pp. 207-219.

6. Murphy, J. D. and Rose, W. C.: Application of the Method of Integral Relations to the Calculation of Incompressible Turbulent Boundary Layers. Computation of Turbulent Boundary Layers, 1968 AFOSR-IFP-Stanford Conference, Vol. I, 1969, pp. 54-75.

7. Laufer, J.: Thoughts on Compressible Turbulent Boundary Layers. Rand Corp. Memorandum RM-5946-PR, Mar. 1969.

8. Probstein, R. F. and Elliott, D.: The Transverse Curvature Effect in Compressible Axially Symmetric Laminar Boundary Layer Flow. Jour. Aero. Sci., vol. 23, p. 208, 1956.

9. Stewartson, K.: Correlated Incompressible and Compressible Boundary Layers. Proc. of the Royal Soc., A, vol. 200, 1949, pp. 85-100.

10. Schlichting, H.: Boundary Layer Theory. Fourth Ed., McGraw-Hill Book Co., Inc., New York, N. Y., 1960, p. 346.

11. Pinckney, S. Z.: Static Temperature Distribution in a Flat-Plate Compressible Turbulent Boundary Layer with Heat Transfer. NASA TN D-4611, June 1968.

12. Morkovin, M. V.: Critical Evaluation of Transition from Laminar to Turbulent Shear Layers with Emphasis on Hypersonically Traveling Bodies. AFFDL-TR-68-149, Mar. 1969.

13. Mack, L. M.: Boundary-Layer Stability Theory. Notes prepared for the AIAA Professional Study Series High-Speed Boundary-Layer Stability and Transition, San Francisco, Calif., June 14-15, 1969.

14. Wazzan, A. R., Okamura, T., and Smith, A. M. O.: Spatial Stability Study of Some Falknar-Skan Similarity Profiles. Proc. Fifth U. S. Natl. Congress of Appl. Mech., A.S.M.E., Univ. of Minnesota, June 1966, p. 836.

15. Kaplan, R. E.: The Stability of Laminar Incompressible Boundary Layers in the Presence of Compliant Boundaries. Mass. Inst. of Tech. Aeroelastic and Structures Research Lab., ASRL-TR-116-1.

16. Donaldson, C. duP.: A Computer Study of an Analytical Model of Boundary-Layer Transition. AIAA Jour., vol. 7, no. 2, Feb. 1969, pp. 271-278.

17. Potter, J. Leith: Observations on the Influence of Ambient Pressure on Boundary-Layer Transition. AEDC TR-68-36, Mar. 1968.

18. Brinich, P. F.: Effect of Leading-Edge Geometry on Boundary Layer Transition at Mach 3.1. NACA TN 3659, Mar. 1956.

19. Pate, S. R. and Schueler, C. J.: Radiated Aerodynamic Noise Effects on Boundary-Layer Transition in Supersonic and Hypersonic Wind Tunnels. AIAA Jour., vol. 7, no. 3, Mar. 1969, pp. 450-457.

20. Pate, S. R.: Measurements and Correlations of Transition Reynolds Numbers on Sharp Slender Cones at High Speeds. AEDC TR-69-172, Dec. 1969.

21. Deem, R. E., Erickson, C. R., and Murphy, J. S.: Flat-Plate Boundary-Layer Transition at Hypersonic Speeds. AFFDL Rep. FDL-TDR-64-129, Oct. 1964.

22. Hopkins, E. J., Jillie, D. W., and Sorensen, V. L.: Charts for Estimating Boundary-Layer Transition on Flat Plates. NASA TN D-5846, June 1970.

23. Bertram, M. H. and Beckwith, I. E.: NASA Langley Boundary-Layer Transition Investigations Paper No. 18. Boundary-Layer Transition Study Group Meeting, Vol. III, Session on Ground Test Transition Data and Correlations, William D. McCauley, Ed., Air Force Rep. BSD-TR-67-213, Vol. III, Aerospace Rep. No. TR-0158(53816-63)-1, Vol. III, Aug. 1967.

24. Van Driest, E. R. and Blumer, C. B.: Boundary-Layer Transition: Free-Stream Turbulence and Pressure Gradient Effects. AIAA Jour., vol. 1, no. 6, June 1963, pp. 1303-1306.

25. Stetson, K. F. and Rushton, G. H.: A Shock Tunnel Investigation of the Effects of Nose Bluntness, Angle of Attack and Boundary Layer Cooling on Boundary Layer Transition at a Mach Number of 5.5. AIAA Paper No. 66-495, presented at the 4th Aerospace Sciences Meeting, Los Angeles, Calif., June 27-29, 1966.

26. Moeckel, W. E.: Some Effects of Bluntness on Boundary-Layer Transition and Heat Transfer at Supersonic Speeds. NACA Rep. 1312, 1957. Supersedes NACA TN 3653, 1956.

27. Holloway, P. F. and Sterrett, J. R.: Effect of Controlled Surface Roughness on Boundary-Layer Transition and Heat Transfer at Mach Numbers of 4.8 and 6.0. NASA TN D-2054, Apr. 1964.

28. Brinich, P. F.: Recovery Temperature, Transition, and Heat Transfer Measurements at Mach 2. NACA TN D-1047, Aug. 1961.

29. Brinich, P. F.: Effect of Bluntness on Transition for a Cone and a Hollow Cylinder at Mach 3.1. NACA TN 3979, May 1957.

30. Eaton, C. J., Pederson, J. R. C., Plane, C. G., and Southgate, A. C.: Experimental Studies at Mach Numbers 3, 4, and 5 of Turbulent Boundary Layer Heat Transfer in Two-Dimensional Flows with Pressure Gradient. British Aircraft Corp. Rep. ST-2310, 1964.

31. Potter, J. Leith and Whitfield, J. D.: Boundary-Layer Transition Under Hypersonic Conditions. AEDC TR-65-99, May 1965, presented at AGARD Specialist Meeting, Naples, May 10-14, 1965.

32. Cary, A. M., Jr.: Turbulent Boundary-Layer Heat Transfer and Transition Measurements with Surface Cooling at Mach 6. NASA TN D-5863, June 1970.

33. Zakkay, V. and Krause, E.: Boundary Conditions at the Outer Edge of the Boundary Layer on Blunted Conical Bodies. Air Force Office of Aerospace Research, Aeronautical Research Lab., ARL 62-386, July 1962.

34. Stainback, P. C.: Effect of Unit Reynolds Number, Nose Bluntness, Angle of Attack, and Roughness on Transition on a $5^{\circ}$ Half-Angle Cone at Mach 8. NASA TN D-4961, Jan. 1969.

35. Softley, E. J., Graber, B. C., and Zempel, R. E.: Experimental Observation of Transition of the Hypersonic Boundary Layer. AIAA Jour., vol. 7, no. 2, Feb. 1969, pp. 257-263.

36. Herring, H. J. and Mellor, G. L.: A Method of Calculating Compressible Turbulent Boundary Layers. NASA CR-1144, Sept. 1968.

37. Maise, G. and McDonald, H.: Mixing Length and Kinematic Eddy Viscosity in a Compressible Boundary Layer. AIAA Paper No. 67-199, presented at the 5th Aerospace Sciences Meeting, New York, N. Y., Jan. 23-26, 1967.

38. Kleinstein, G.: Generalized Law of the Wall and Eddy-Viscosity Model for Wall Boundary Layers. AIAA Jour., vol. 5, no. 8, Aug. 1967, pp. 1402-1407.

39. Martelucci, A., Rie, H., and Sontowski, J. F.: Evaluation of Several Eddy Viscosity Models Through Comparison with Measurements in Hypersonic Flows. AIAA Paper No. 69-688, presented at AIAA Fluid and Plasma Dynamics Conference, San Francisco, Calif., June 16-18, 1969.

40. Clauser, F. H.: The Turbulent Boundary Layer. Advances in Appl. Mech., Vol. IV, Academic Press, Inc., 1956, pp. 1-52.

41. Harris, J. E.: Numerical Solution of the Compressible Laminar, Transitional, and Turbulent Boundary Layer Equations with Comparisons to Experimental Data. Ph.D. Dissertation, Virginia Polytechnic Inst., May 1970.

42. Emmons, H. W.: The Laminar-Turbulent Transition in a Boundary Layer. Jour. Aero. Sci., vol. 18, 1951, p. 490.

43. Mitchner, M.: Propagation of Turbulence from an Instantaneous Point Disturbance. Jour. Aero. Sci., vol. 27, 1954, pp. 350-351.

44. Schubauer, G. B. and Klebanoff, P. S.: Contributions on the Mechanics of Boundary-Layer Transition. NACA Rep. 1289, 1956. (Supersedes NACA TN 3489, Sept. 1955.)

45. James, C. S.: Observations of Turbulent-Burst Geometry and Growth in Supersonic Flow. NACA TN 4235, Apr. 1958.

46. Elder, J. W.: An Experimental Investigation of Turbulent Spots and Breakdown to Turbulence. Jour. Fluid Mech., vol. 9, no. 2, Oct. 1960, pp. 235-246.

47. Dhawan, S. and Narasimha, R.: Some Properties of Boundary Layer Flow During the Transition from Laminar to Turbulent Motion. Jour. Fluid Mech., vol. 3, 1958, p. 418.

48. Nagel, A. L.: Compressible Boundary Layer Stability by Time Integration of the Navier-Stokes Equations and an Extension of Emmons' Transition Theory to Hypersonic Flow. Boeing Flight Sci. Lab. Rep. No. 119, Sept. 1967.

49. Owen, F. K.: Transition Experiments on a Flat Plate at Subsonic and Supersonic Speeds. AIAA Paper No. 69-9, presented at the 7th Aerospace Sciences Meeting, New York, N. Y., Jan. 20-22, 1969.

50. Corrsin, S. and Kistler, A. L.: Free Stream Boundaries of Turbulent Flow. NACA Rep. 1244, 1955. (Supersedes NACA TN 3133, 1954.)

51. Lees, L. and Reshotko, E.: Stability of the Compressible Laminar Boundary Layer. Jour. of Fluid Mech., vol. 12, Pt. 4, Apr. 1962.

52. Fischer, M. C.: An Experimental Investigation of Boundary-Layer Transition on a $10^{o}$ Half-Angle Cone at Mach 6.9. NASA TN D-5766, Apr. 1970.

53. DiCristina, V.: Three-Dimensional Laminar Boundary-Layer Transition on a Sharp $8^{o}$ Cone at Mach 10. AIAA Jour., vol. 8, no. 5, May 1970, pp. 852-856.

54. Jones, J. J.: Experimental Investigation of the Heat-Transfer Rate to a Series of $20^{o}$ Cones of Various Surface Finishes at a Mach Number of 4.95. NASA Memo 6-10-59L, June 1959.

55. Softley, E. J.: Boundary Layer Transition on Hypersonic Blunt Slender Cones. AIAA Paper No. 69-705, presented at AIAA Fluid and Plasms Dynamics Conf., San Francisco, Calif., June 16-18, 1969.

56. Softley, E. J., Graber, B. C., and Zempel, R. E.: Transition of the Hypersonic Boundary Layer on a Cone. Part 1 - Experiments at $M_\infty$ = 12 and 15. General Electric Rep. No. 67 SD39, Contract No. AF 04(694)772, Nov. 1967.

57. Mateer, G. G. and Larson, H. K.: Unusual Boundary-Layer Transition Results on Cones in Hypersonic Flow. AIAA Jour., vol. 7, no. 5, Apr. 1969, pp. 660-664.

58. Rumsey, C. B. and Lee, D. B.: Measurements of Aerodynamic Heat Transfer and Boundary-Layer Transition on a 15° Cone in Free Flight at Supersonic Mach Numbers up to 5.2. NASA TN D-888, Aug. 1961.

59. Van Driest, E. R. and Boison, J. C.: Experiments on Boundary-Layer Transition at Supersonic Speeds. Jour. Aeronautical Sci., vol. 24, no. 12, Dec. 1957, pp. 885-899.

60. Merlet, C. F. and Rumsey, C. B.: Supersonic Free-Flight Measurement of Heat Transfer and Transition on a 10° Cone Having a Low Temperature Ratio. NASA TN D-951, Aug. 1961.

61. Rumsey, C. B. and Lee, D. B.: Measurements of Aerodynamic Heat Transfer and Boundary-Layer Transition on a 10° Cone in Free Flight at Supersonic Mach Numbers up to 5.9. NASA TN D-745, May 1961.

62. Cary, A. M., Jr.: Summary of Available Information on Reynolds Analogy for Zero-Pressure-Gradient, Compressible Turbulent-Boundary-Layer Flow. NASA TN D-5560, Jan. 1970.

63. Hildebrand, F. B.: Introduction to Numerical Analysis. McGraw-Hill Book Co., New York, 1956, Chapter 6.

64. Zakkay, V., Bos, A., and Jensen, P. F., Jr.: Laminar, Transitional, and Turbulent Flow with Adverse Pressure Gradient on a Cone-Flare at Mach 10. AIAA Paper No. 66-493, presented at the 4th Aerospace Sciences Meeting, Los Angeles, Calif., June 27-29, 1966.

65. Van Driest, E. R.: On Turbulent Flow Near a Wall. Jour. of Aero. Sci., vol. 23, no. 11, Nov. 1956.

66. Bushnell, D. M. and Beckwith, I. E.: Calculation of Nonequilibrium Hypersonic Turbulent Boundary Layers and Comparisons with Experimental Data. AIAA Paper No. 69-684, presented at AIAA Fluid and Plasma Dynamics Conf., San Francisco, Calif., June 16-18, 1969.

67. Winter, K. G., Smith, K. G., and Rotta, J. C.: Turbulent Boundary Layer Studies on a Waisted Body of Revolution in Subsonic and Supersonic Flow. AGARD - Recent Developments in Boundary-Layer Research, proc. of a Specialist Meeting sponsored by AGARD Fluid Dynamics Panel, Naples, Italy, May 10-15, 1965, p. 933.

68. Sims, J. L.: Tables for Supersonic Flow Around Right Circular Cones at Zero Angle of Attack. NASA SP-3004, 1964.

69. Cebeci, T., Smith, A. M. O., and Mosinskis, G.: Calculation of Compressible Adiabatic Turbulent Boundary Layers. AIAA Paper No. 69-687, presented at AIAA Fluid and Plasma Dynamics Conf., San Francisco, Calif., June 16-18, 1969.

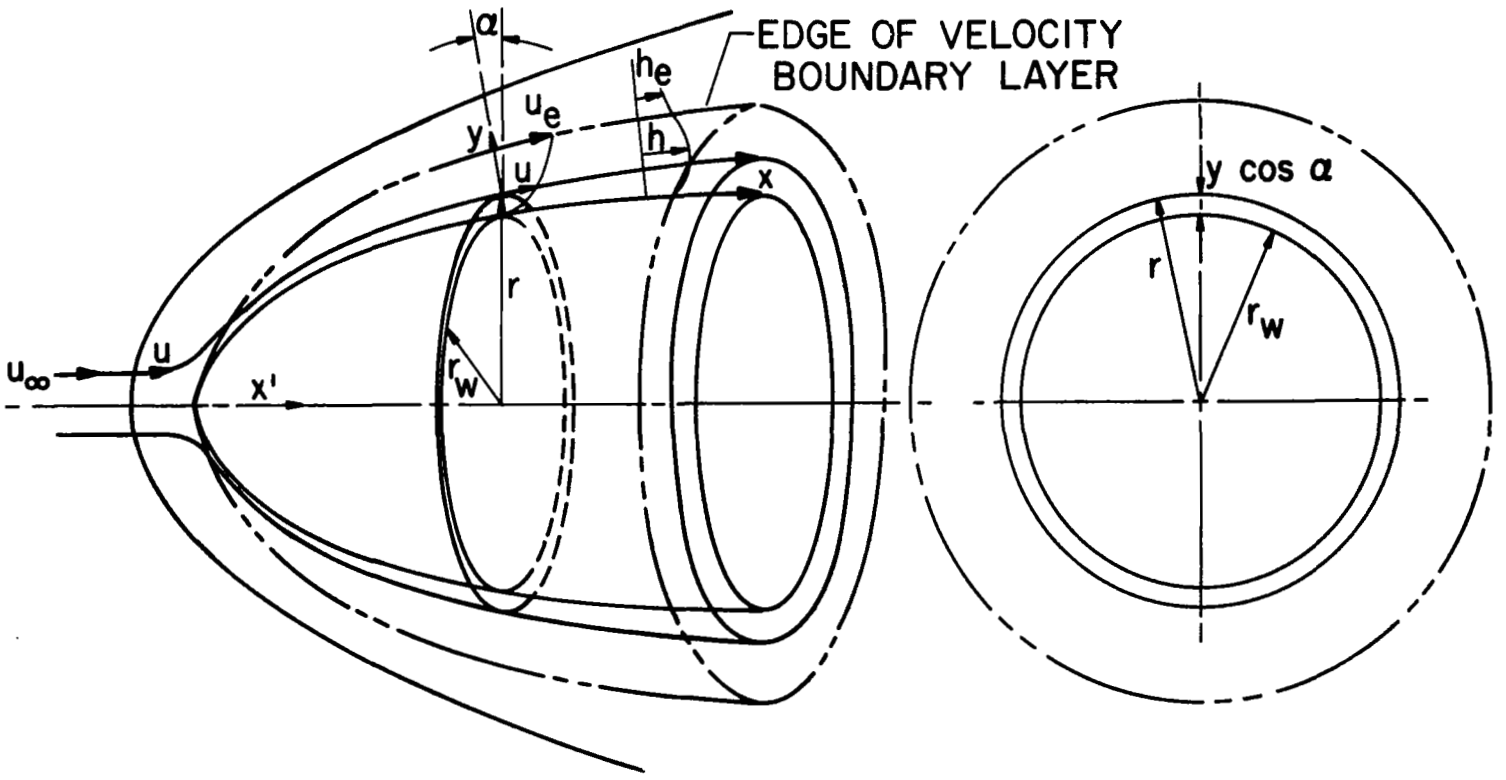


(a) Axisymmetric configuration.

Figure 1.- Boundary-layer coordinate system.

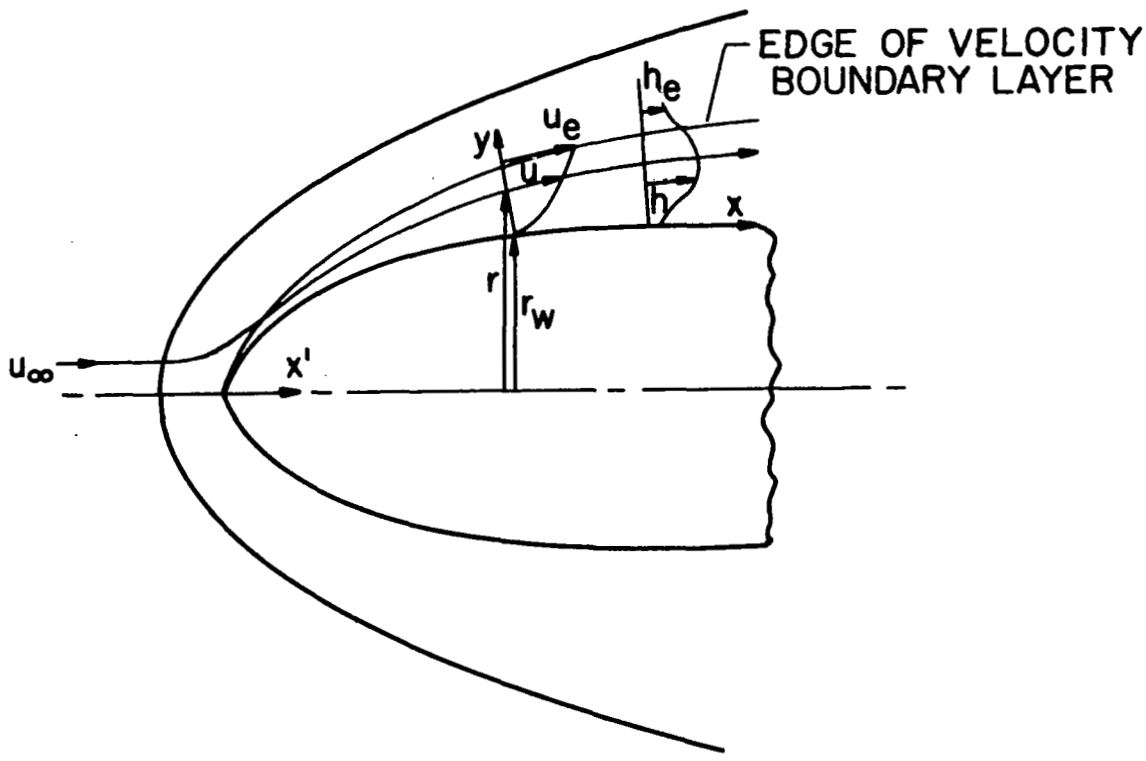


(b) Two-dimensional configuration.

Figure 1.- Concluded.

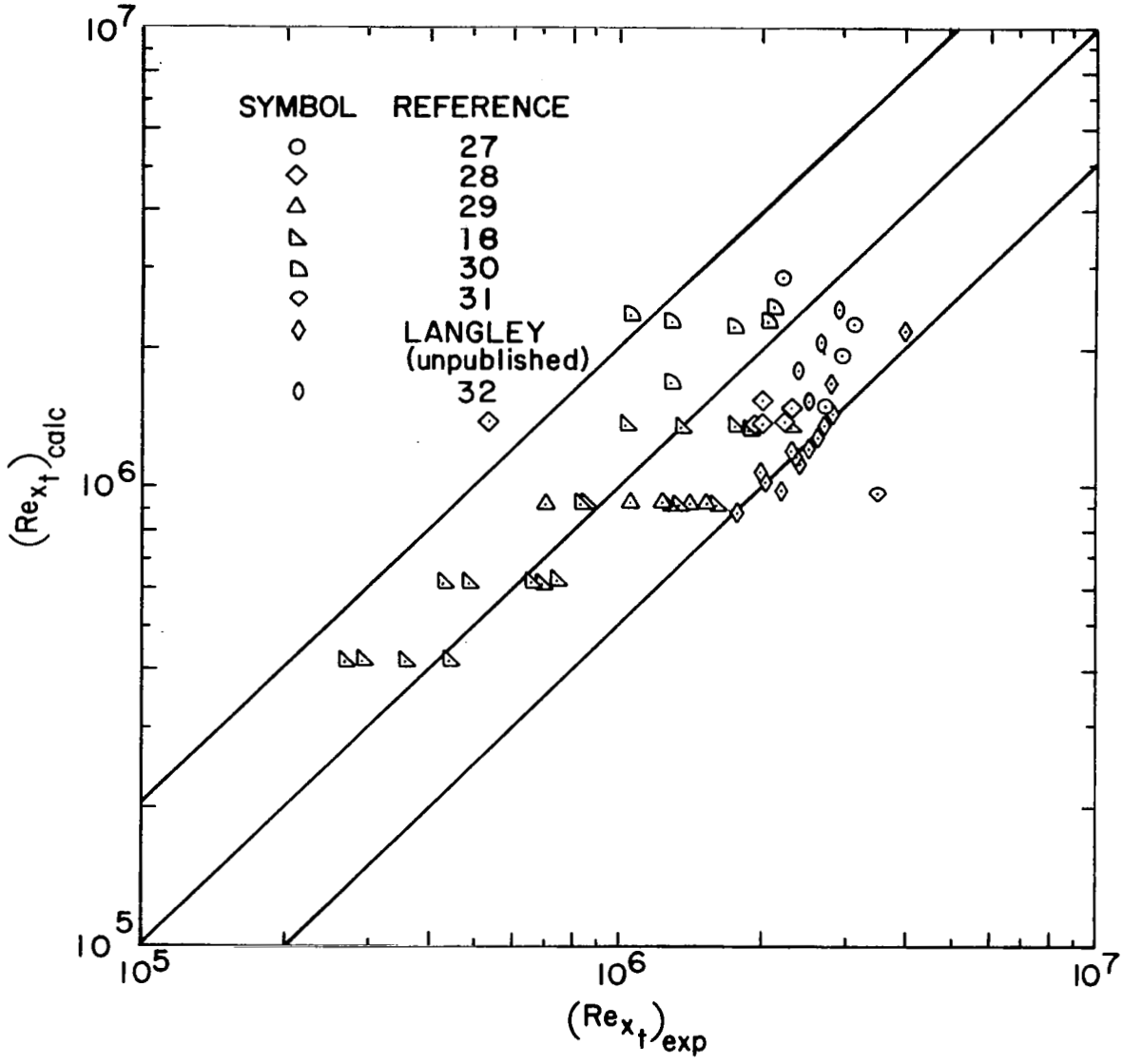


Figure 2.- Comparison of experimental data with predicted transition Reynolds numbers on flat plates.

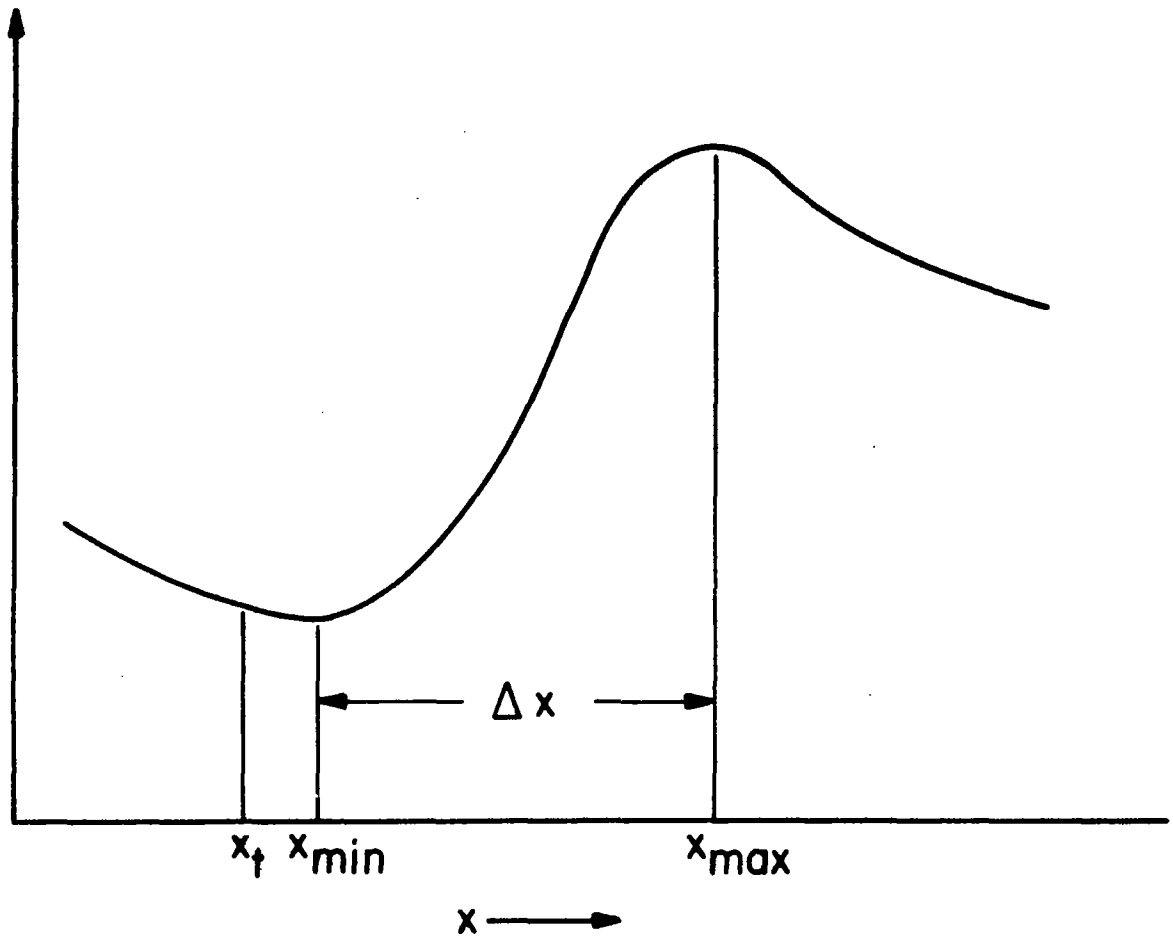


Figure 3.- Typical distribution of a surface quantity in a transitional boundary layer.

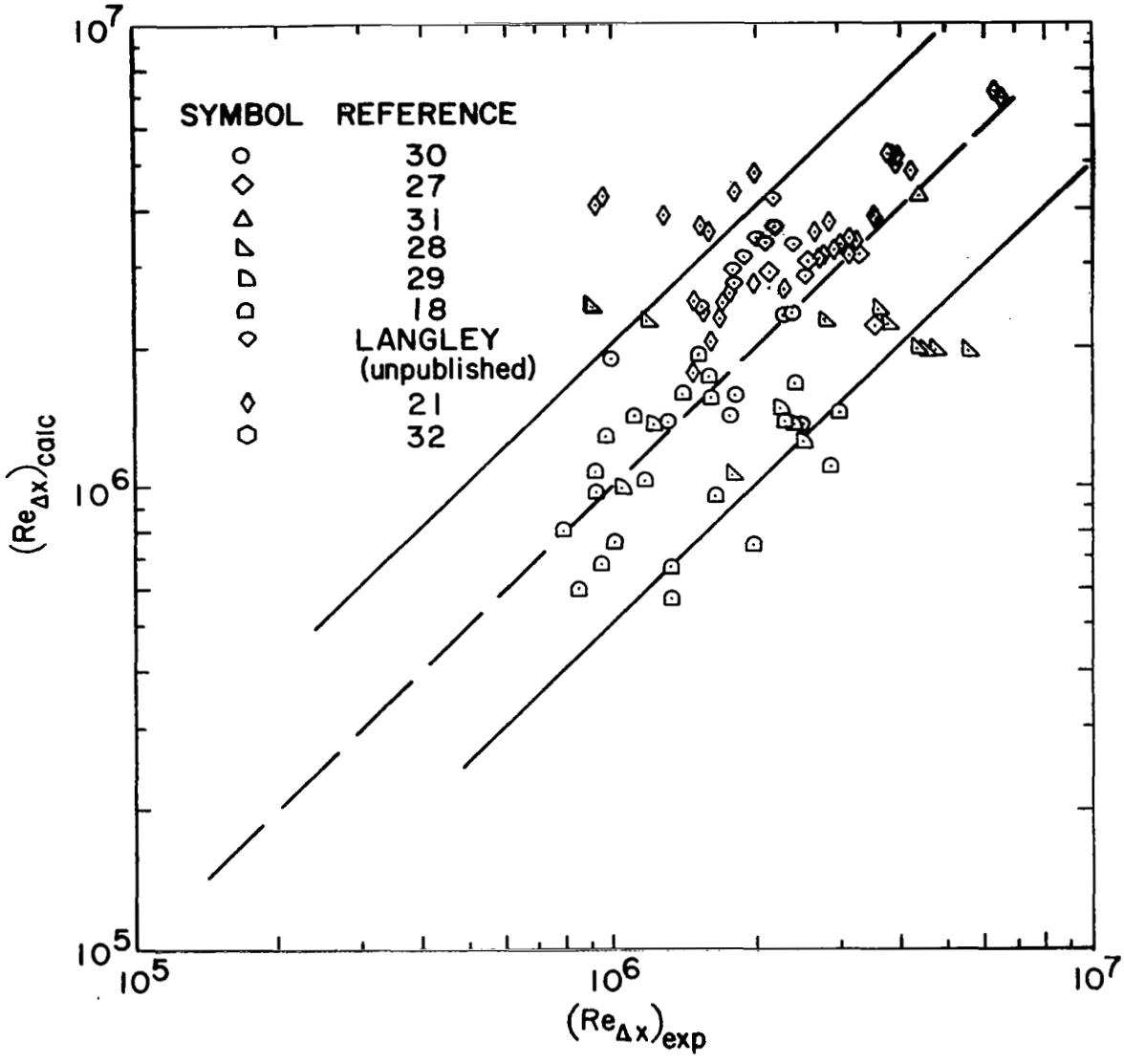


(a) Flat plates and hollow cylinders.

Figure 4.- Comparison of experimental data for length of transition region with predicted values.

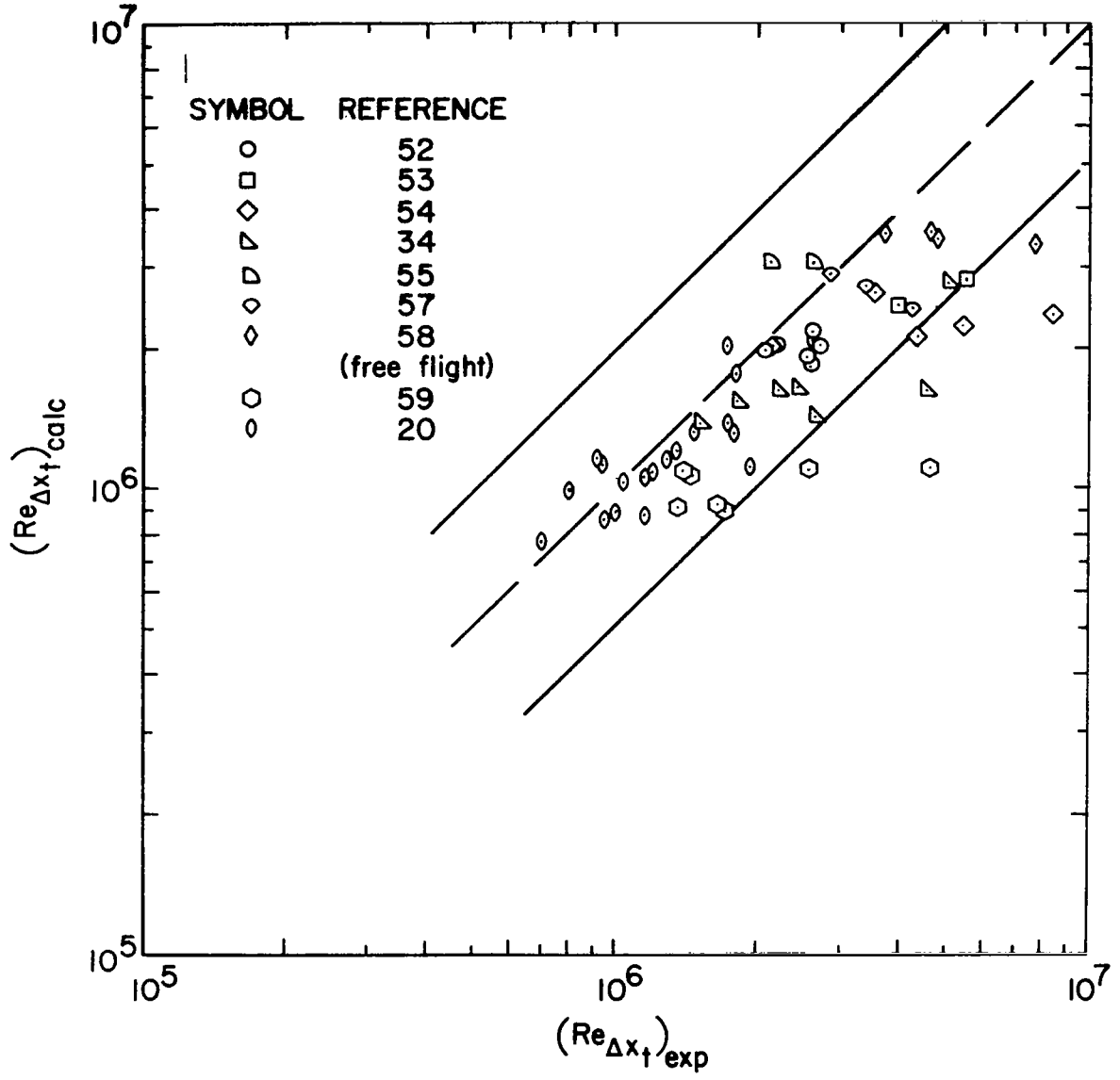


(b) Cones.

Figure 4.- Concluded.

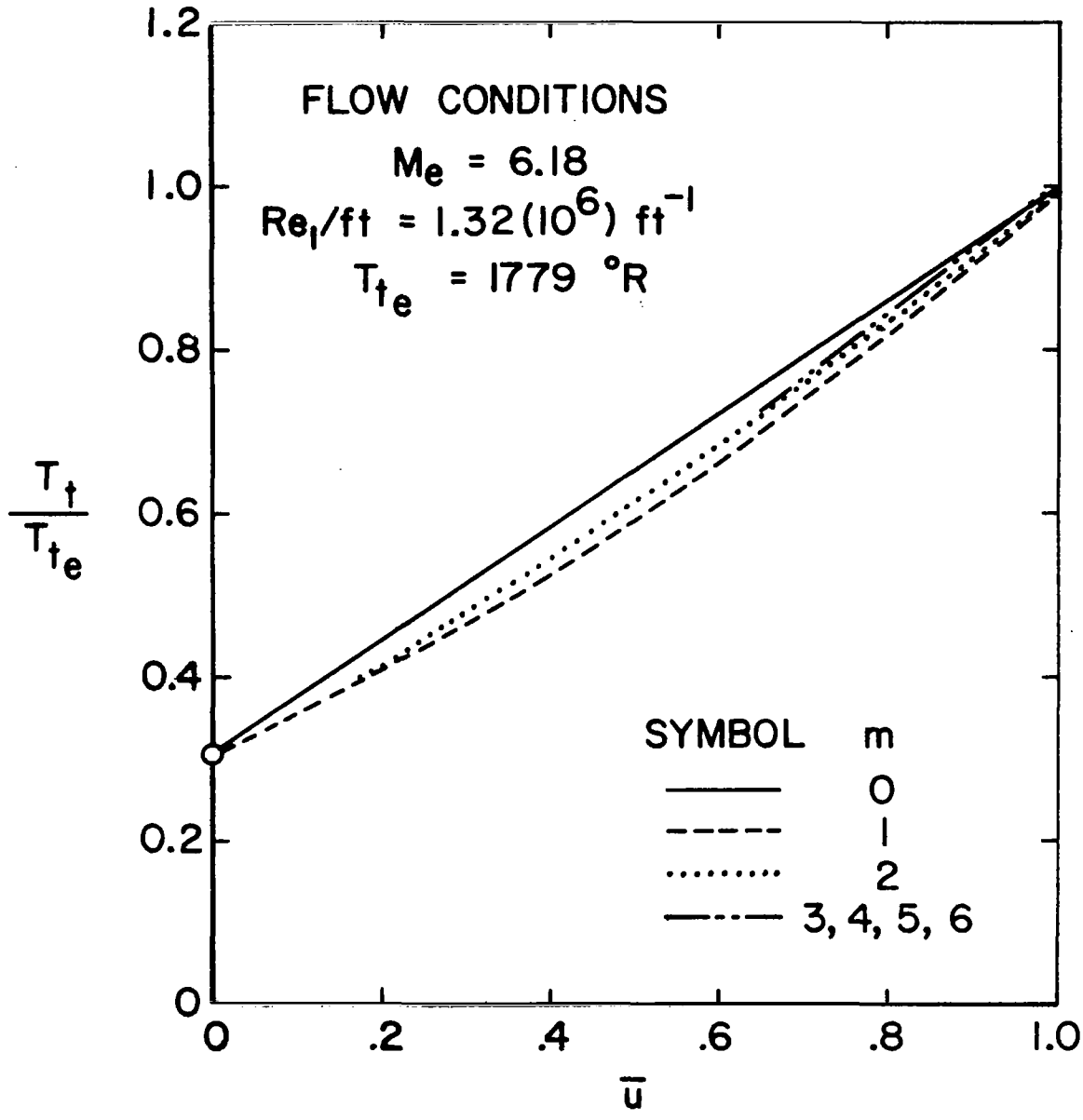


Figure 5.- Variation of total temperature in a laminar boundary layer for different orders of approximation.

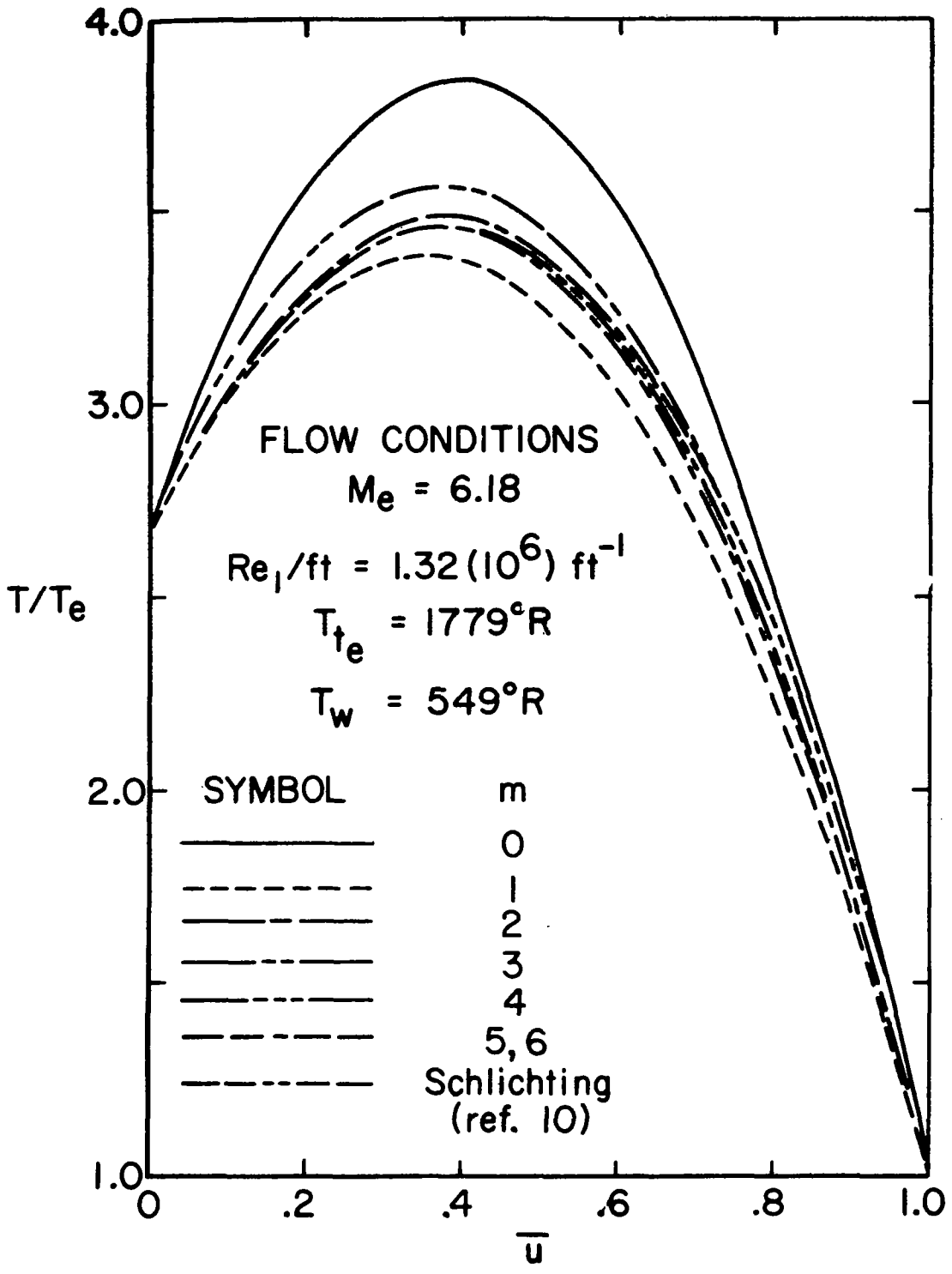


Figure 6.- Variation of static temperature in a laminar boundary layer for different orders of approximation.

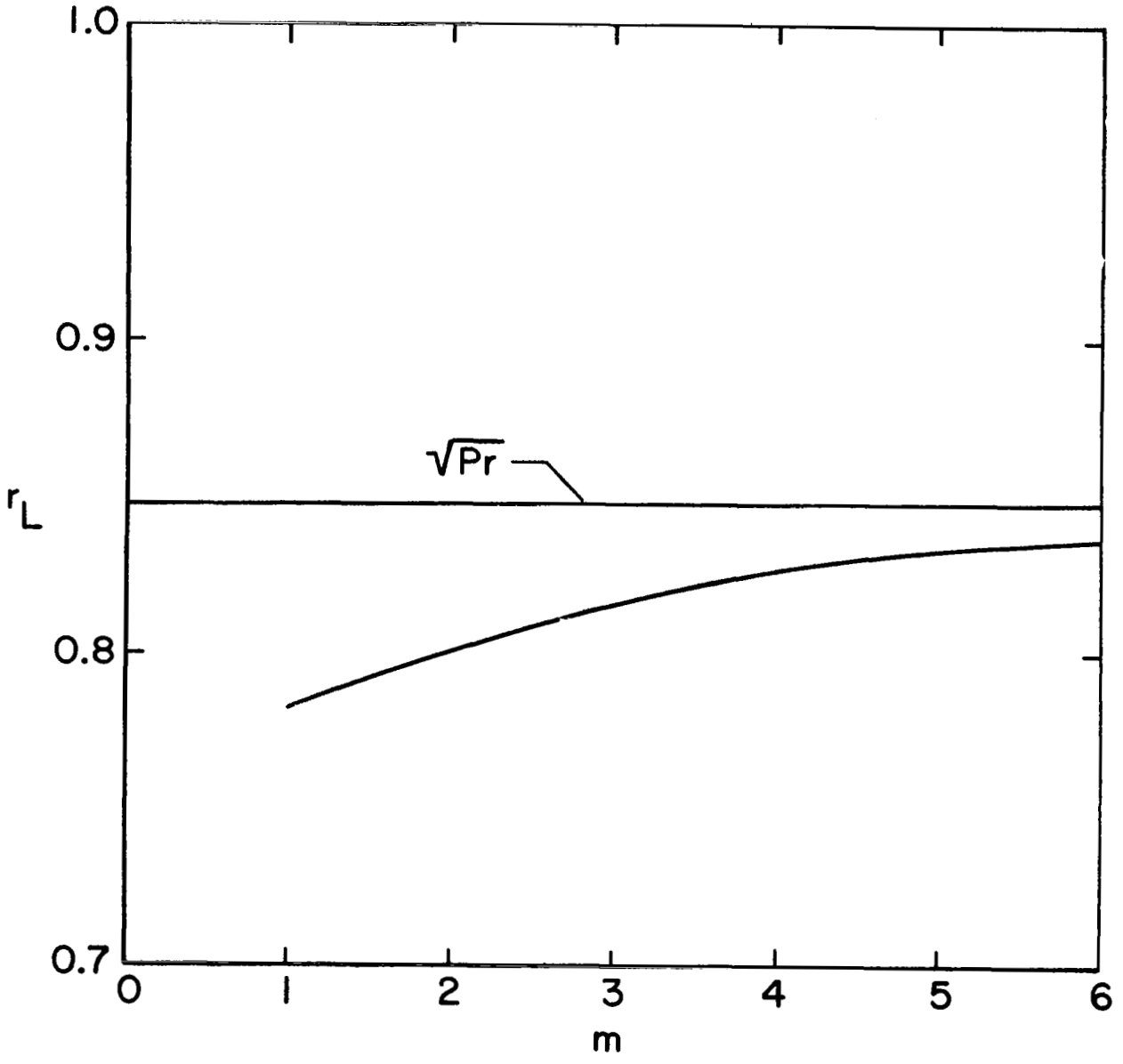


Figure 7.- Variation of laminar recovery factor with order of approximation of enthalpy function.

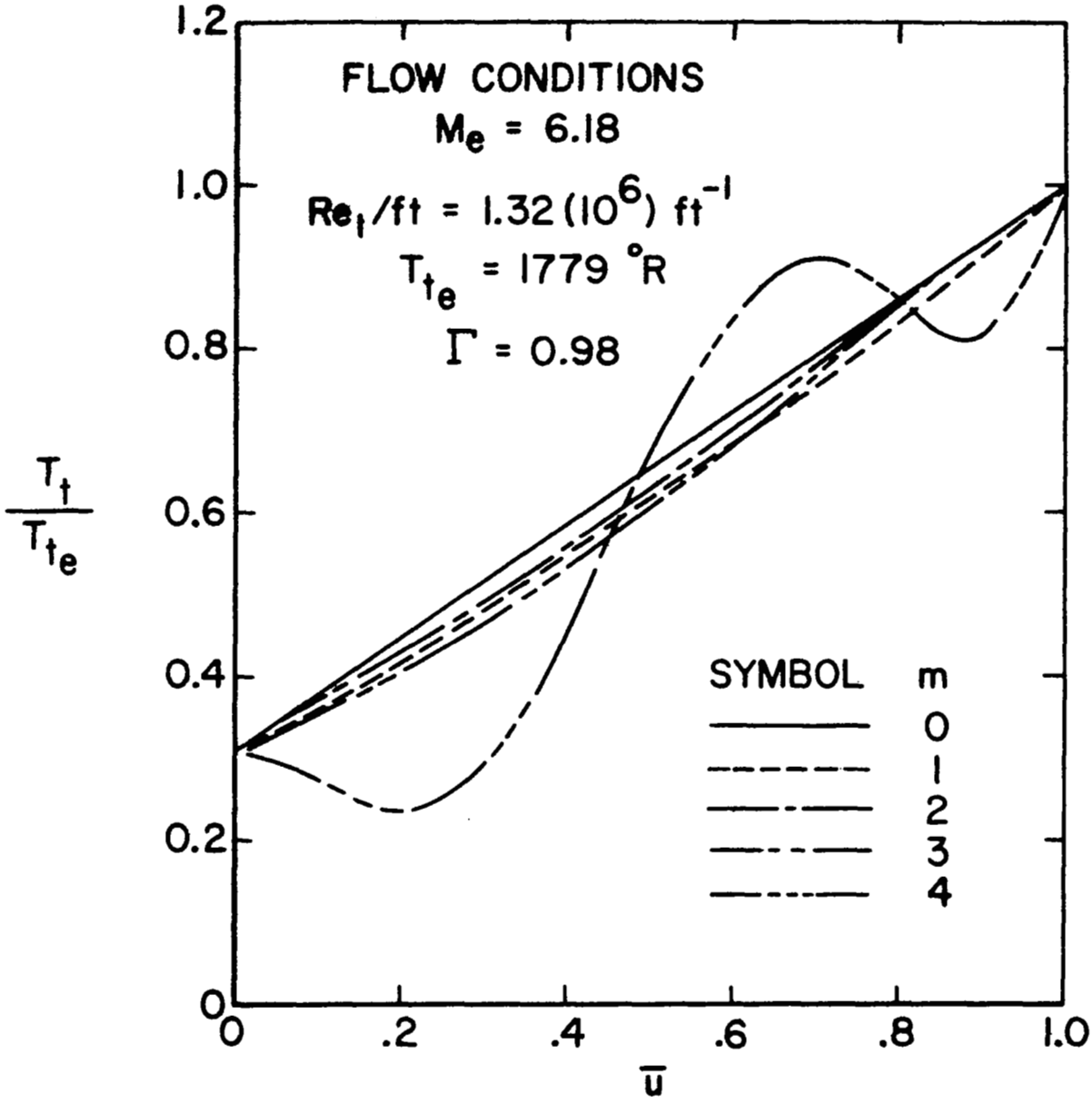


Figure 8.- Variation of total temperature in a nearly turbulent boundary layer for different orders of approximation.

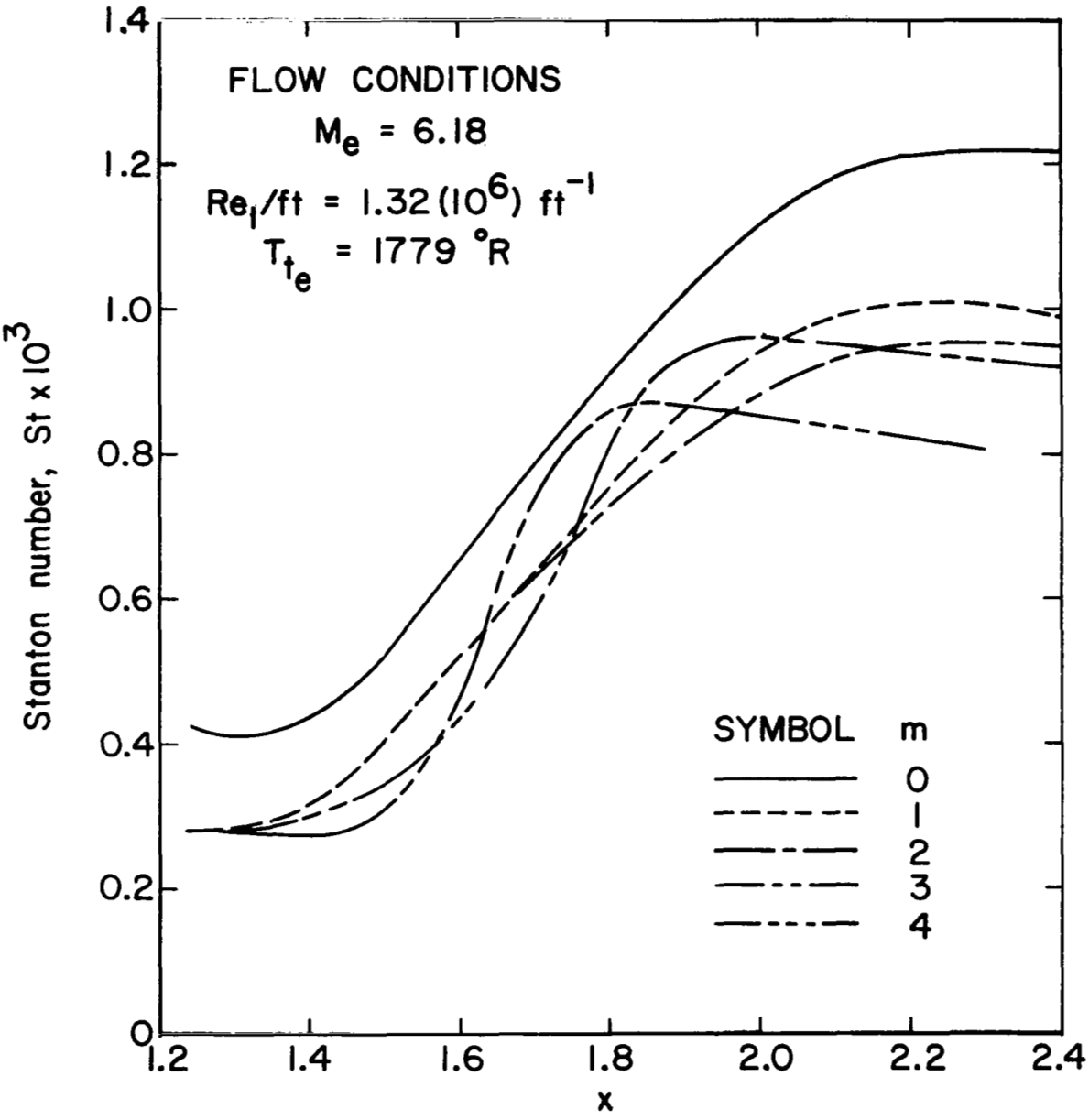


Figure 9.- Stanton number distribution in a transitional boundary layer for various orders of approximation of the enthalpy profile.

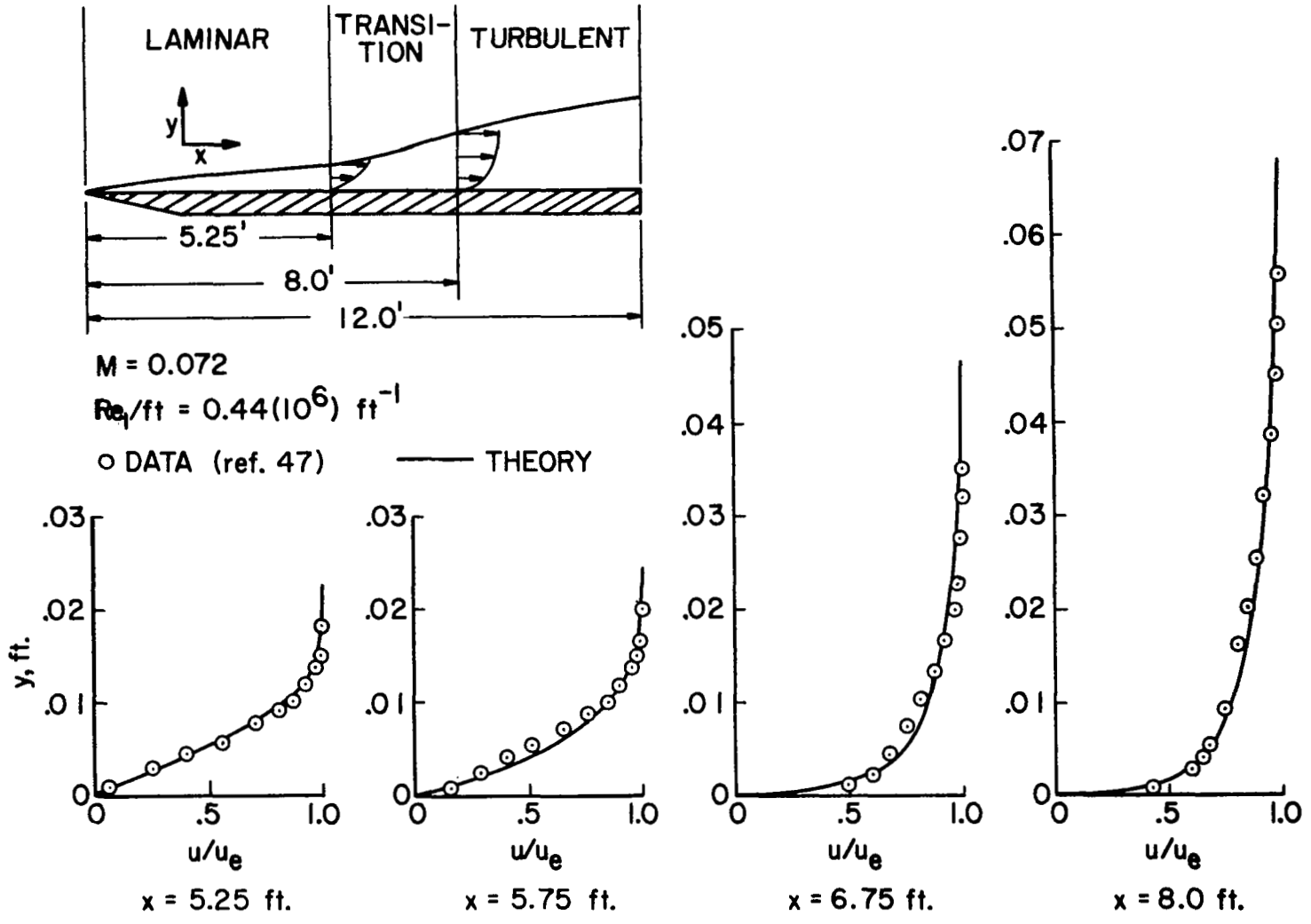


(a) Velocity profiles.

Figure 10.- Comparison of theoretical and experimental quantities in transitional flow on a flat plate.

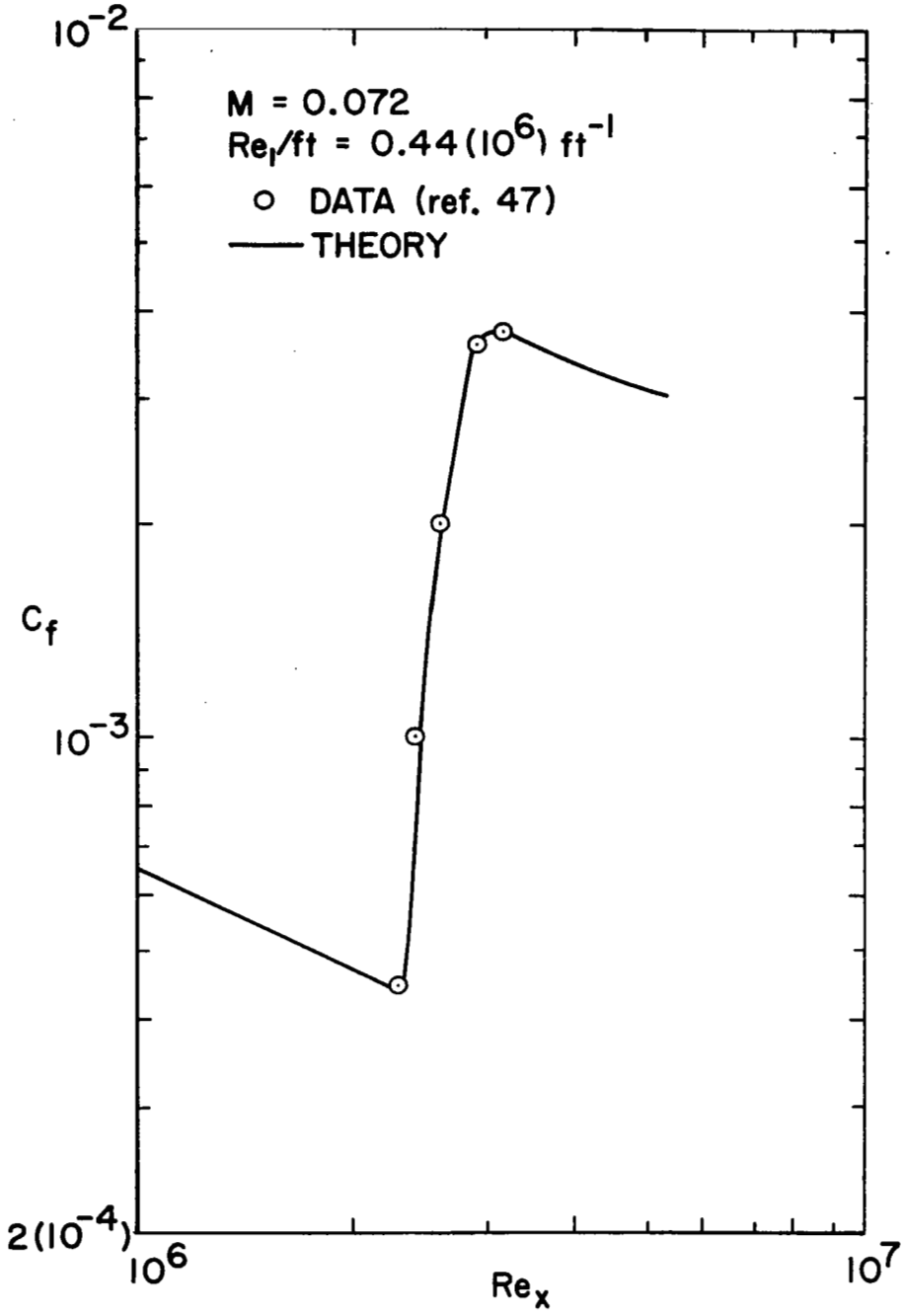


(b) Skin-friction coefficient.

Figure 10.- Concluded.

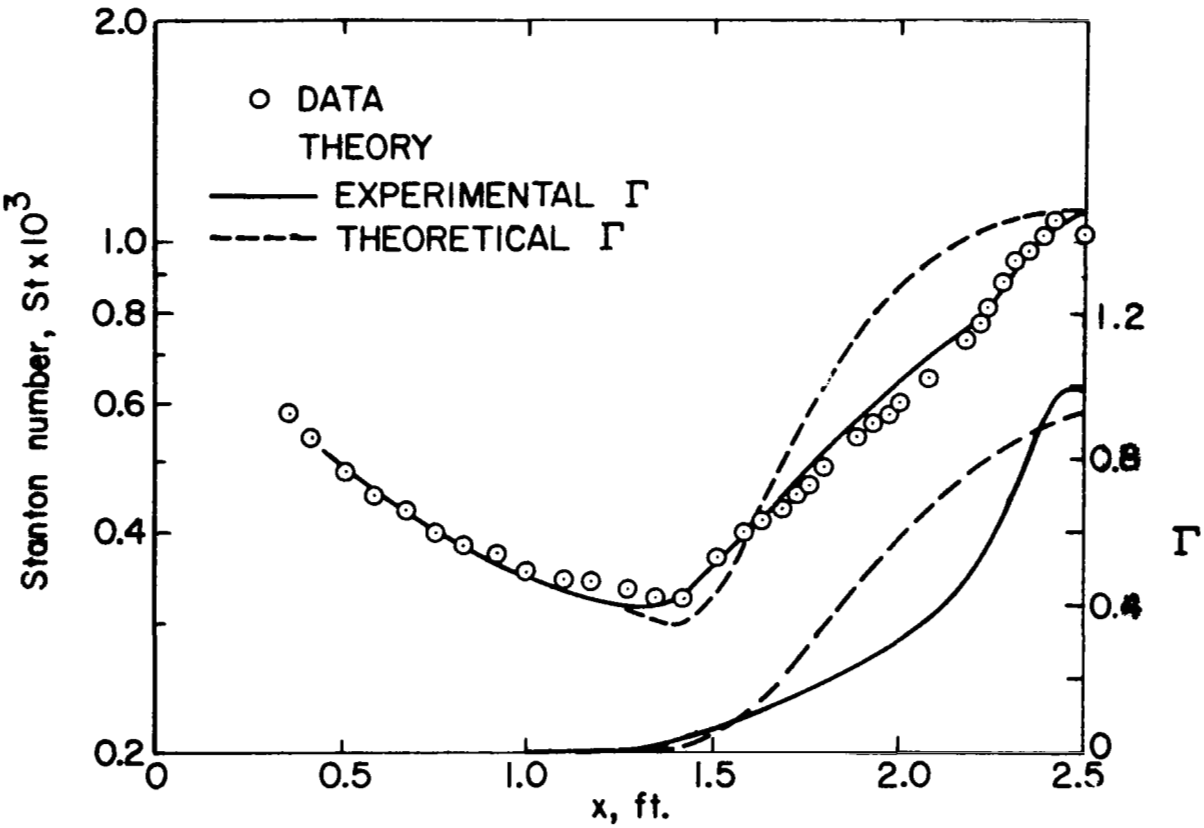


(a) $M_e = 6.18$, $Re_1 = 1.32(10^6)$ $ft^{-1}$, $T_t = 1860^oR$, $T_w = 549^oR$.

Figure 11.- Comparison of theoretical and experimental Stanton number distributions on a sharp-leading-edge flat plate.

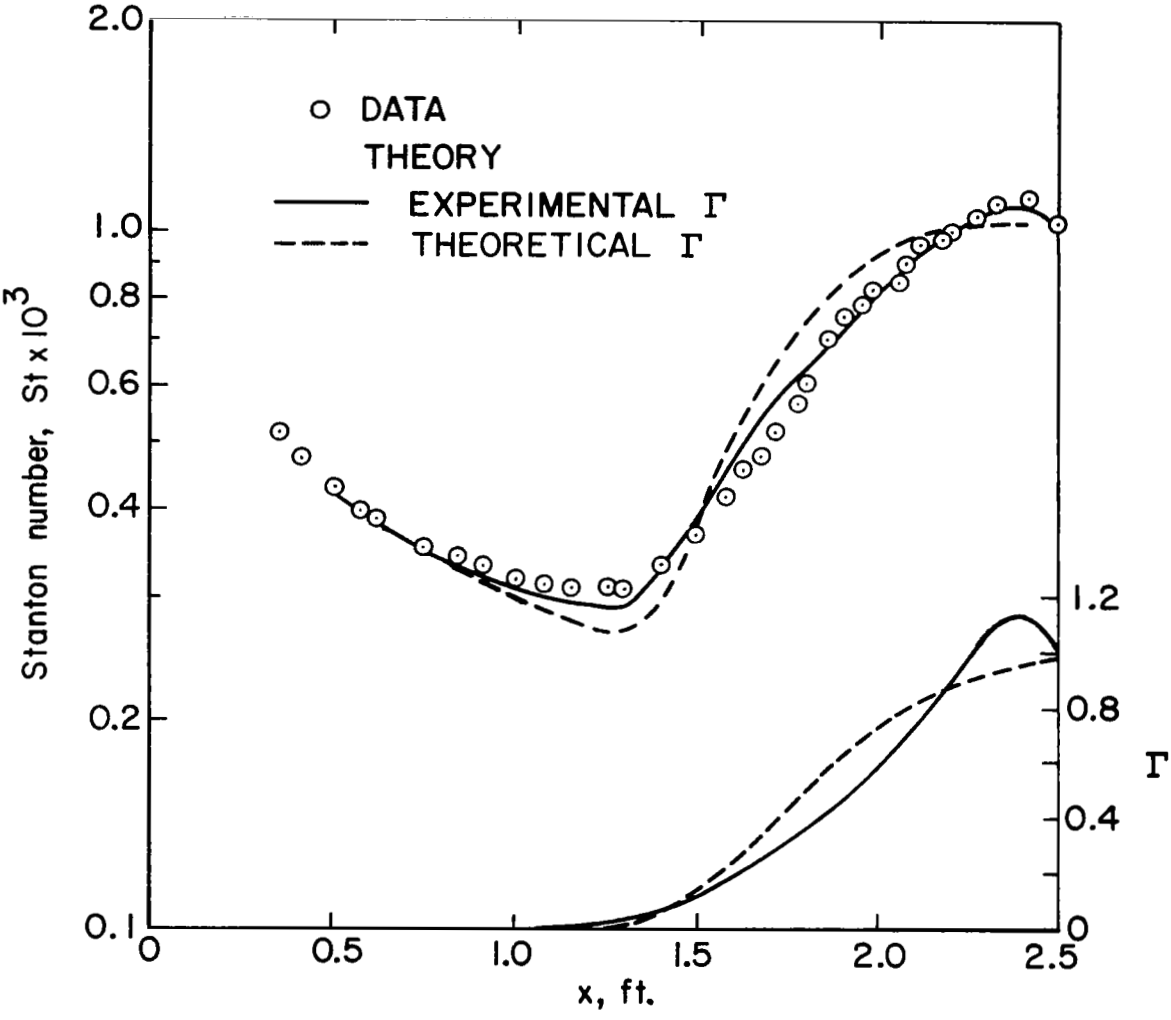


(b) $M_e$ = 6.18, $Re_1$ = 1.63($10^6$) $ft^{-1}$, $T_t$ = 1815°R, $T_w$ = 552°R.

Figure 11.- Continued.

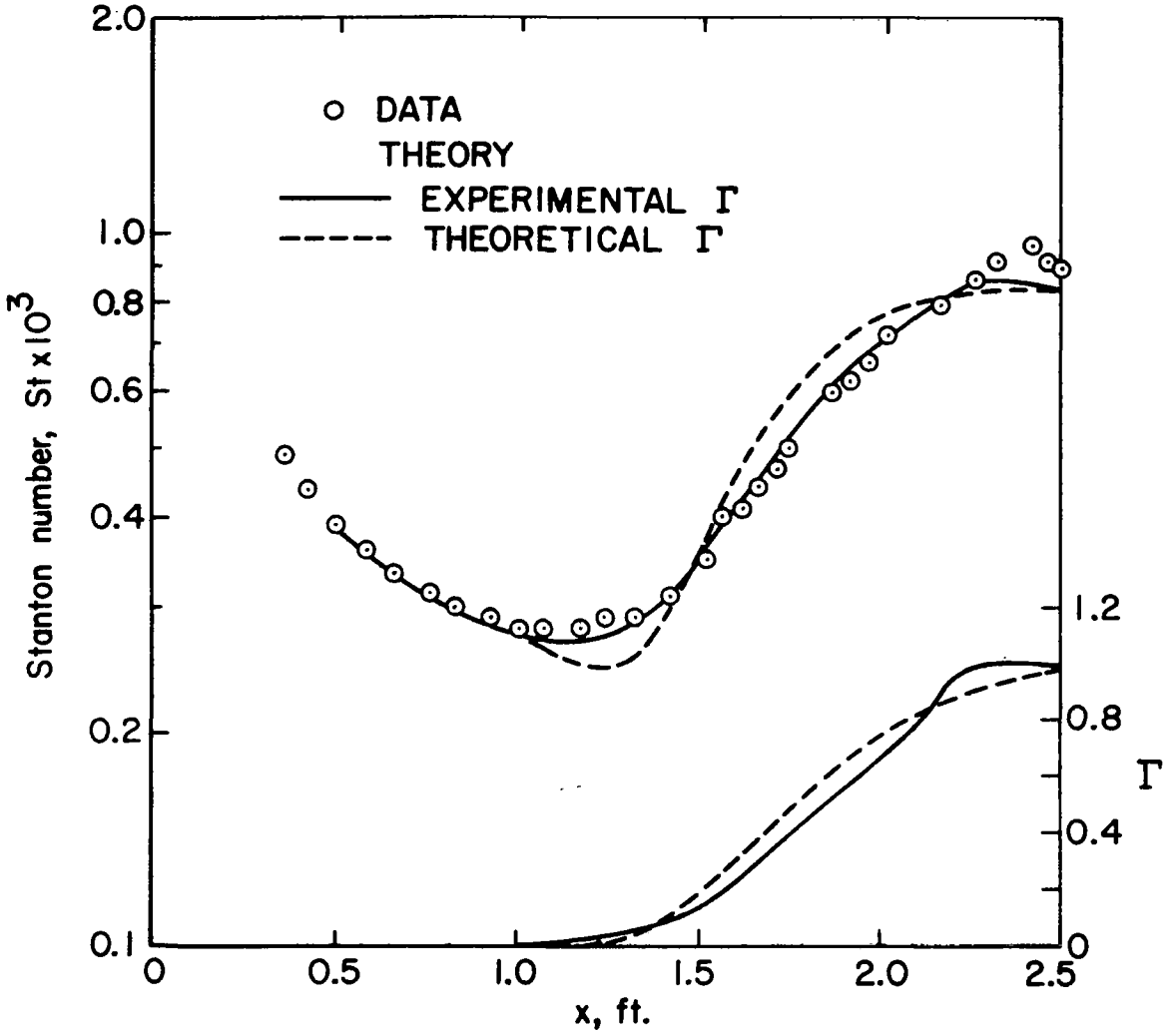


(c) $M_e$ = 7.45, $Re_1$ = 2.03($10^6$) $ft^{-1}$, $T_t$ = 1829°R, $T_w$ = 553°R.

Figure 11.- Concluded.

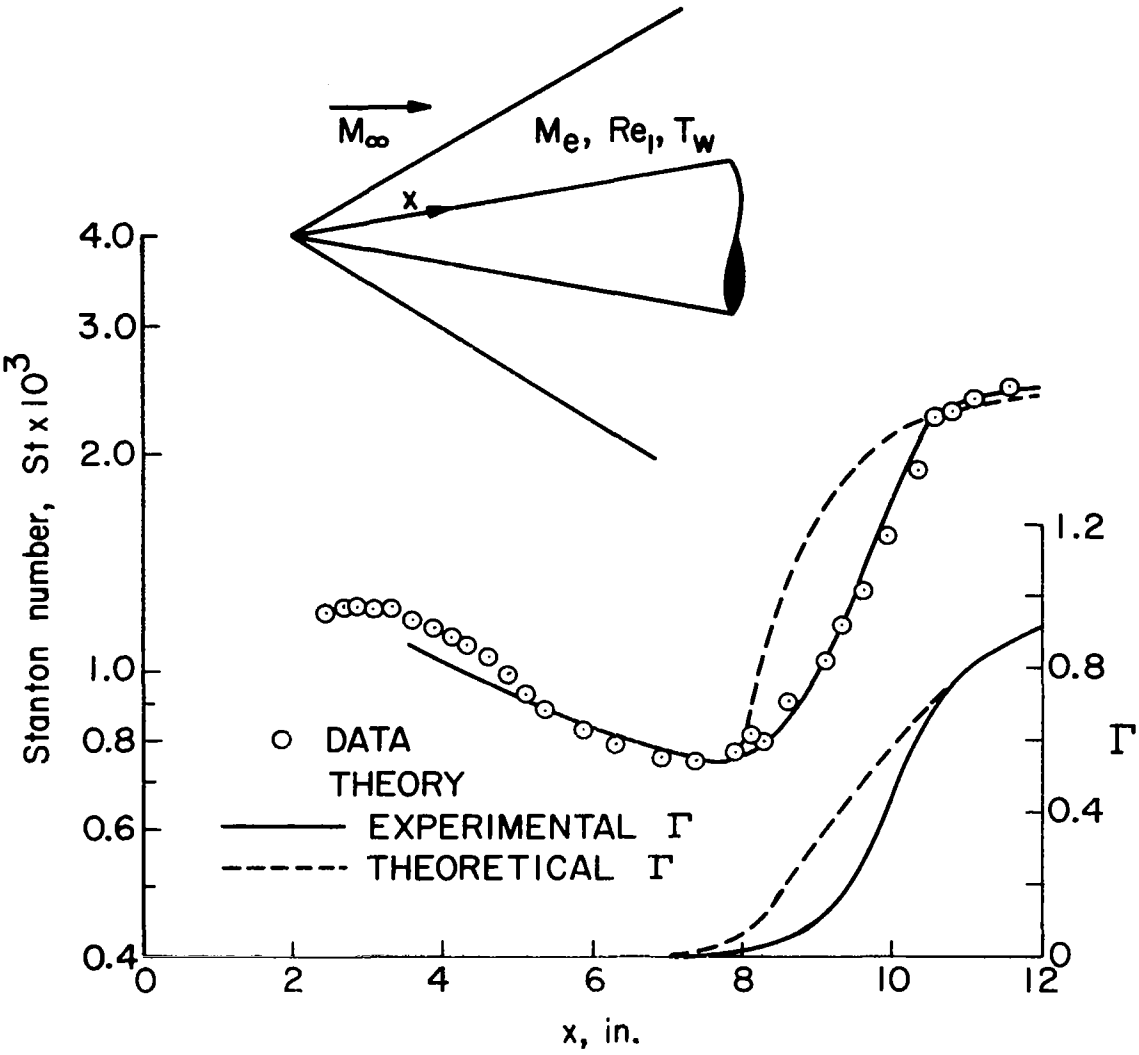


(a) $Re_1 = 6.69(10^6)$ $ft^{-1}$, $T_t = 1040^\circ R$, $T_w = 551^\circ R$.

Figure 12.- Comparison between theoretical and experimental Stanton number distributions on a sharp-nosed cone at $M_\infty = 7$.

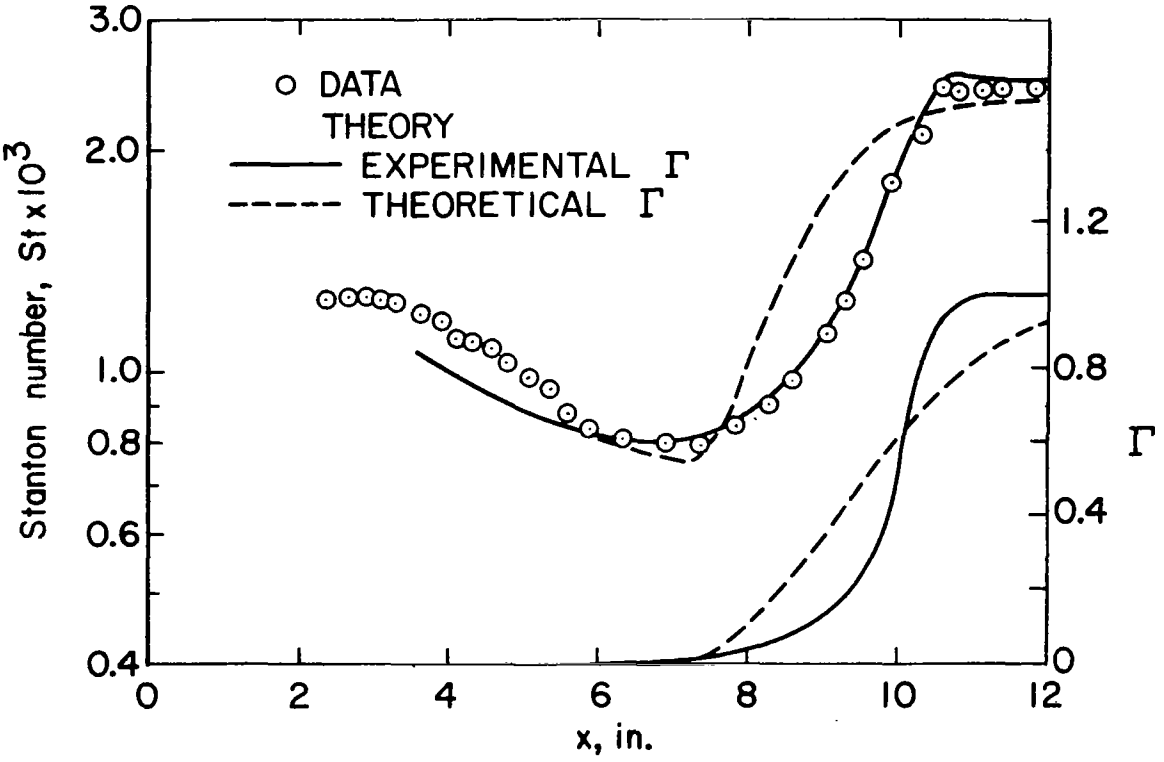


(b) $Re_1 = 7.01(10^6)$ $ft^{-1}$, $T_t = 1070^{\circ}R$, $T_w = 556^{\circ}R$.

Figure 12.- Continued.

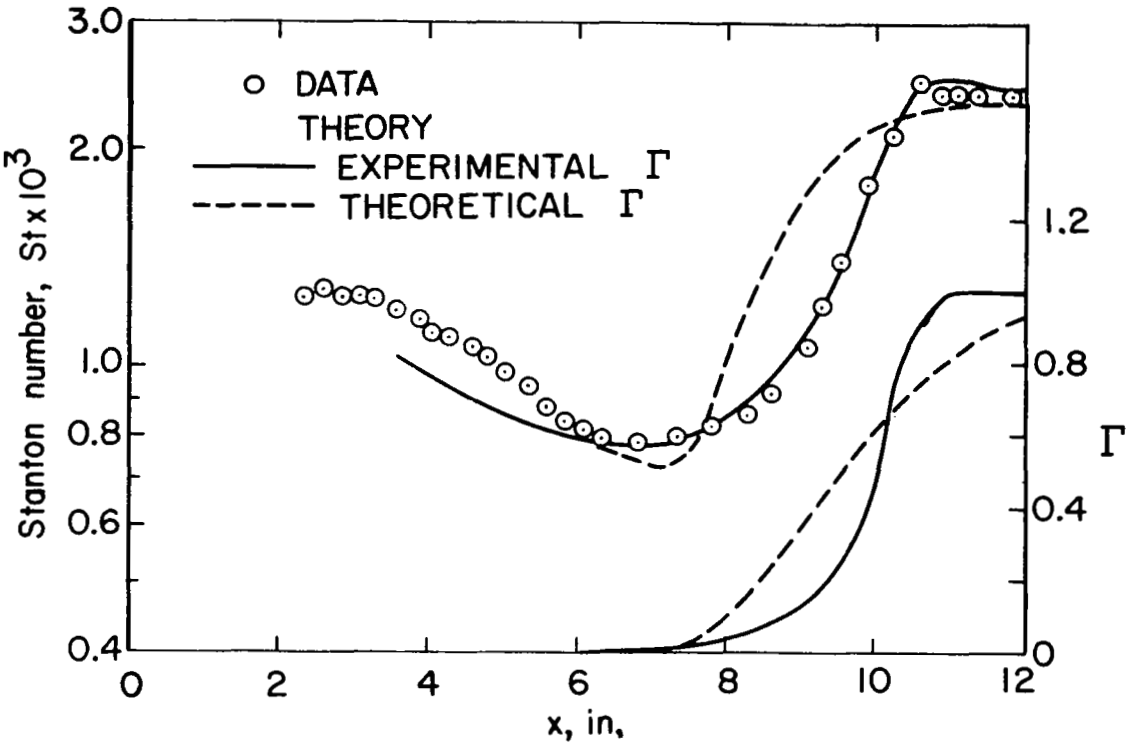


(c) $Re_1 = 7.48(10^6)$ $ft^{-1}$, $T_t = 1075^{\circ}R$, $T_w = 548^{\circ}R$.

Figure 12.- Concluded.

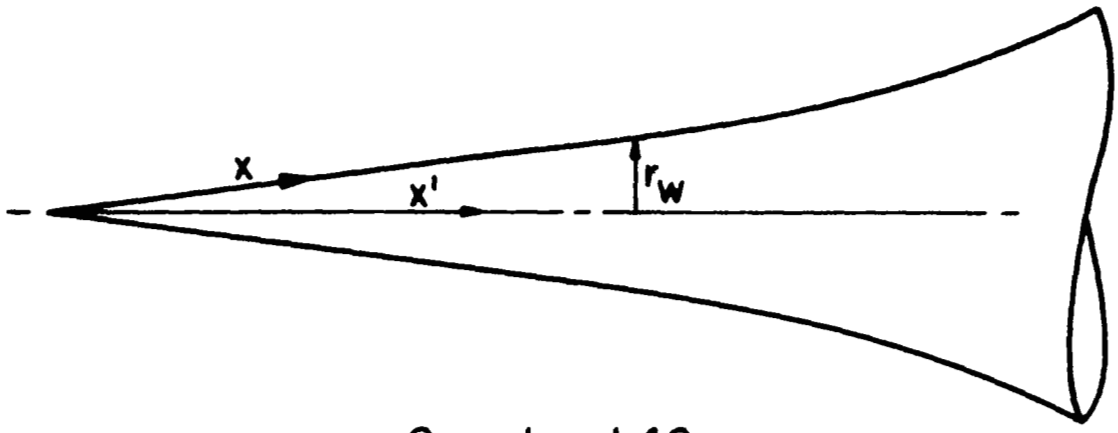


$$0 \leq x' \leq 1.46$$

$$r_w = 0.1318\, x'$$

$$0 \leq x' \leq 2.33$$

| $x'$ | $r_w$ |
|---|---|
| 1.5 | 0.1977 |
| 1.5833 | .2092 |
| 1.6667 | .2258 |
| 1.75 | .2458 |
| 1.8333 | .2683 |
| 1.9167 | .2933 |
| 2.0 | .3217 |
| 2.0833 | .3517 |
| 2.1667 | .3883 |
| 2.25 | .4267 |
| 2.33 | .4683 |

Figure 13.- Cone-flare configuration.

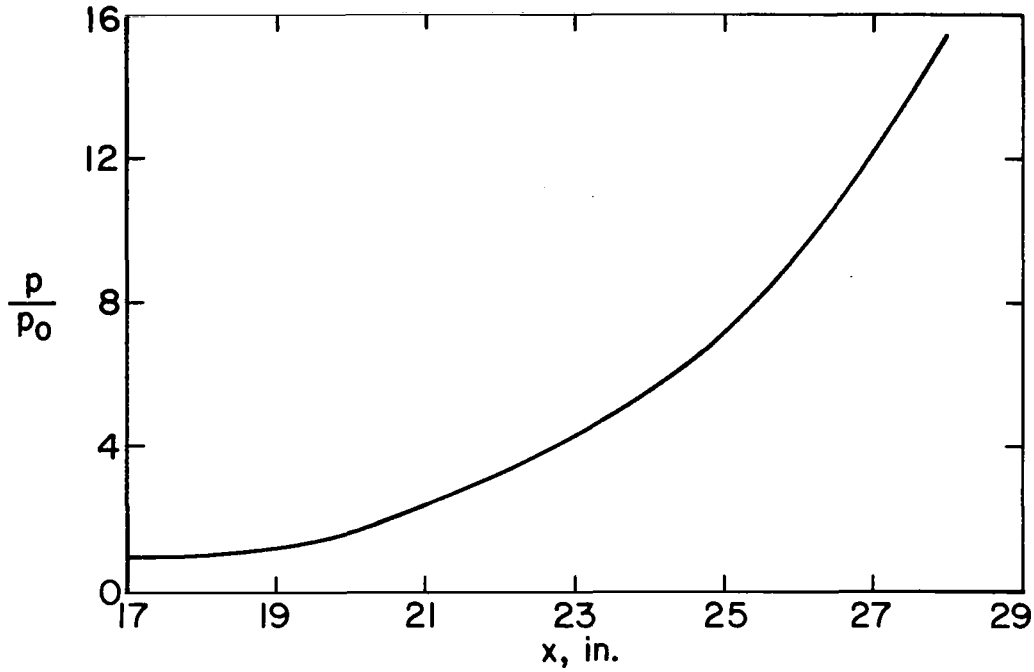


(a) Pressure distribution on the flare.

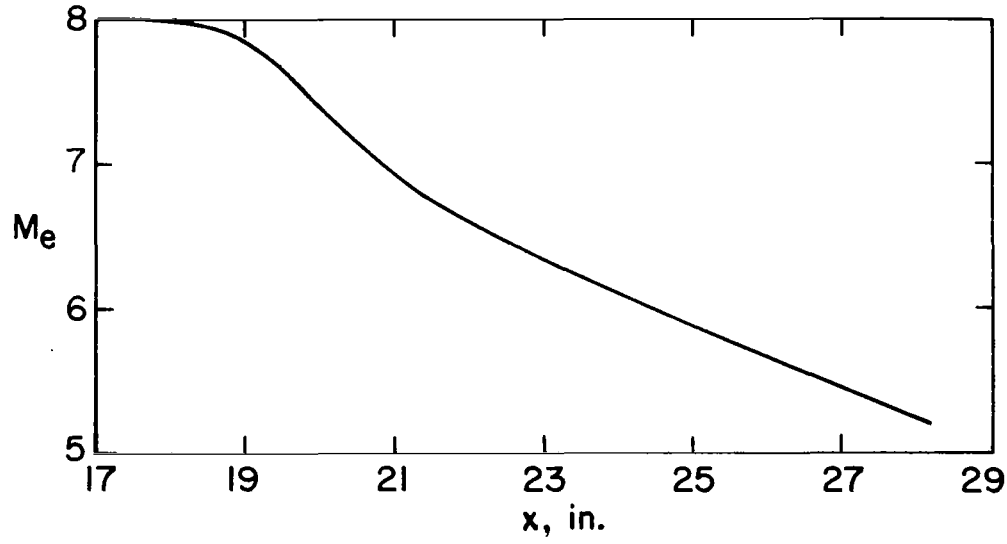


(b) Mach number on the flare.

Figure 14.- Conditions at the edge of the boundary layer on an axisymmetric cone-flare.

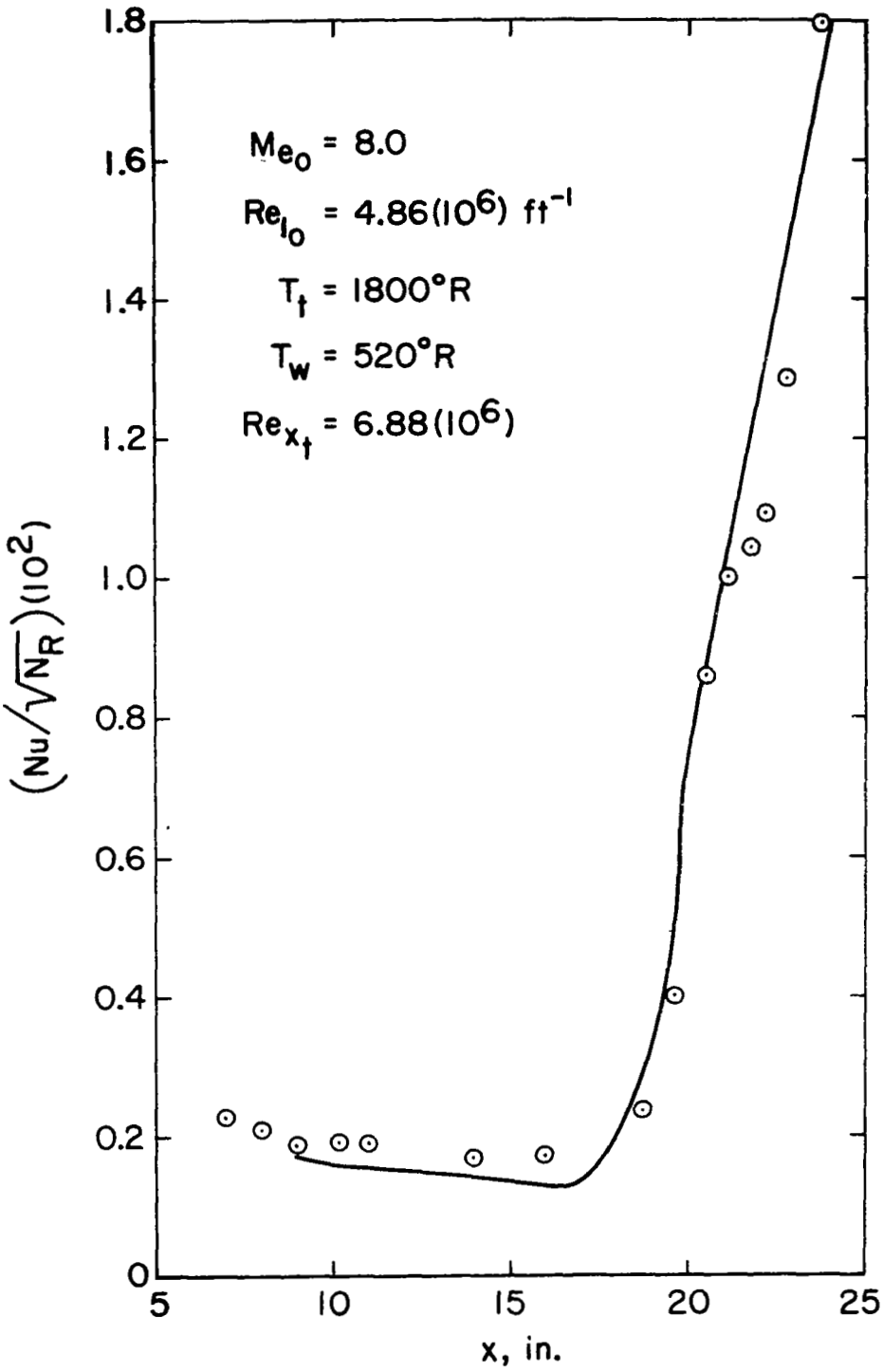


Figure 15.- Comparison between the predicted and experimental heat transfer distributions on a cone-flare.

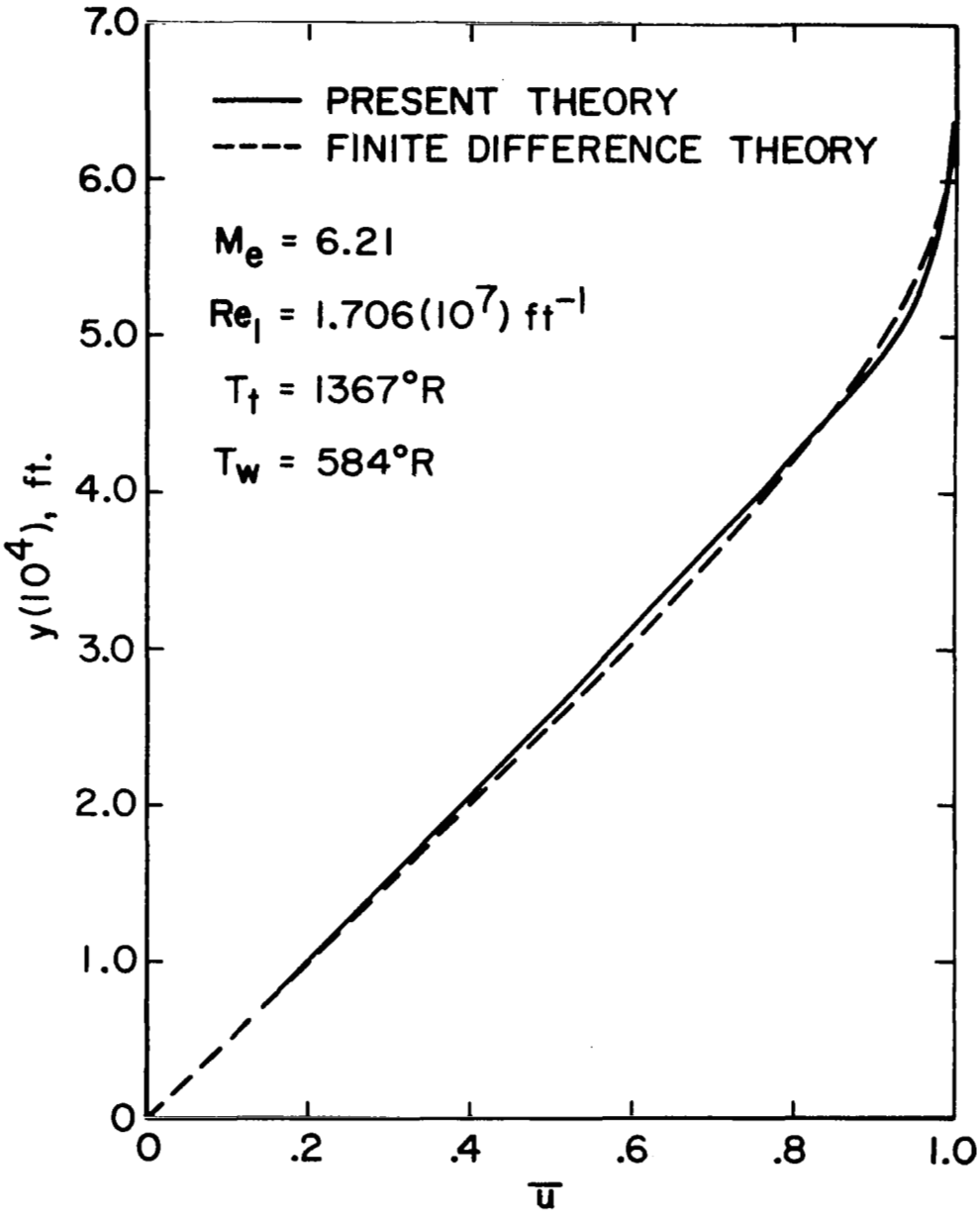


(a) Initial velocity profile (x = 0.1 ft.).

Figure 16.- Comparison of two theoretical calculations of the boundary layer on a sharp cone.

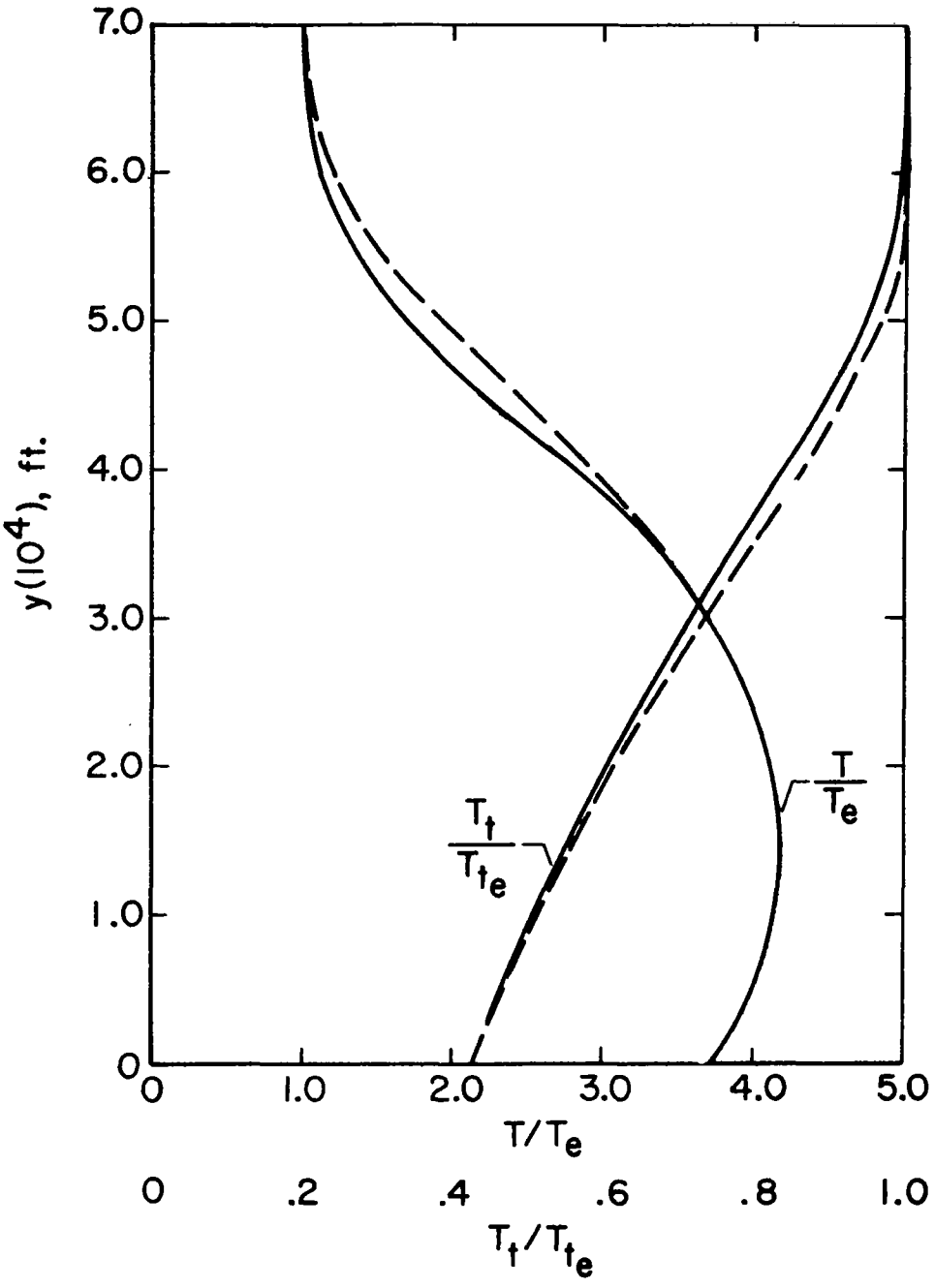


(b) Initial static and total temperature profiles in the boundary layer (x = 0.1 ft.).

Figure 16.- Continued.

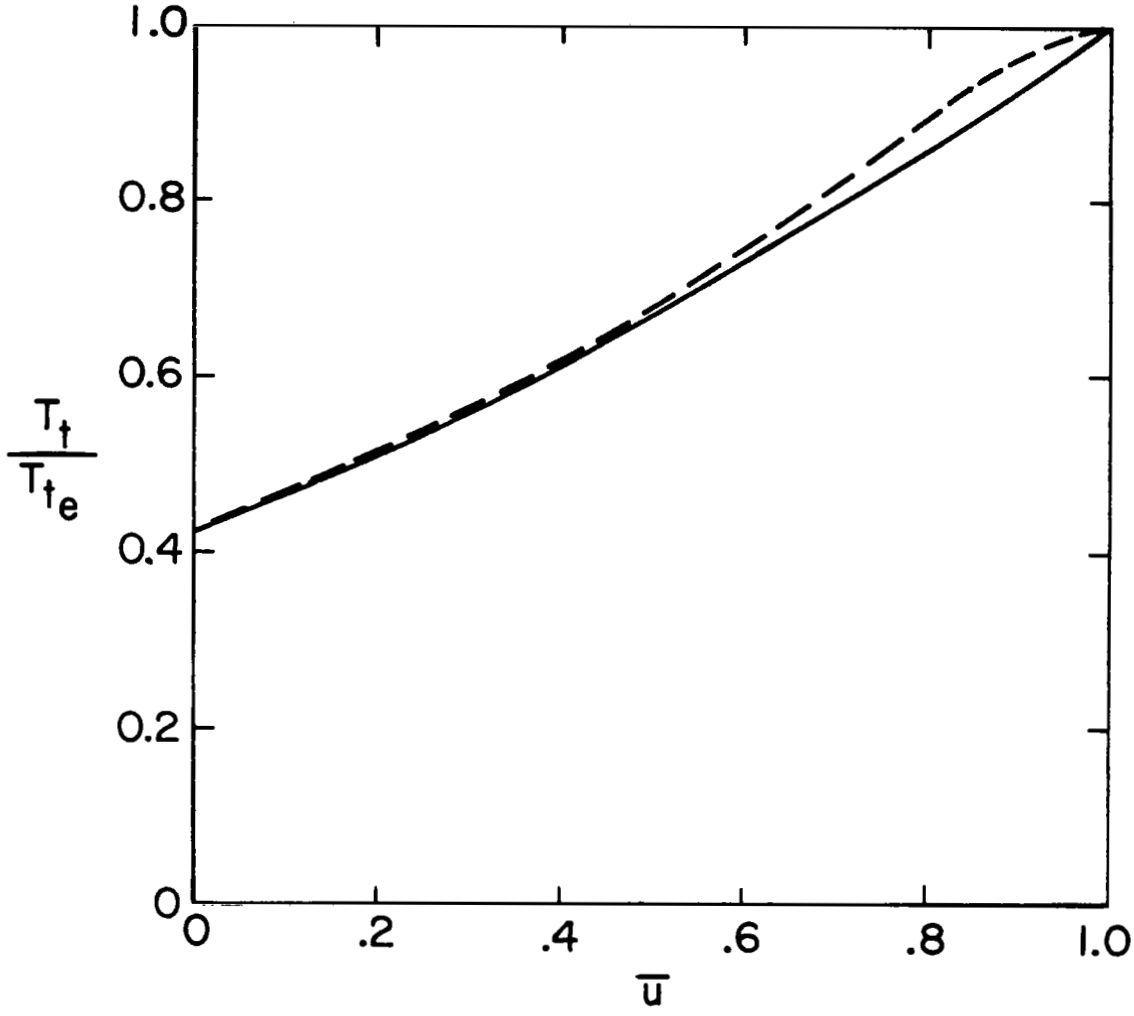


(c) Initial total temperature profiles (x = 0.1 ft.).

Figure 16.- Continued.

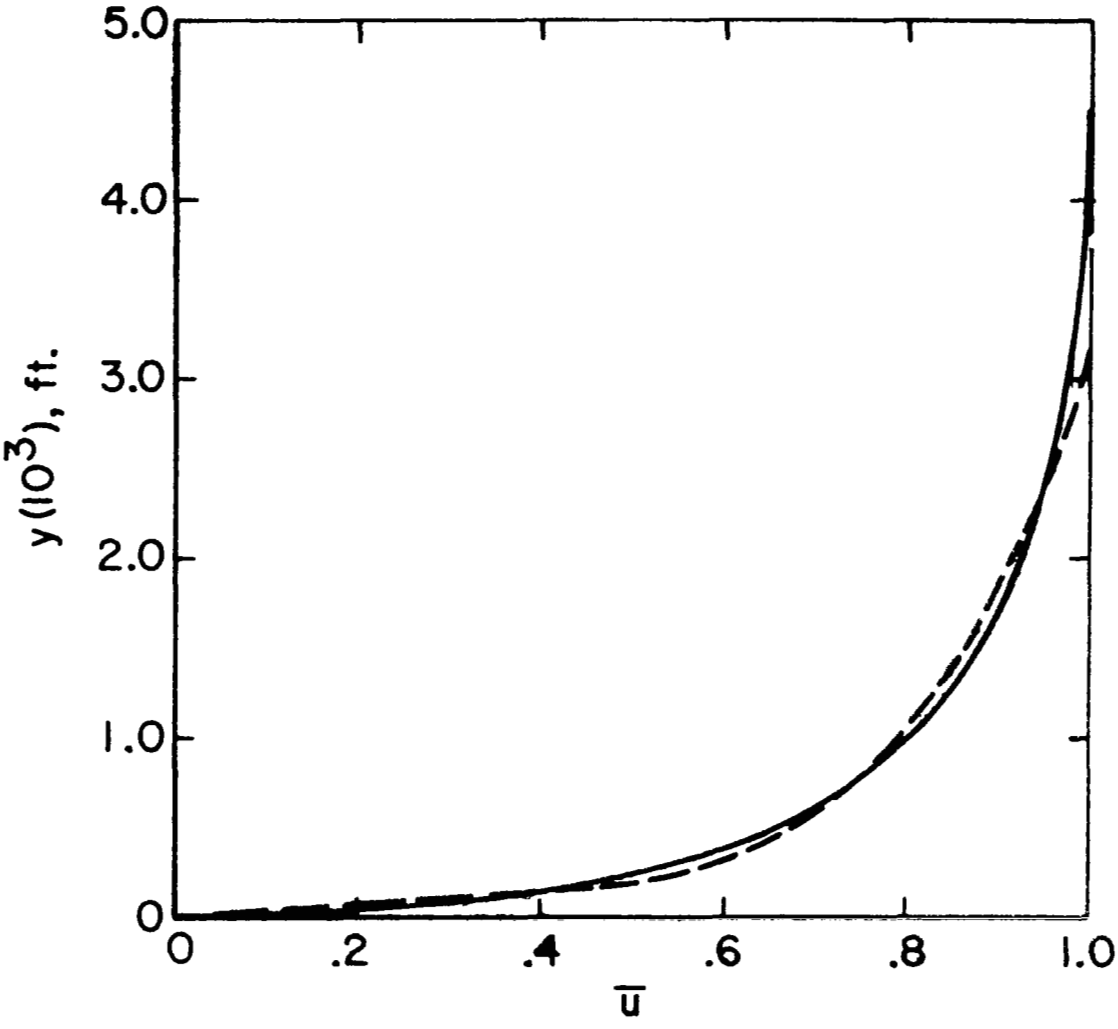


(d) Velocity profile at end of transition (x = 0.5 ft.).

Figure 16.- Continued.

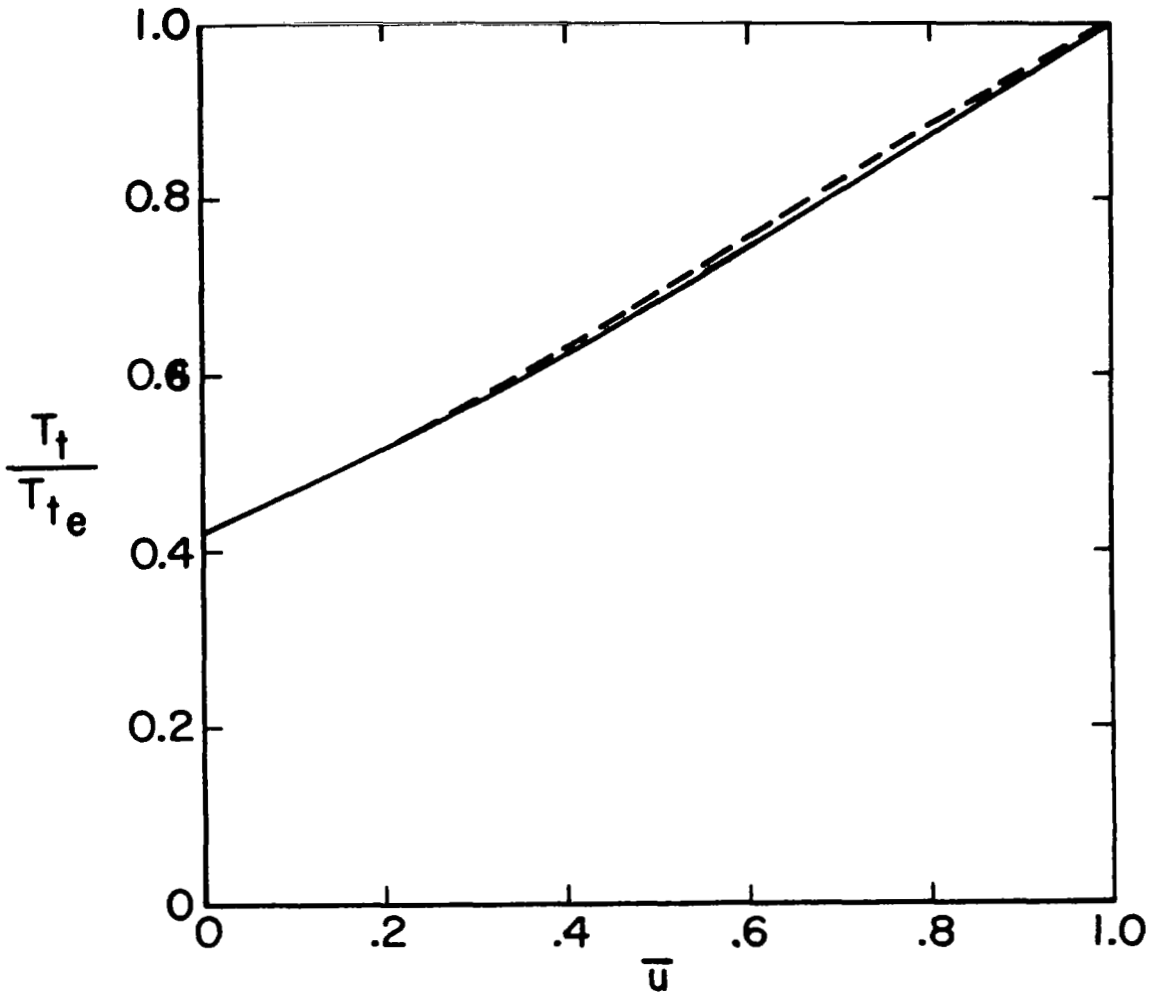


(e) Total temperature profile at end of transition (x = 0.5 ft.).

Figure 16.- Continued.

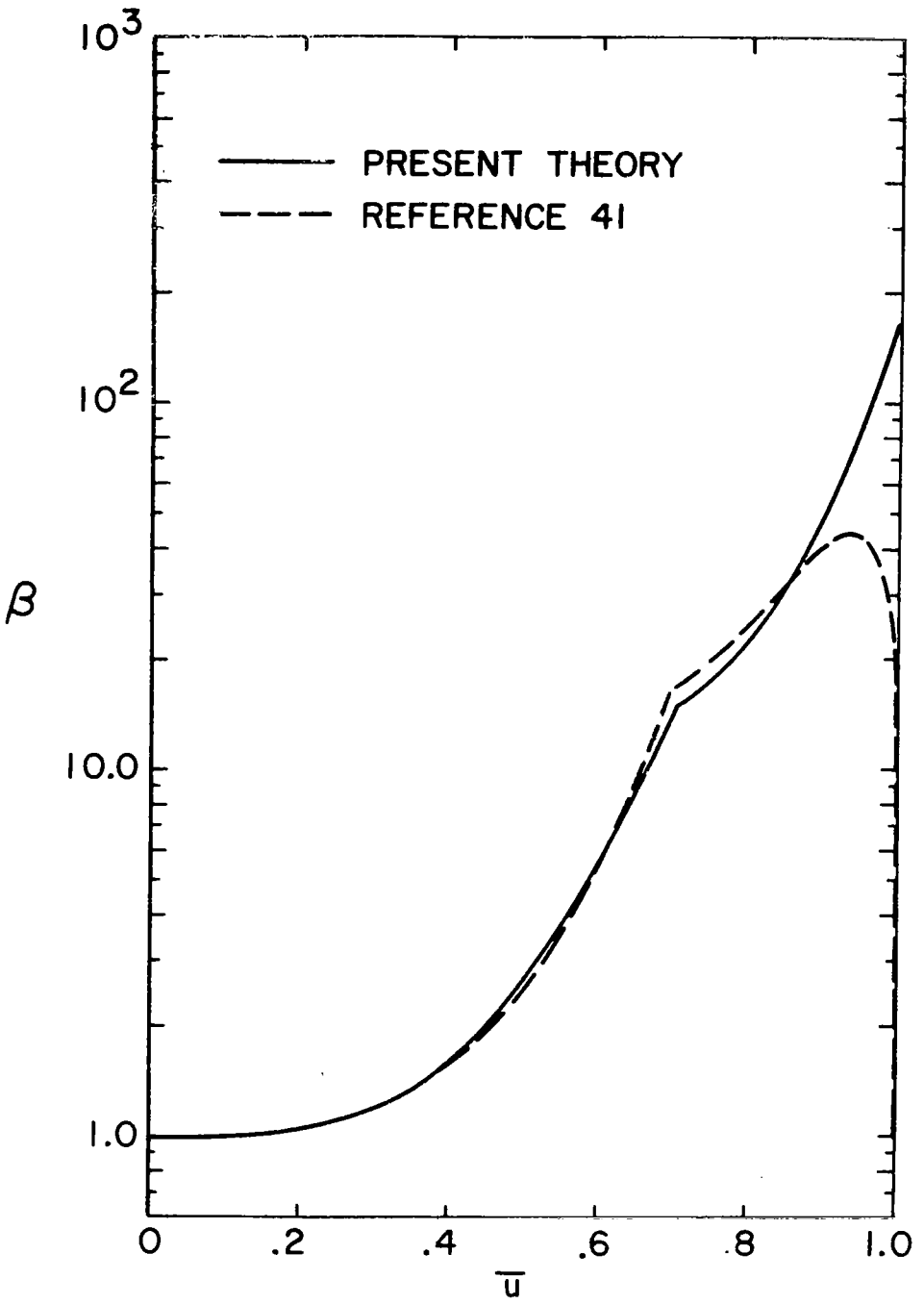


(f) Eddy viscosity at end of transition (x = 0.5 ft.).

Figure 16.- Continued.

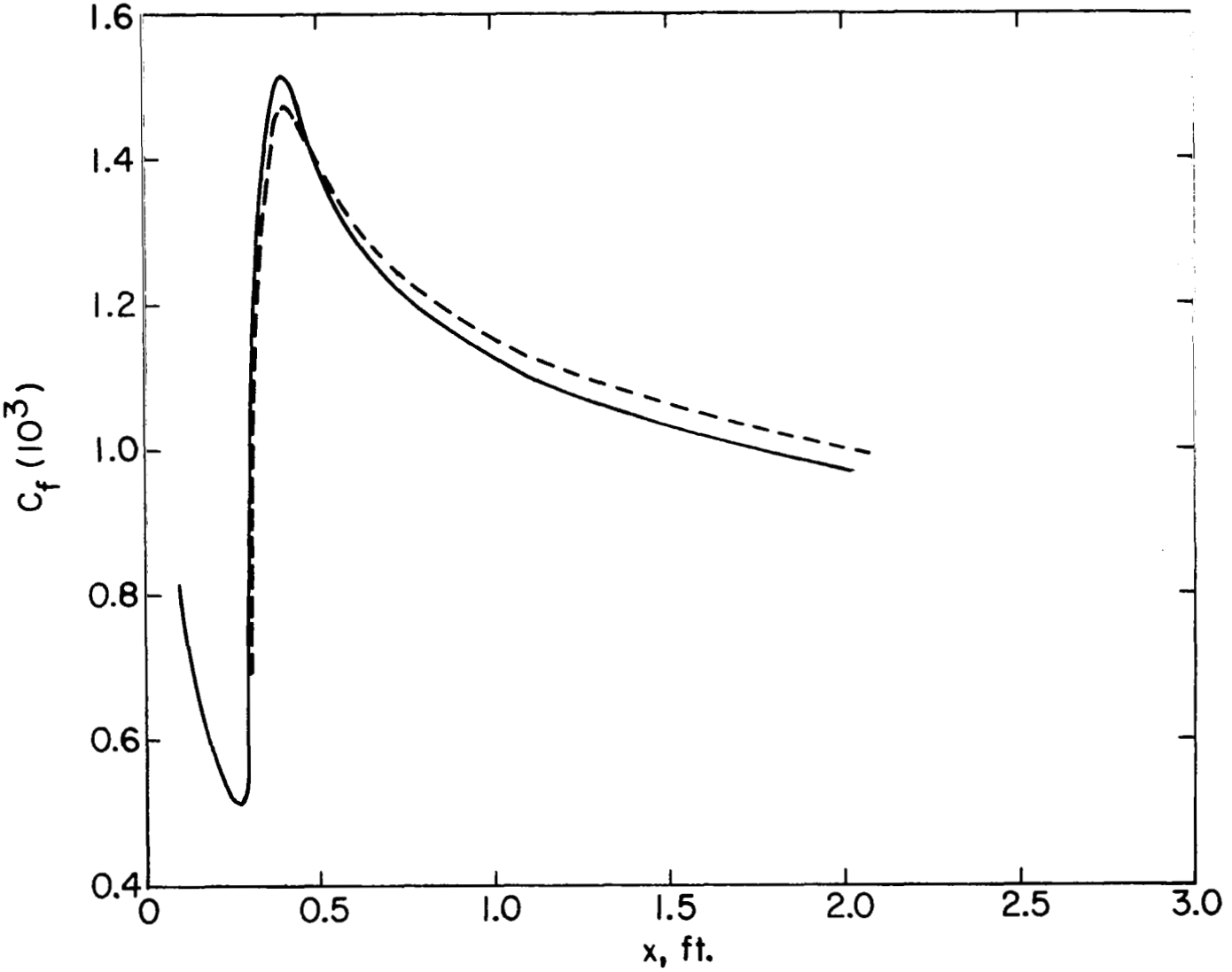


(g) Skin-friction coefficient.

Figure 16.- Continued.

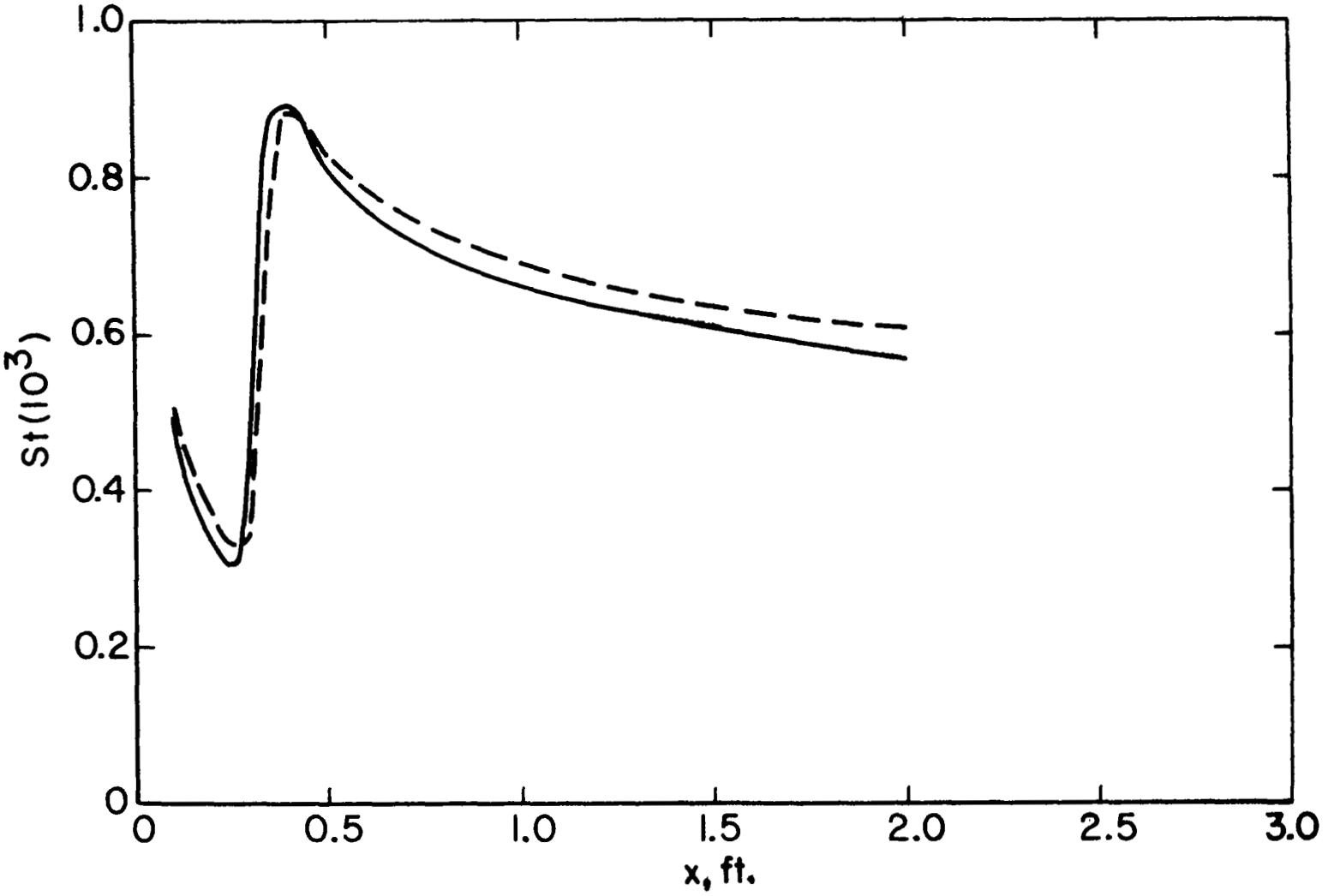


(h) Stanton number.

Figure 16.- Continued.

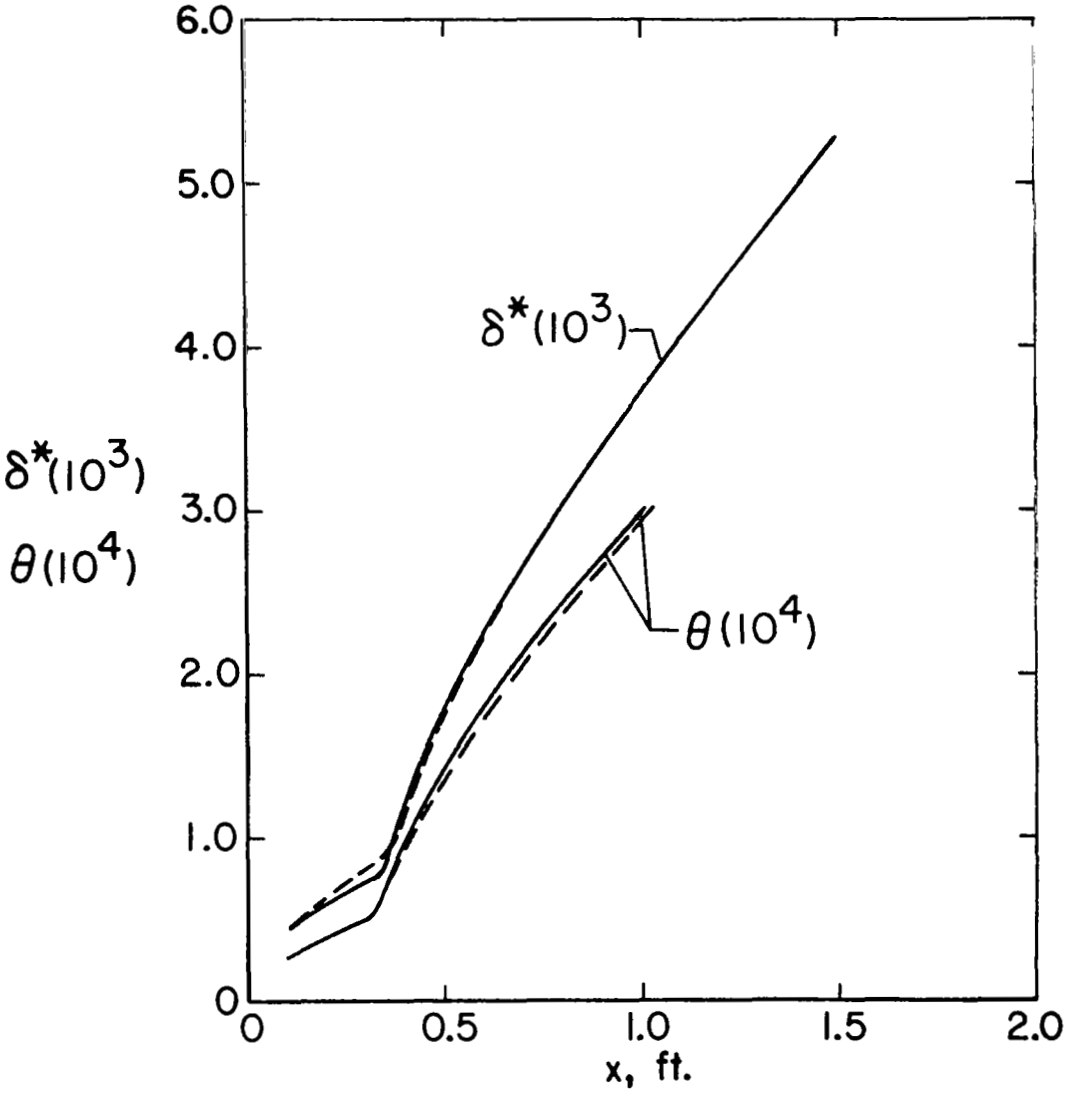


(i) Displacement and momentum thickness, ft.

Figure 16.- Concluded.

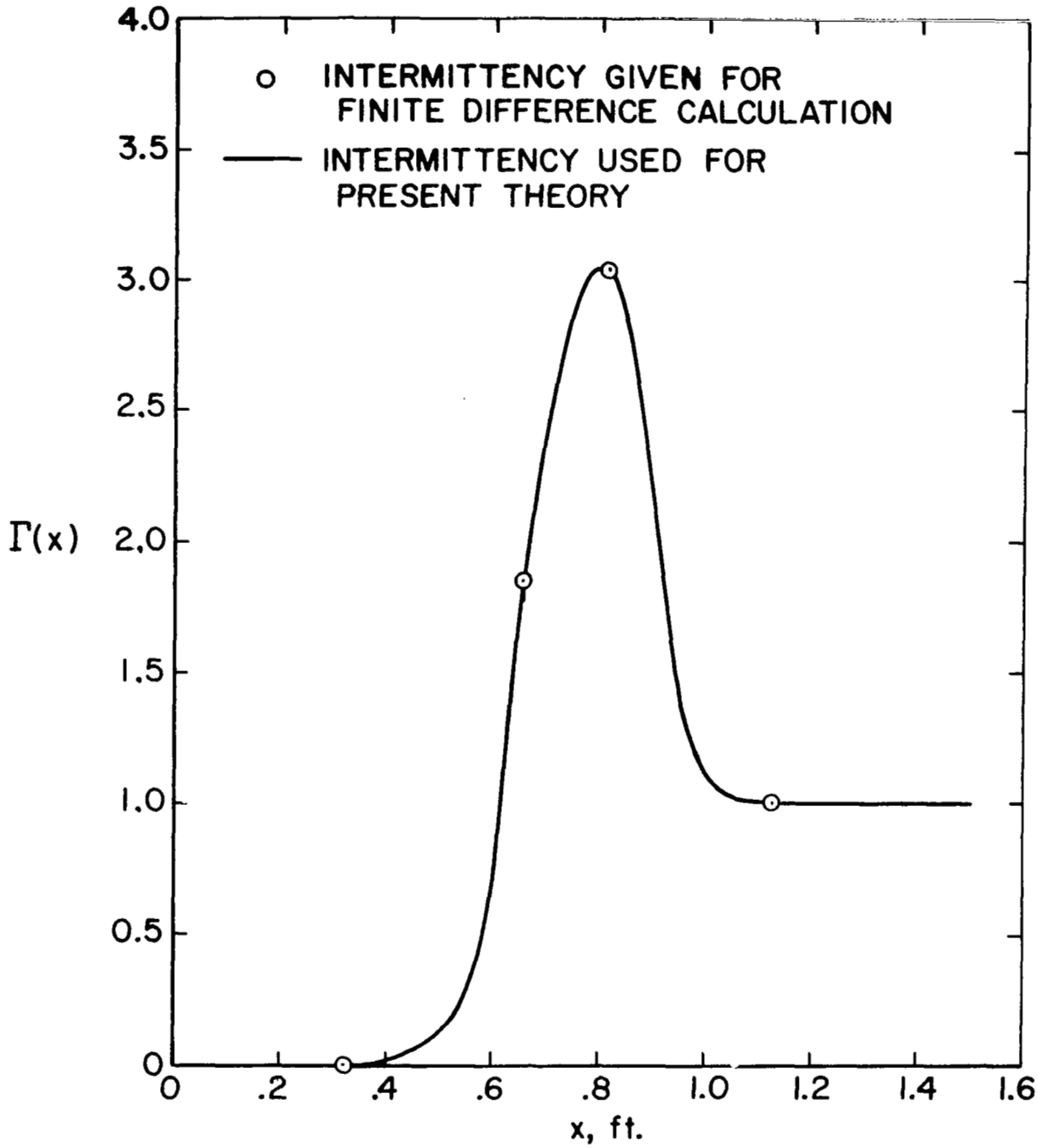


(a) Distribution of intermittency.

Figure 17.- Comparison of finite-difference theory and present theory for different initial conditions on a flat plate.

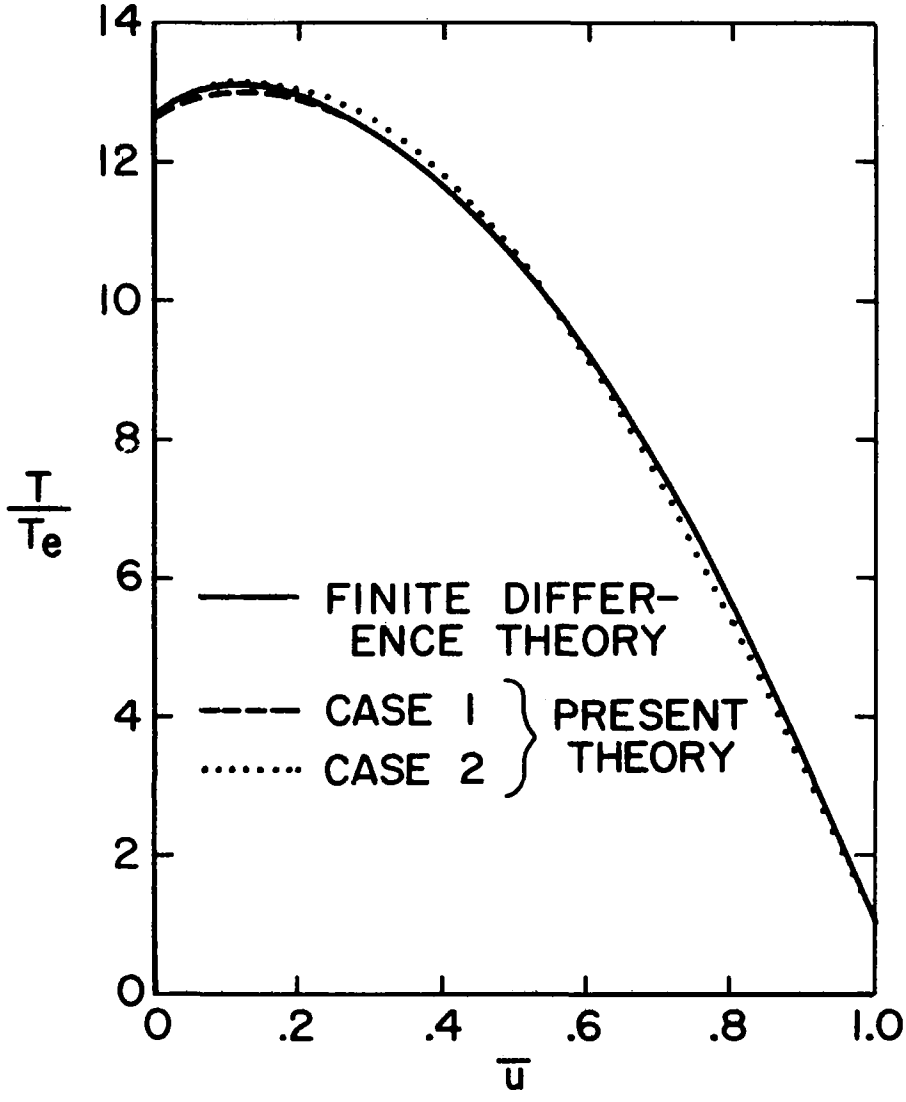


(b) Initial static temperature profiles (x = 0.325 ft.).

Figure 17.- Continued.

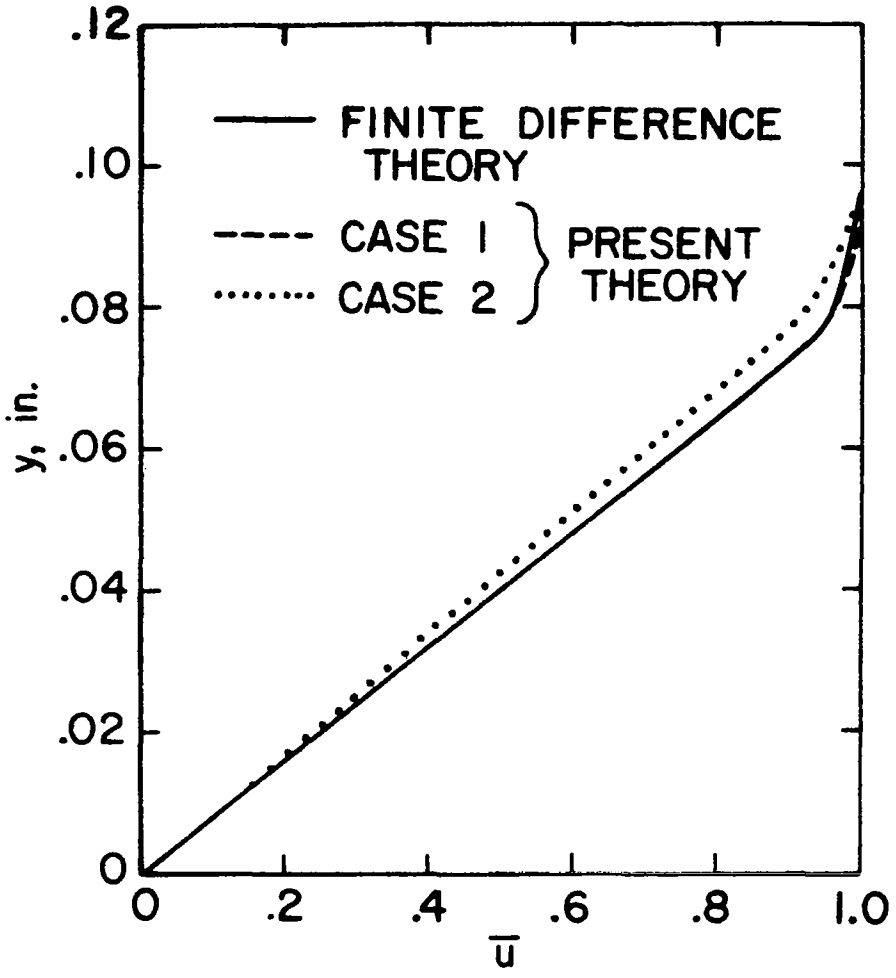


(c) Initial velocity profiles (x = 0.325 ft.).

Figure 17.- Continued.

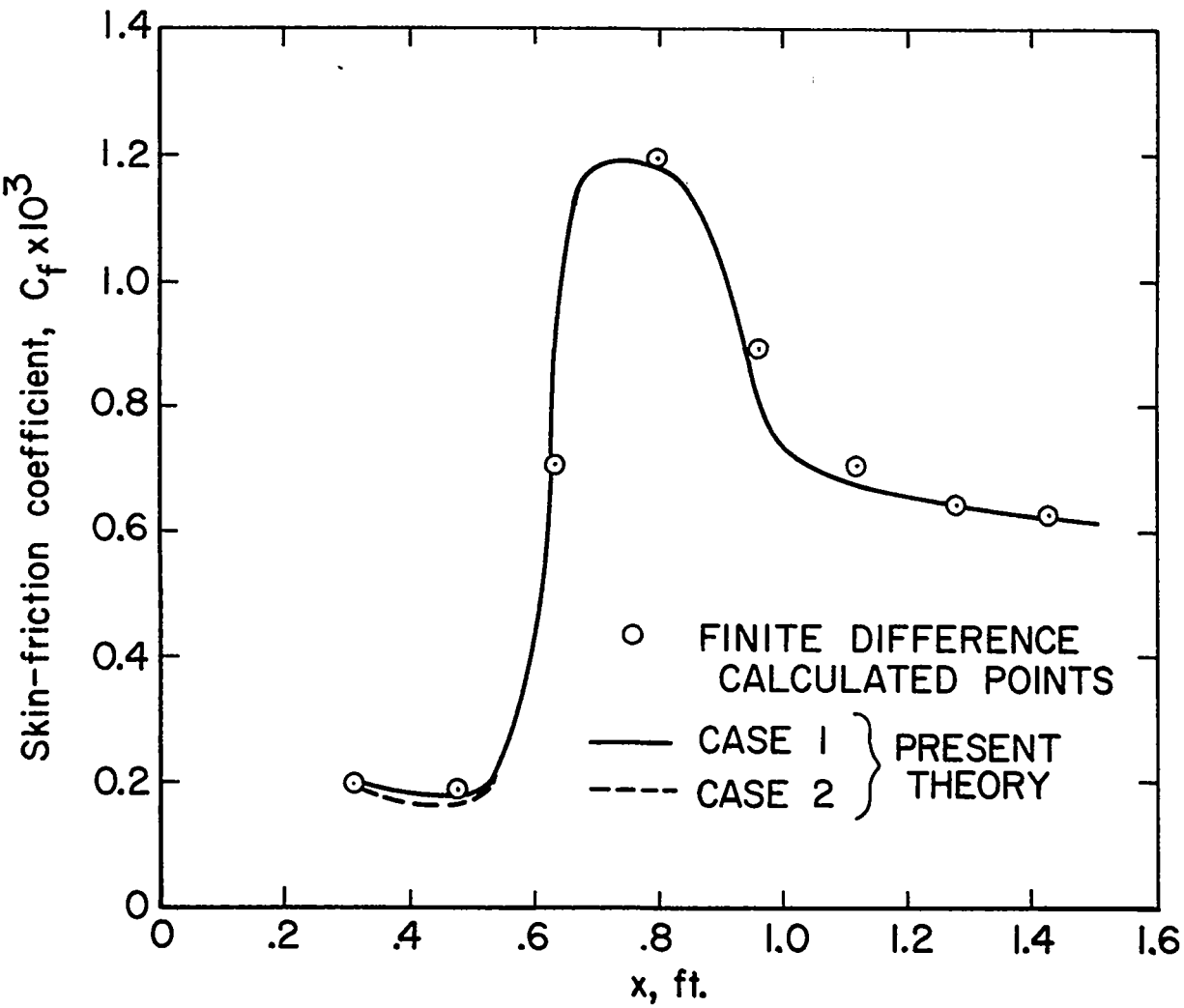


(d) Skin-friction coefficient.

Figure 17.- Continued.

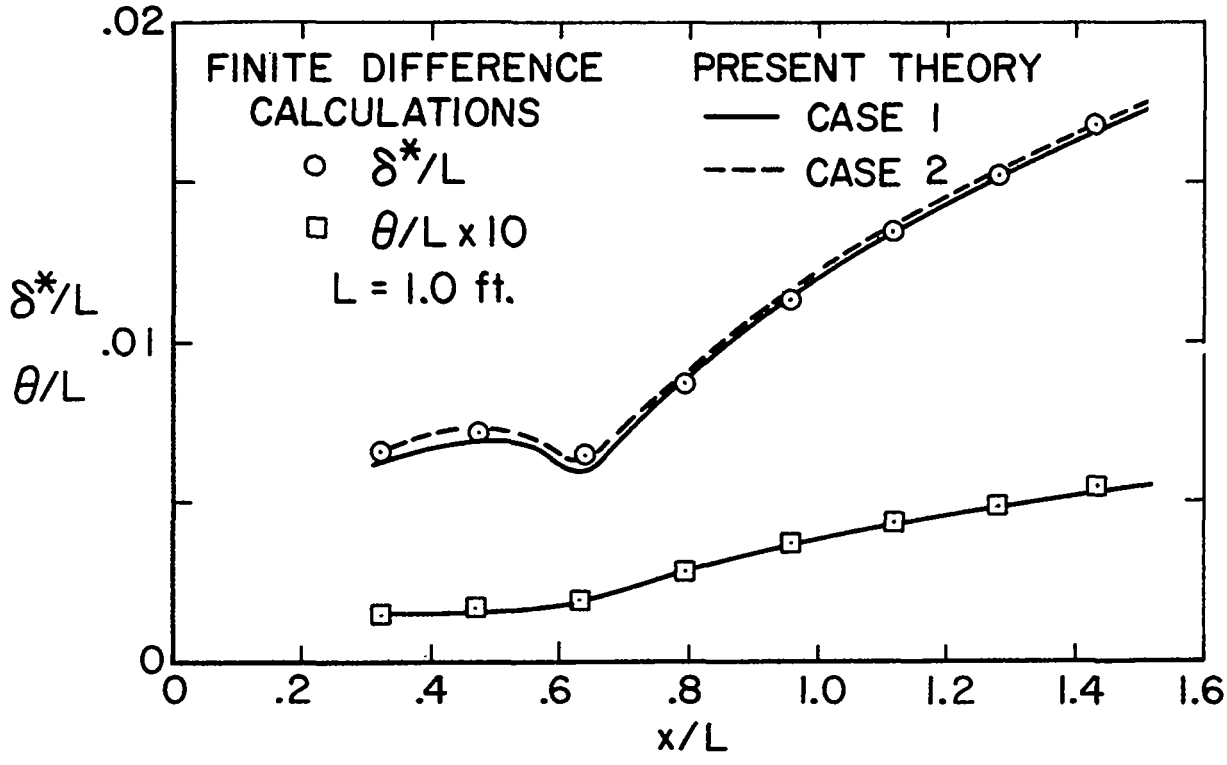


(e) Displacement and momentum thickness.

Figure 17.- Continued.

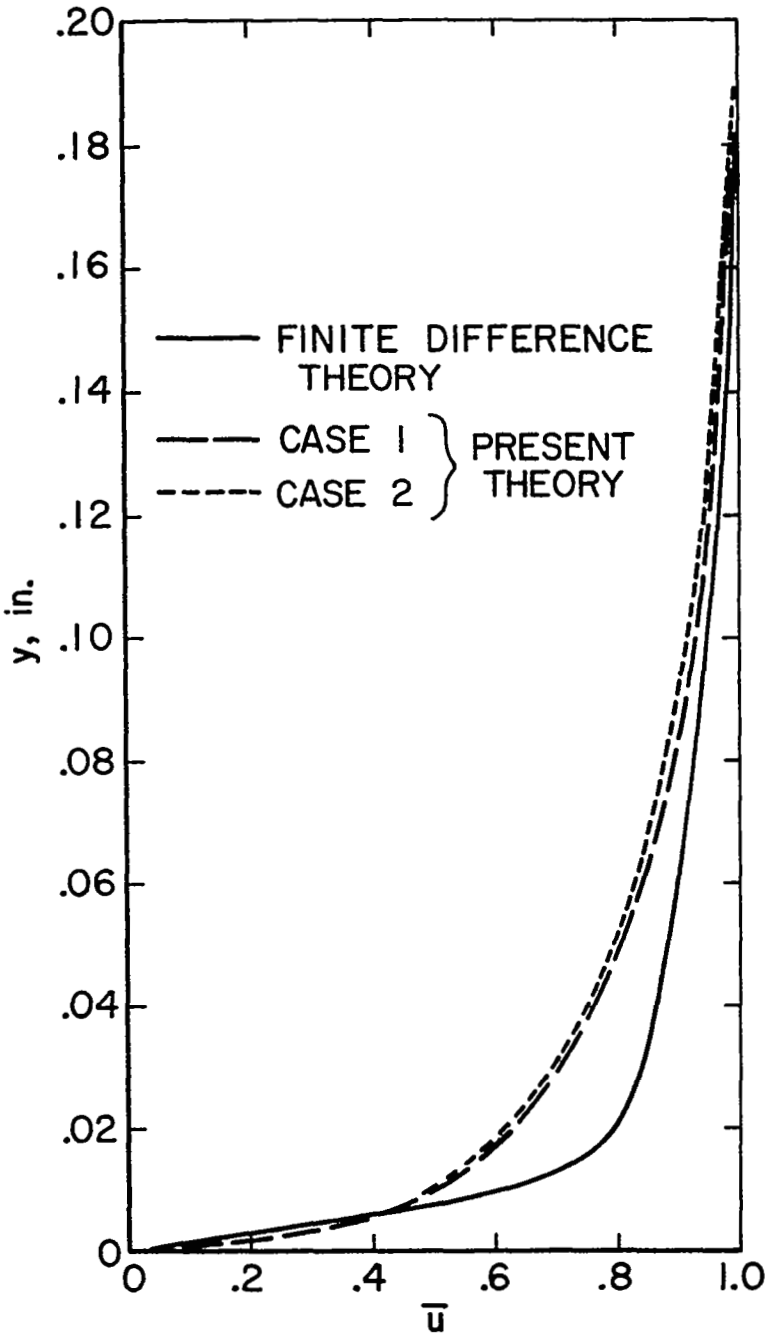


(f) Velocity profiles in transition region ($x = 0.825$ ft., $\Gamma \doteq 3$).

Figure 17.- Continued.

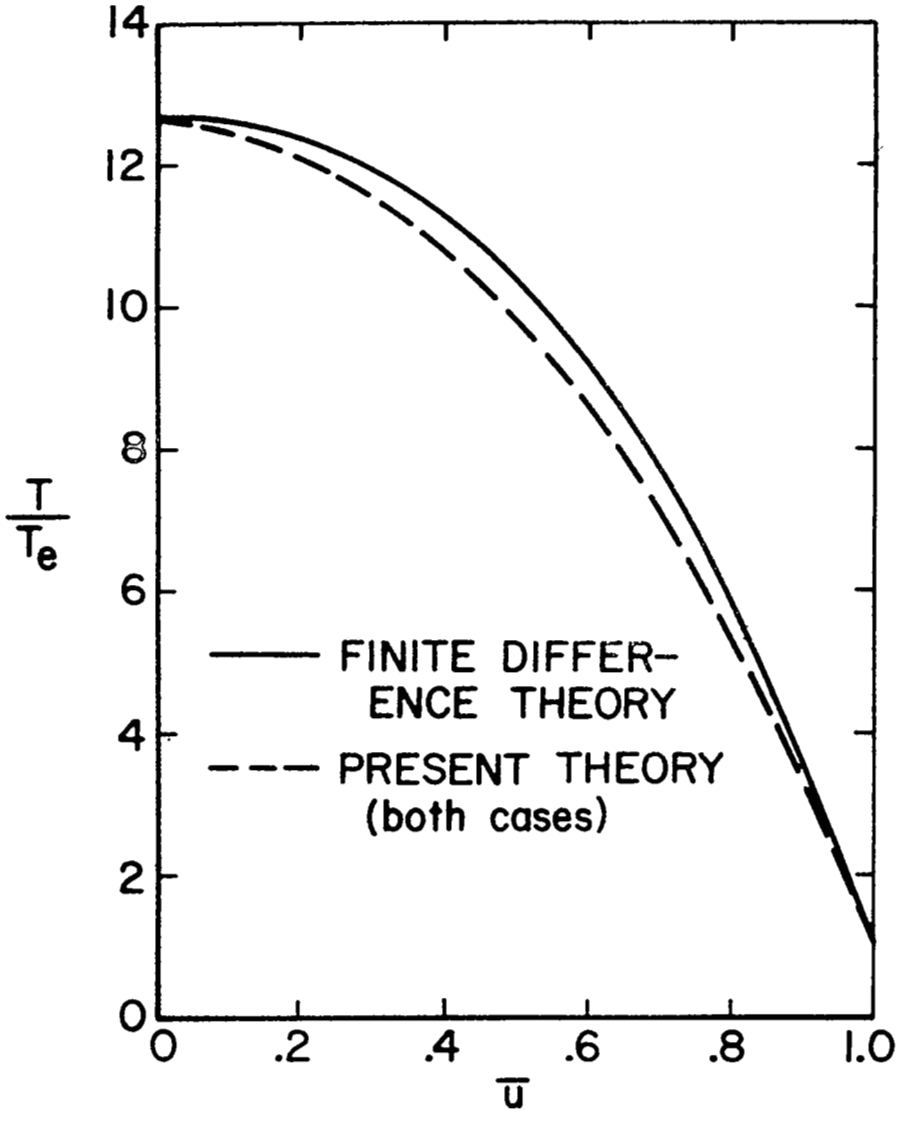


(g) Total temperature profile in transition region ($x = 0.825$ ft., $\Gamma = 3$).

Figure 17.- Continued.

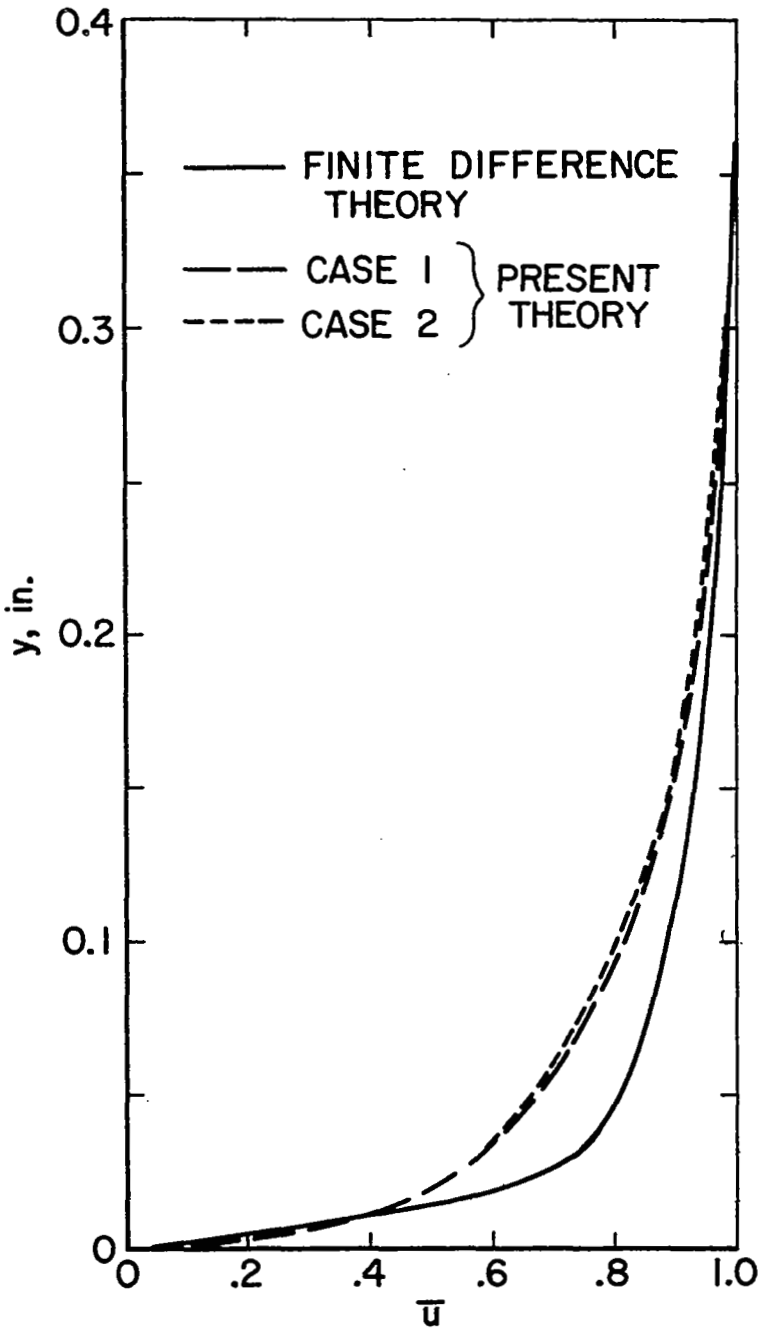


(h) Velocity profiles in turbulent region ($x = 1.43$, $\Gamma = 1$).

Figure 17.- Continued.

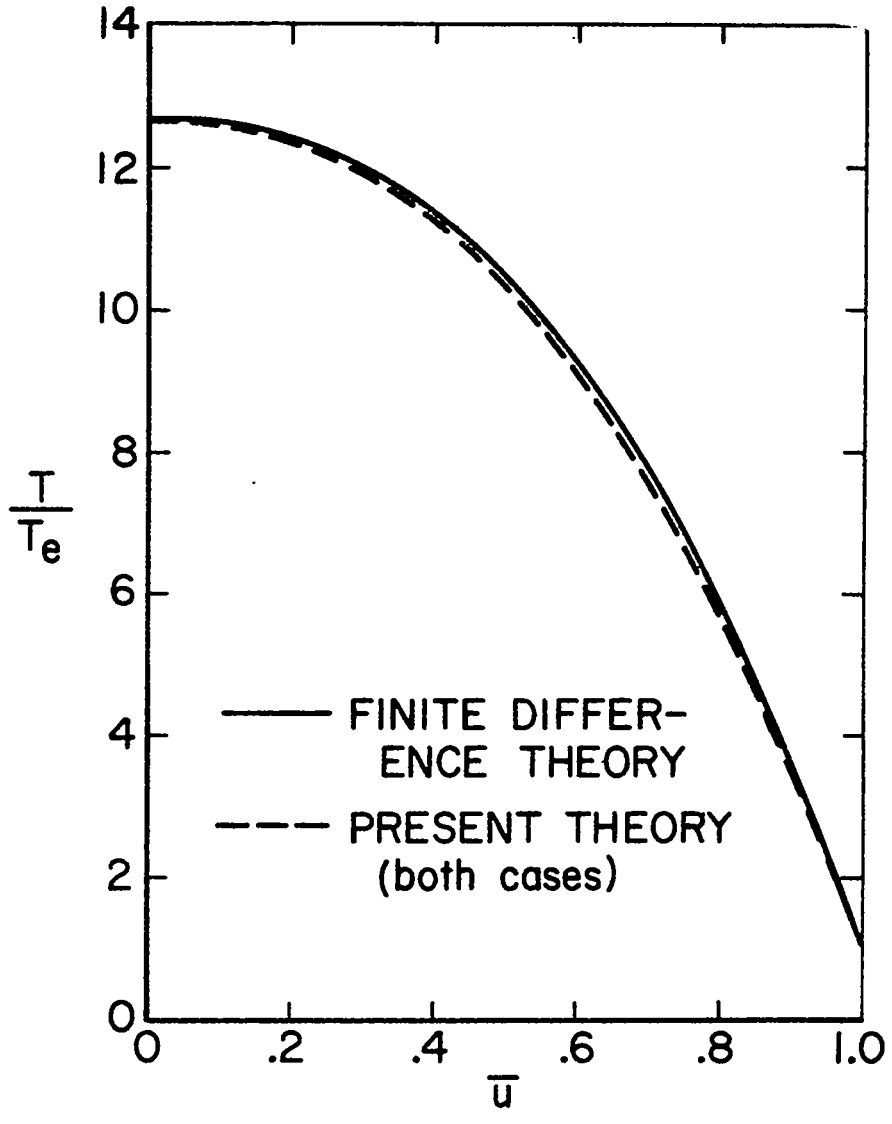


(i) Total temperature in turbulent region ($x = 1.43$, $\Gamma = 1$).

Figure 17.- Concluded.

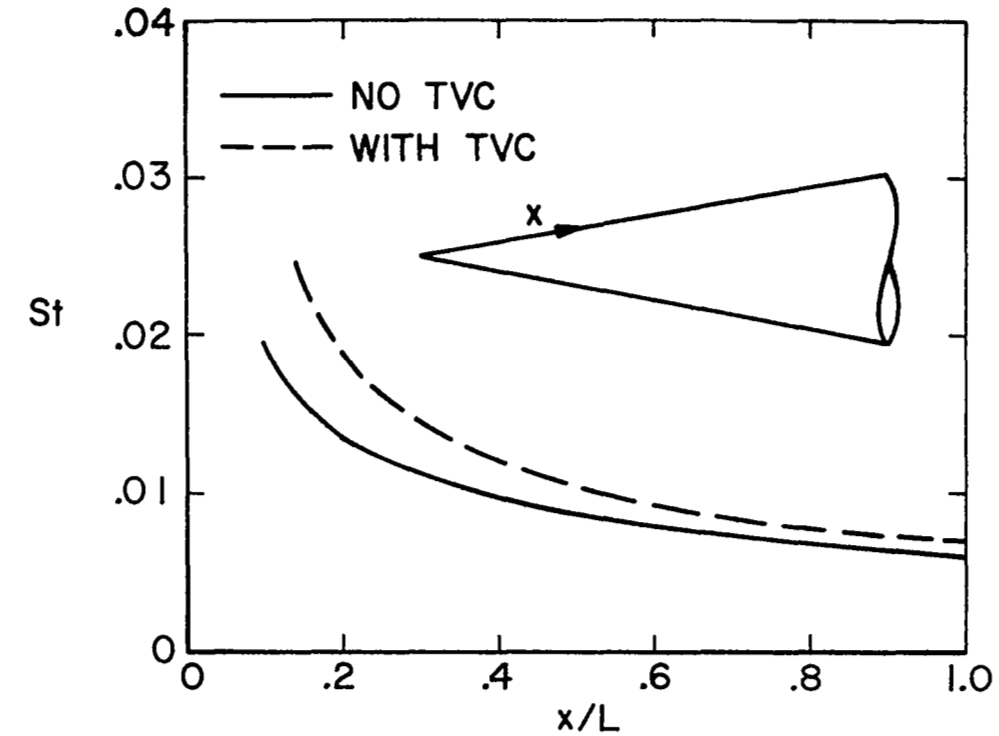


(a) Stanton number.

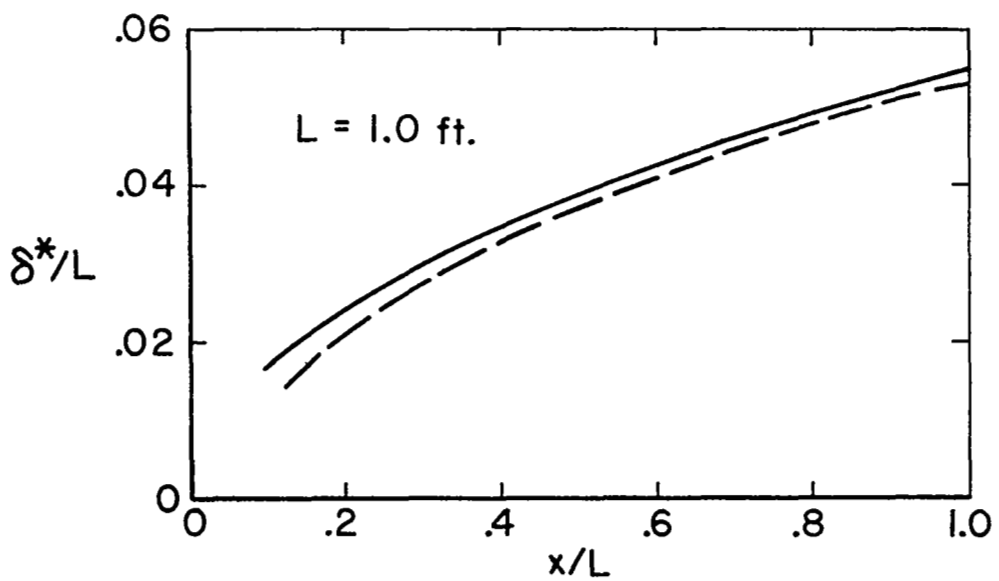


(b) Displacement thickness.

Figure 18. Calculation showing the effect of transverse curvature on a laminar boundary layer on a cone; $M_e = 5.54$, $Re_1 = 10^4$ ft$^{-1}$.

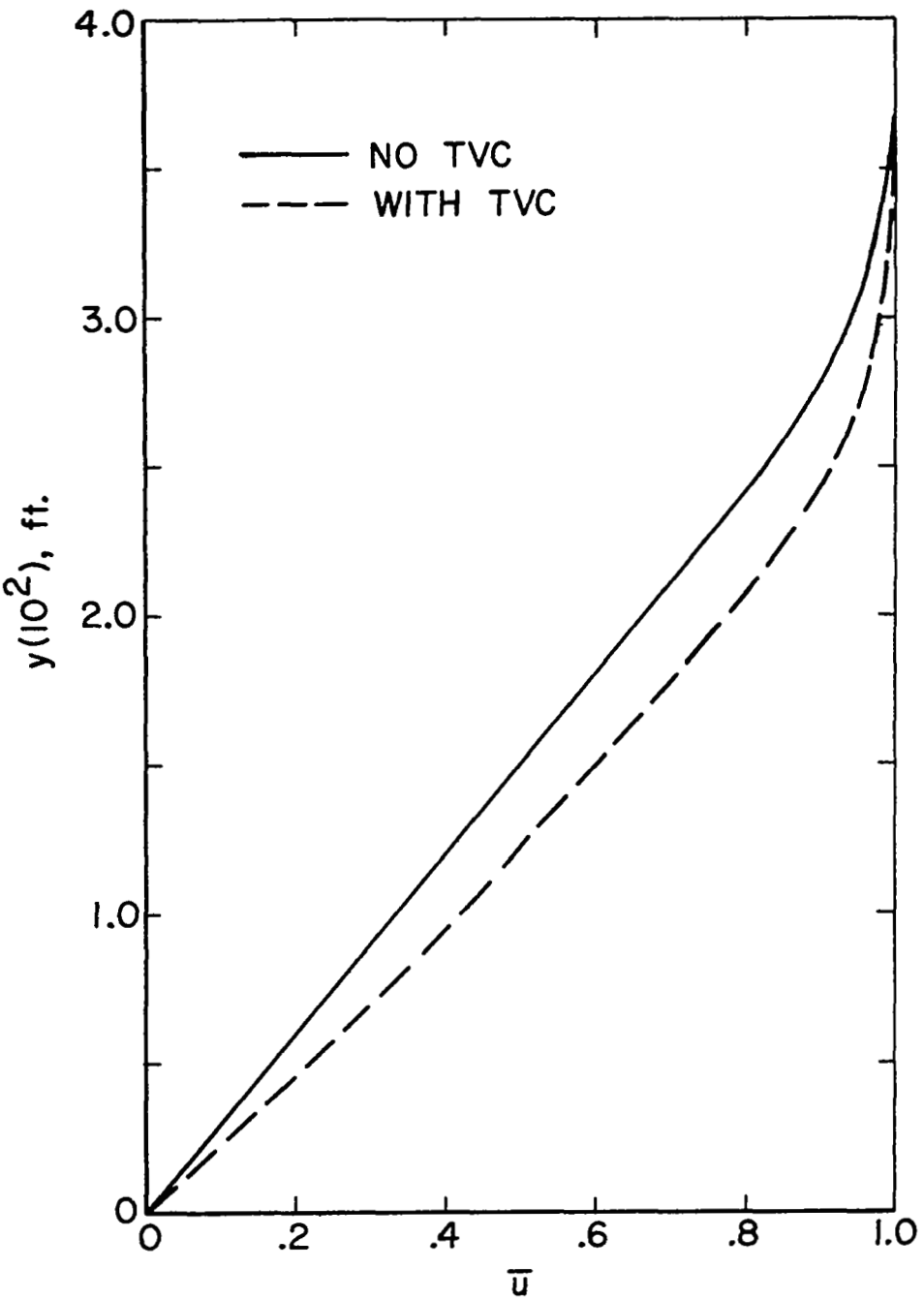


(c) Velocity profiles (x/L = 0.2).

Figure 18.- Continued.

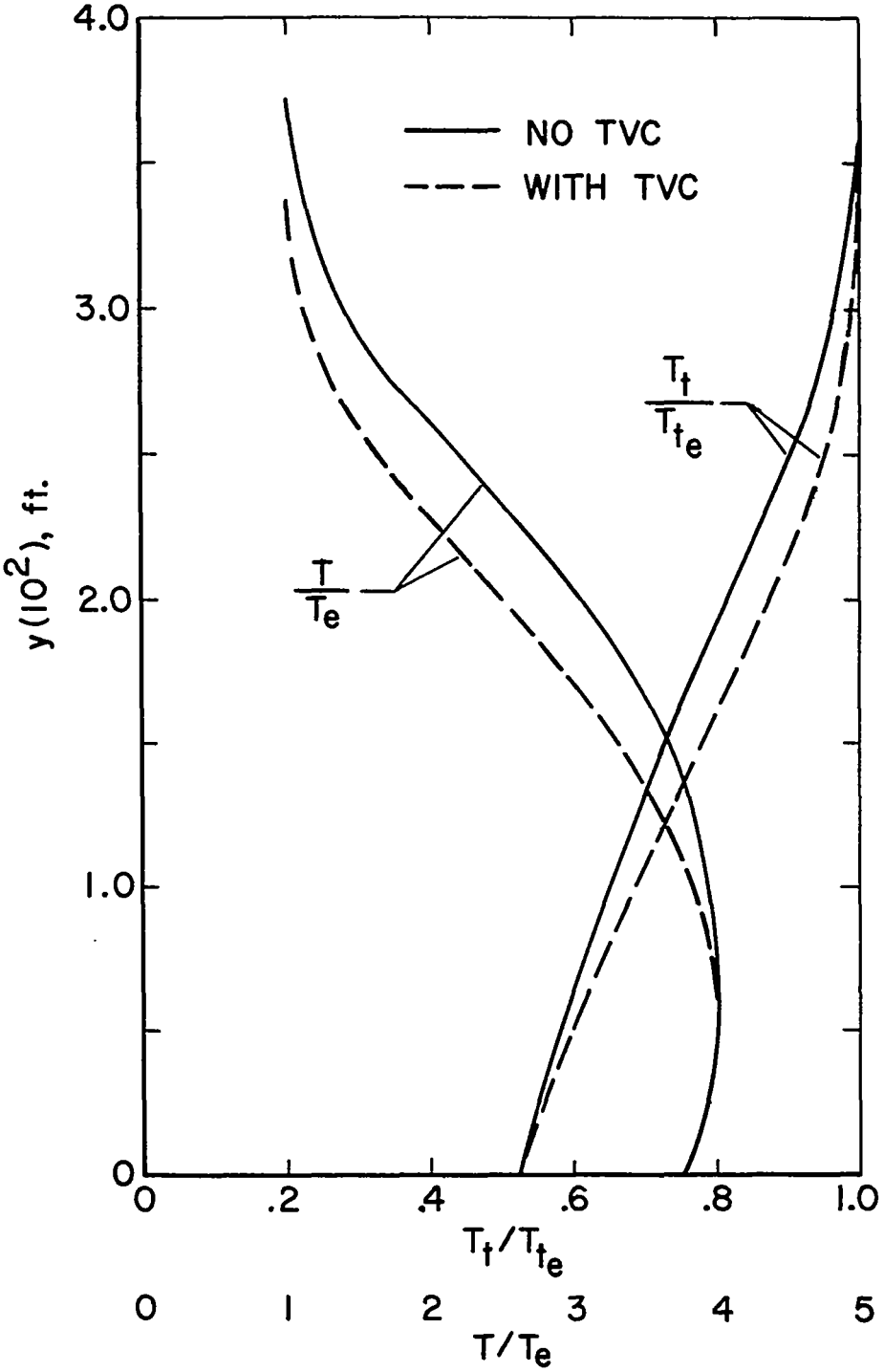


(d) Static and total temperature profiles (x/L = 0.2).

Figure 18.- Concluded.

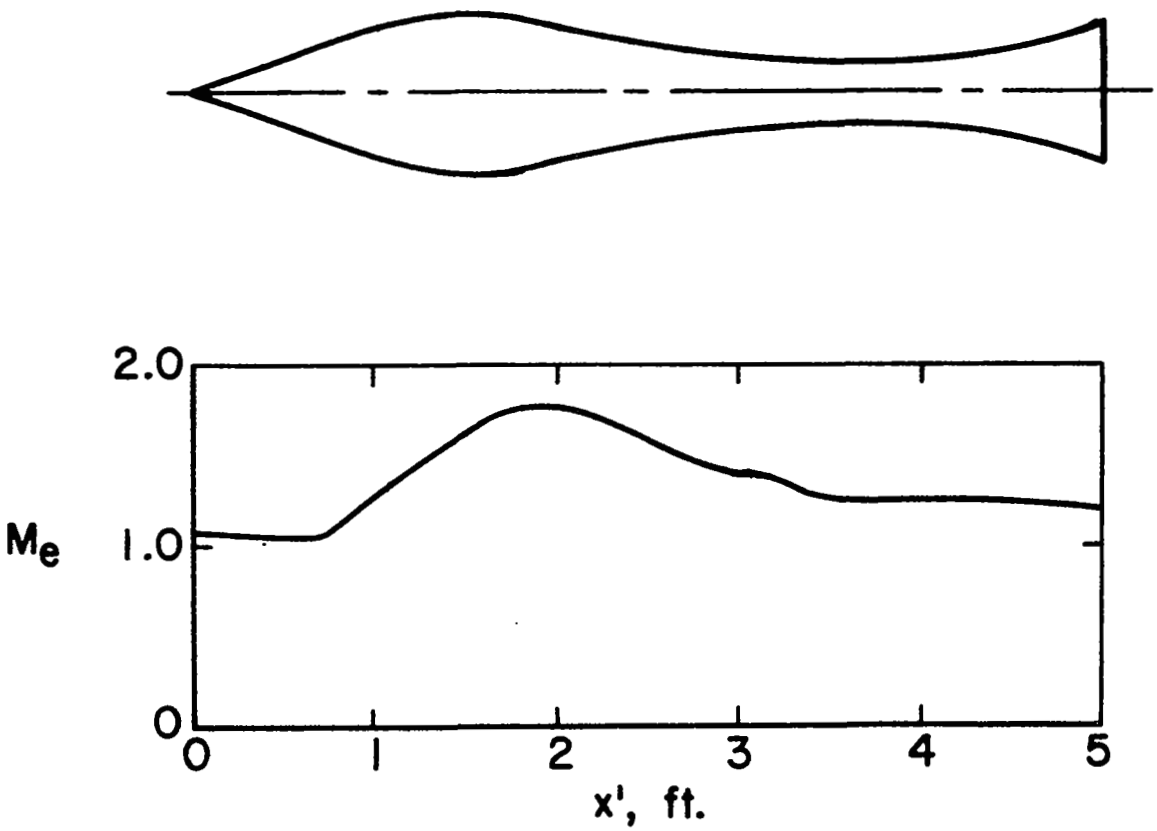


Figure 19.- Experimental Mach number distribution on a waisted body of revolution.

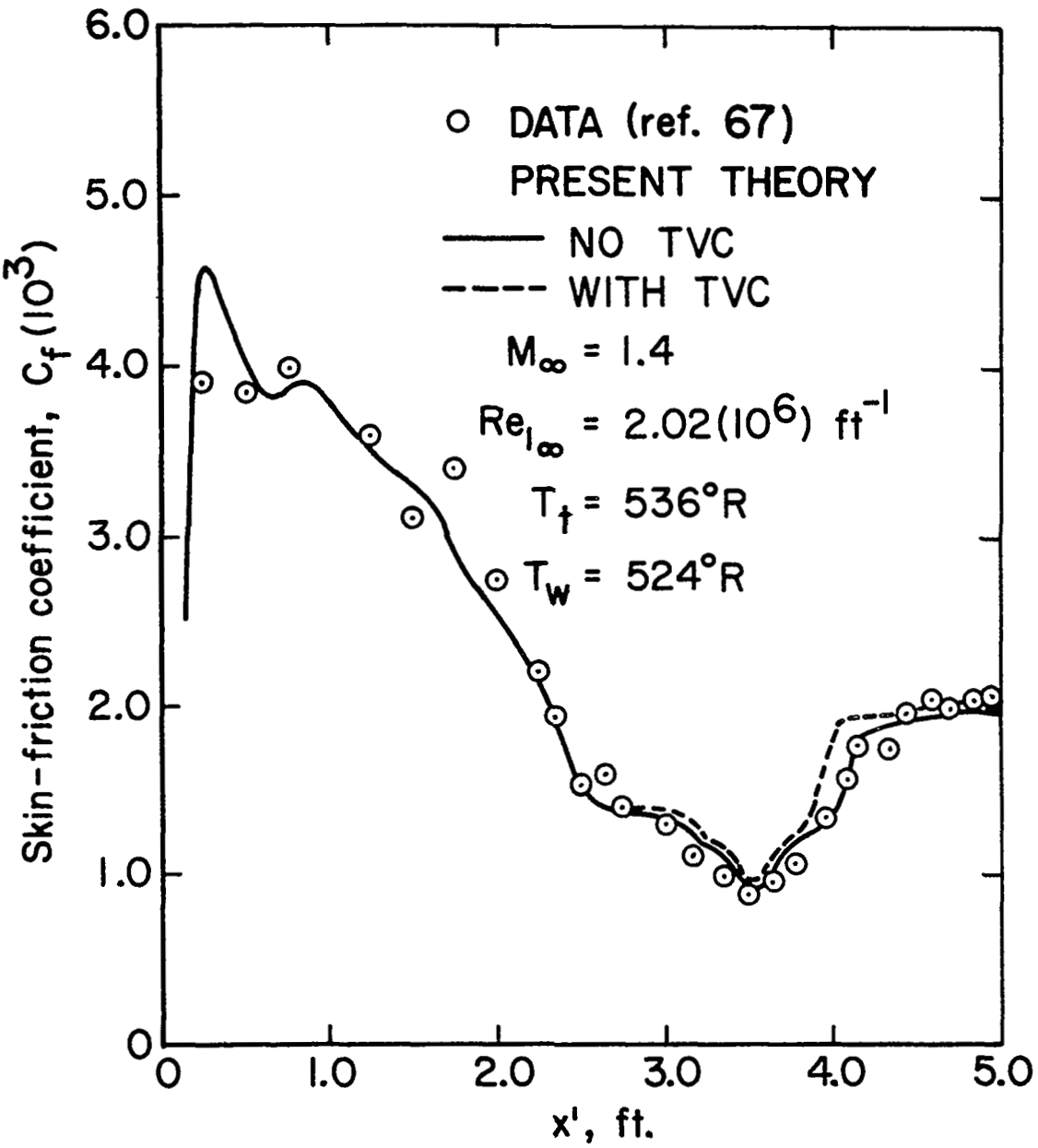


(a) Skin-friction coefficient.

Figure 20.- Comparison of theory and experimental data on a waisted body of revolution.

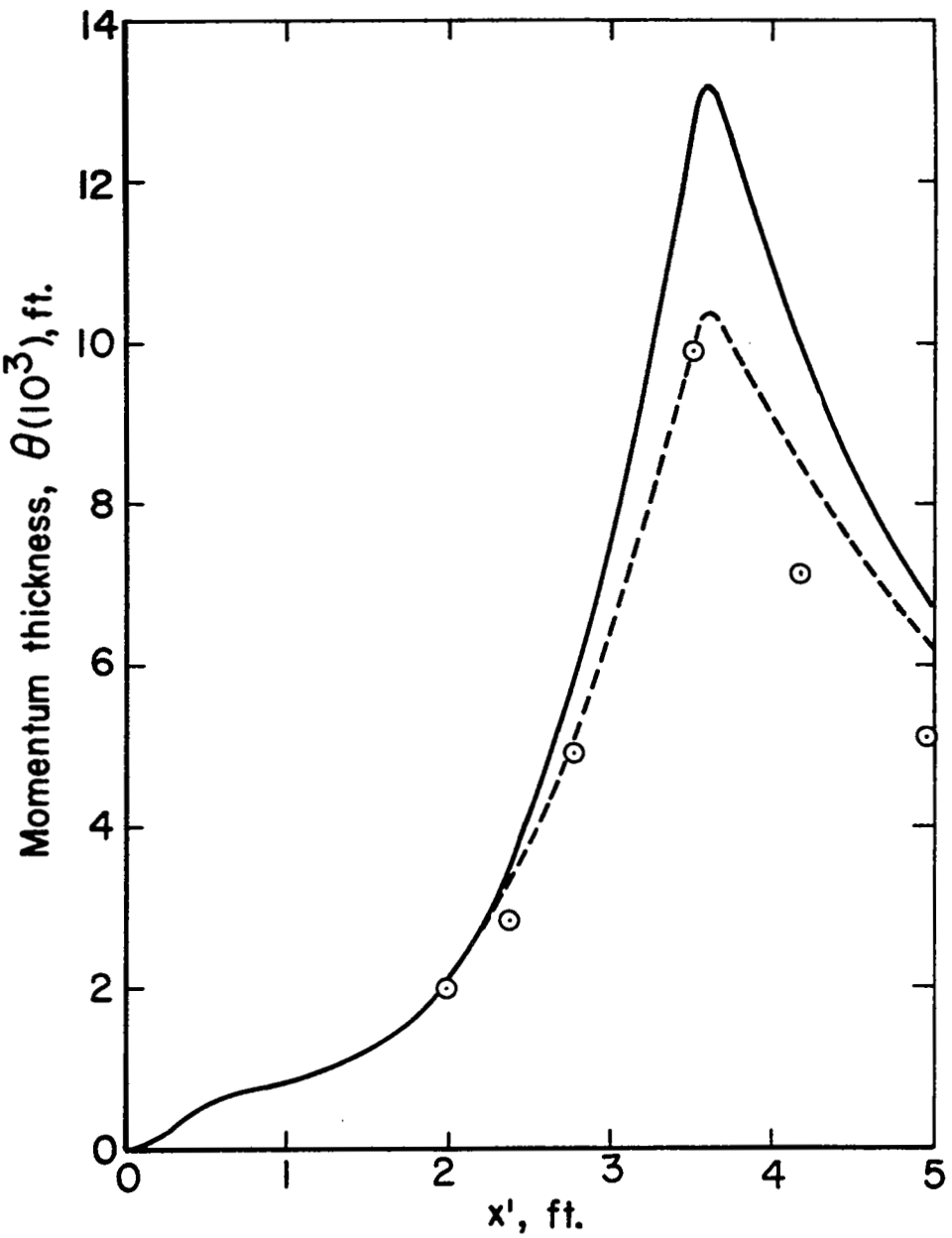


(b) Momentum thickness.

Figure 20.- Concluded.



NASA-Langley, 1971 —— 12 CR-1797